AN ABSTRACT OF THE THESIS OF

M. Kevin Drost for the degree of Doctor of Philosophy in Mechanical Engineering presented on April 29, 1985

Title: Volumetric Receiver Development - A Heat Transfer and Design Evaluation of an Advanced Air Heating Solar Thermal Central Receiver Concept

Redacted for Privacy

Abstract approved: James R. Welty

The volumetric receiver is an advanced solar central receiver concept designed to produce high temperature air. This document presents the results of a heat transfer and performance evaluation of the volumetric receiver concept.

The volumetric receiver consists of an array of ceramic fins or fibers arranged in concentric rows around a central manifold. Solar energy is absorbed on the fins or fibers and is used to heat ambient air which is drawn into the receiver by an induced draft fan.

The unusual features of the volumetric receiver required the development of analytical models for radiation heat transfer, convection and receiver performance. Radiation heat transfer was calculated using a Monte Carlo model where an innovative numerical scheme was used to improve computation speed. Convective heat transfer correlations used were obtained from a review of existing

literature. The receiver performance was predicted using a transient simulation which calculated the equilibrium temperature distribution.

The results of an extensive parametric investigation of five volumetric receiver design variations are reported and the most attractive design is identified. This design consists of a large number of small diameter ceramic fibers enclosed in a shroud. Convection from the fibers is enhanced by inducing a swirl in the incoming ambient air. The combination of small ceramic fibers and the induced swirl produces very efficient heat transfer. Performance results showed that the volumetric receiver has a predicted efficiency of 86% as compared to other high temperature receivers where the efficiency is estimated to be 81%.

# Volumetric Receiver Development - A Heat Transfer and Design Evaluation of an Advanced Air Heating Solar Thermal Central Receiver Concept

by

M. Kevin Drost

A THESIS

submitted to

Oregon State University

in partial fulfillment of
the requirements for the
degree of

Doctor of Philosophy

April 29, 1985

Commencement June 1985

APPROVED:

Redacted for Privacy

Professor of Mechanical Engineering in charge of major

Redacted for Privacy

Chairman of department of Mechanical Engineering

Redacted for Privacy

Dean of Graduate School

Date thesis is presented April 29, 1985

Typed by Sadie's Word Processing for M. Kevin Drost

## ACKNOWLEDGEMENTS

This work was supported by the Pacific Northwest Laboratory (PNL) as part of the Volumetric Receiver Development Program. The PNL program was in turn supported by Sandia National Laboratories as part of the U.S. Department of Energy's Solar Thermal Central Receiver Program. The author would like to acknowledge the assistance and guidance provided by Dr. Ben Johnson of PNL and Dr. James Welty of Oregon State University and the other members of my committee. Finally, I dedicate this work to my father. Any small success I have had in life is due to his example.

TABLE OF CONTENTS

LIST OF FIGURES

LIST OF TABLES

# VOLUMETRIC RECEIVER DEVELOPMENT - A HEAT TRANSFER AND DESIGN EVALUATION OF AN ADVANCED AIR HEATING SOLAR THERMAL CENTRAL RECEIVER CONCEPT

## CHAPTER I

## INTRODUCTION

This document reports the results of an analysis and design of a volumetric air heating receiver for use in a solar central receiver energy generation facility. Section 1.1 of the introduction will present an overview of solar thermal technology and indicate the role of the volumetric air heating receiver in the development of advanced solar technology. Section 1.2 will present a brief description of concept and describe the generic features of the volumetric receiver. Section 1.3 includes a discussion of the results of previous investigations of the volumetric concept and Section 1.4 presents a statement of the objective of the research documented in this study.

### 1.1 SOLAR THERMAL TECHNOLOGY

High temperature solar thermal technology for either power generation or process heat has been a major focus of energy research. All high temperature solar thermal facilities can be divided into five subsystems. The concentrator collects the solar radiation from the sun (insolation) and focuses it on a receiver which absorbs the radiant energy and transfers it to some heat transfer media. The energy stored in the heat transfer media is transported by a transport subsystem either to a storage subsystem or to the end use.

The end use can either be a process heat application or an energy conversion devise (power generation). A schematic diagram showing the main subsystems is presented in Figure 1.1.

A variety of solar thermal concepts have been developed. They can be characterized by the type of concentration (point focus, line focus or non focusing) and the type of receiver (distributed receiver or central receiver). The various generic solar thermal concepts have been compared for small power generation applications (Laity et al., 1979), large power generation applications (Apley et al., 1980), and process heat applications (Bird et al., 1981). In all three cases the point focus central receiver cost concept has proved to be the most attractive solar thermal concept for most combinations of plant size and capacity factor.

The point focus central receiver concept, normally identified as a central receiver system, consists of a field of mirrors or heliostats which completely or partially surround a tower mounted receiver. The heliostats can move about two axes and track the sun as it moves through the sky, concentrating the insolation on the tower-mounted receiver. The receiver absorbs the insolation and transfers it to a heat transfer medium. Usually the heat transfer medium is transported to ground level where it provides energy for power generation or process heat. In order to extend the amount of time that a central receiver can provide energy a storage subsystem is included. When the facility is in operation some fraction of the energy

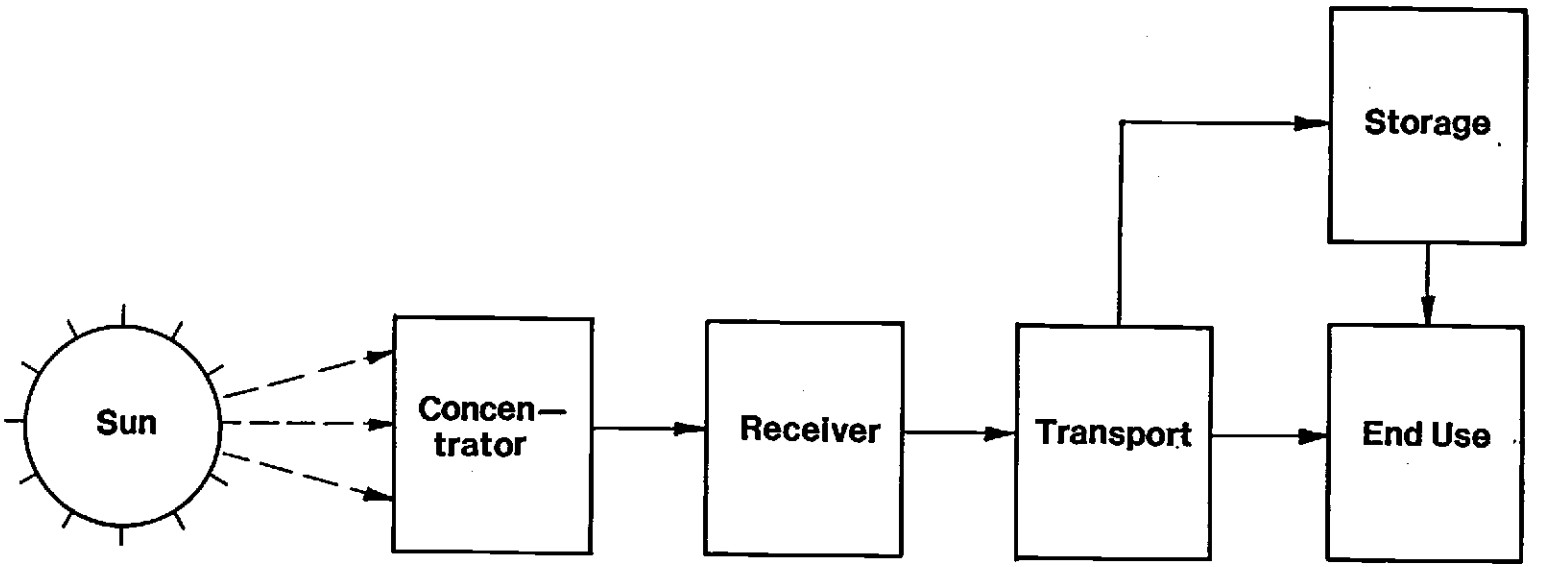


Figure 1.1. Schematic arrangement of solar thermal subsystems

collected by the plant is stored for use when isolation is not available. A schematic drawing of a central receiver power plant is shown in Figure 1.2 and an artist's rendition is presented in Figure 1.3.

The receiver is either an open receiver where the absorbing surface is completely exposed to the surroundings or a cavity receiver where the absorbing surface is encased in a cavity with an opening (aperture) to allow insolation to enter the receiver. High temperature applications tend to use cavity receivers.

The central receiver has been primarily considered for power generation. The one operating solar central receiver power plant is located at Barstow, California. In this concept, superheated steam is generated in the receiver. The steam is then used in a conventional Rankine cycle to produce electric power. Liquid sodium and molten salts have also been considered as heat transfer fluids. Either liquid sodium or molten salt is heated in the receiver and used to generate steam in a heat exchanger. Economic comparison studies have shown that, for power generation, the molten-salt central receiver systems are the most attractive alternatives when compared to other solar thermal concepts.

Most electric power generation schemes either directly or indirectly use the solar energy to generate steam in a Rankine power cycle. This limits the required temperature from the receiver to around 866K (1100F). Above 866K the choice of a heat transfer medium is much more limited. Air has been studied as a heat transfer medium for both power generation and process heat applications.

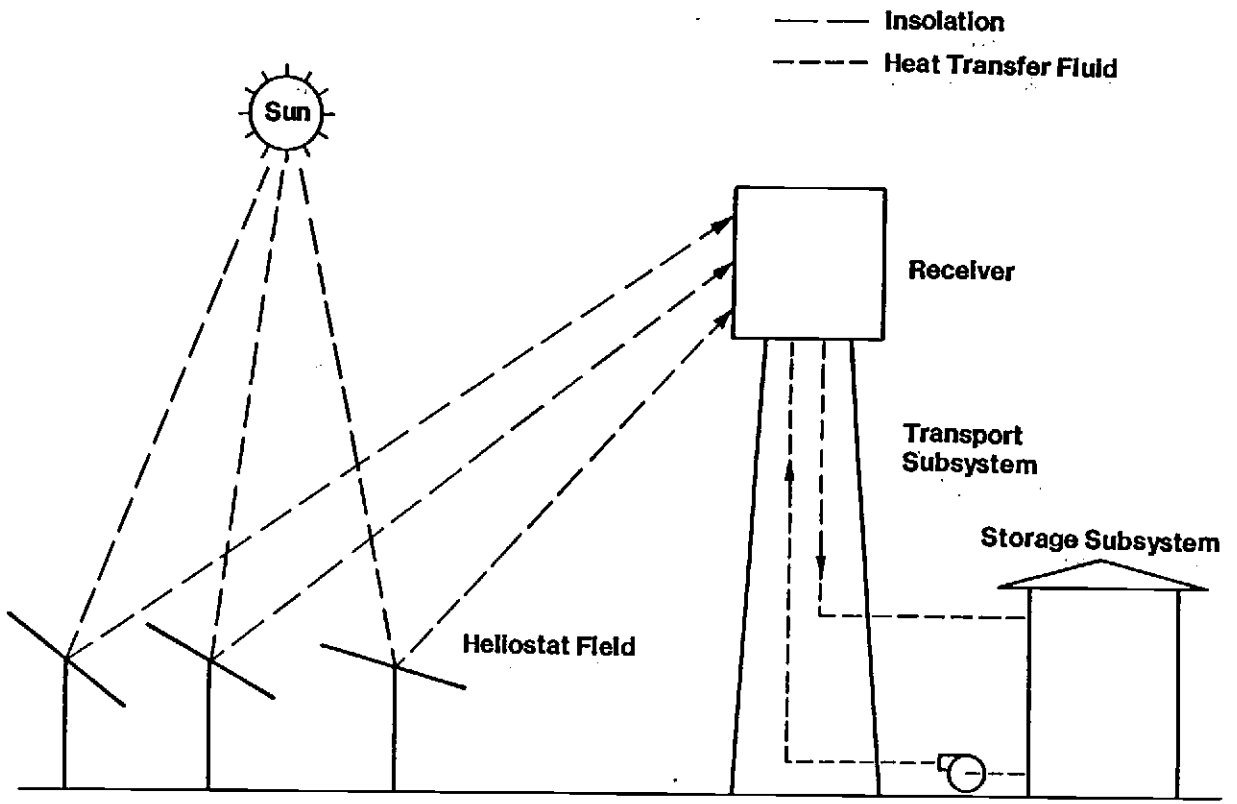


Figure 1.2. Schematic arrangement of solar process heat facility

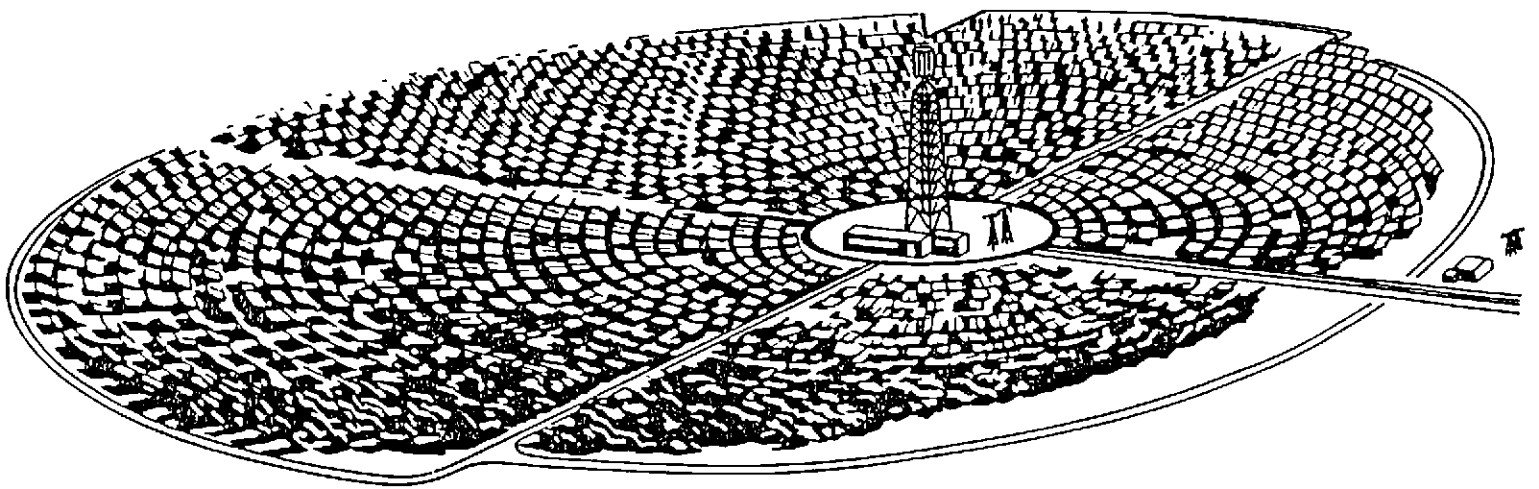

Figure 1.3. Solar central receiver concept

Other media such as sand and certain types of molten salts have also been proposed.

In 1981, the United States Department of Energy funded a study of air heating receivers (Bird et al., 1982) and a study of complete process heat facilities using air as the working fluid (Delaquil et al., 1983). One of the concepts included in the air heating receiver study was the volumetric air heating receiver. This concept had been developed at the Pacific Northwest Laboratory (Drost and Eyler, 1981). Based on the results of these studies, the volumetric receiver was identified as an attractive concept and a study was funded at the Pacific Northwest Laboratory (PNL). The purpose of the investigation was to study the volumetric concept in more depth. The research described in this document is part of the PNL investigation.

## 1.2 CONCEPT DESCRIPTION

The original volumetric receiver concept consisted of an array of fins arranged in concentric cylindrical rows around an inlet manifold. The outer row of fins is made up of wedge shaped fins (reflecting fins) with specular reflecting surfaces. Insolation strikes the receiver and is reflected into the interior of the receiver by the reflecting fins. The radiant energy is then absorbed on the interior fins. As the insolation is absorbed on the various surfaces, they increase in temperature and thermal energy is removed by convection to ambient air being drawn past the receiver surfaces. Ultimately the air is drawn into the inlet manifold and finally

through the downcomer to ground level. The absorbing surfaces will also reradiate energy to the surroundings. The wedge-shaped reflecting zones will reduce reradiation by either absorbing the reradiated energy or reflecting it back into the receiver. This version of the volumetric receiver is shown in Figure 1.4.

The volumetric receiver concept shown in Figure 1.4 includes the primary features of all volumetric receiver designs. These are:

- o Volumetric Absorbing Array - The volumetric absorbing array is the primary absorber in the receiver. The array is intended to absorb insolation and transfer the thermal energy to the air being drawn past the surfaces of the array. This should be done with minimum pressure drop and reradiation losses. The absorbing array can consist of fins pins or small fibers arranged in a variety of configurations.
- o Inlet Manifold/Terminal Absorber - The Inlet Manifold serves two purposes. First, it is designed to evenly distribute air flow through the receiver. Second, the inlet manifold also acts as the terminal absorber which absorbs any insolation which has passed through the volumetric absorbing array. The inlet manifold is located at the discharge of the absorbing array.
- o Geometric Loss Reducer - The reflection and reradiation losses from the absorbing array can be further reduced by using a geometric loss reducer. The geometric loss

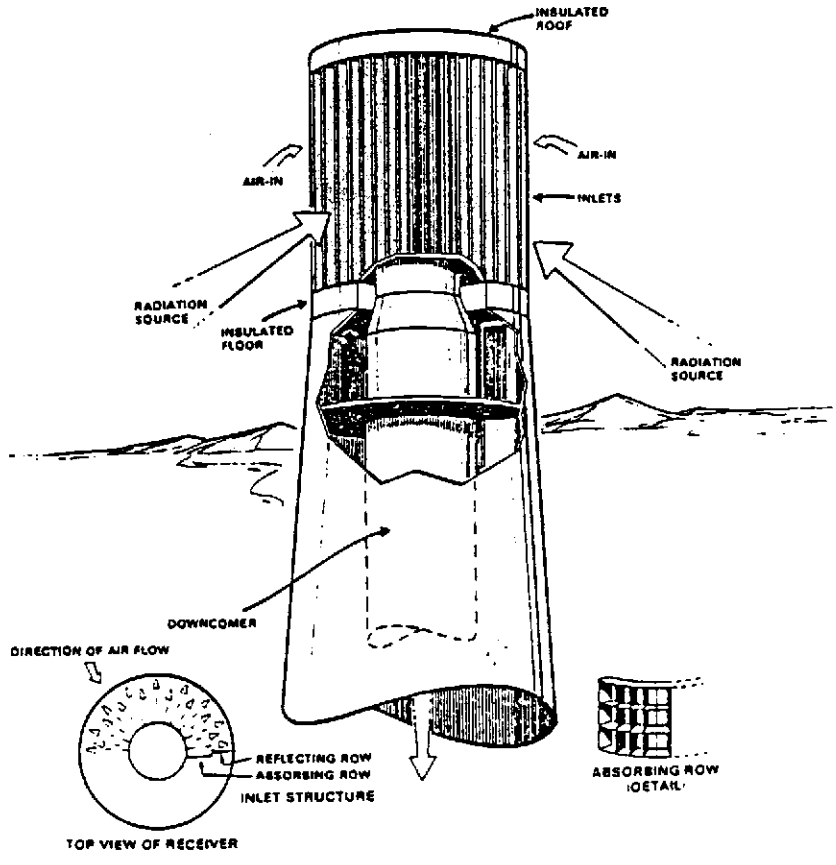


Figure 1.4. Volumetric receiver (Bird et al., 1982)

reducer lets insolation enter the receiver while inhibiting the reradiation or reflection of energy from the receiver. This effect is obtained solely by the geometric arrangements of surfaces rather than any special surface coating or coverglass. One common geometric loss reducer is a cavity around the absorber. A second type considered in this study is the inclusion of a row of wedge-shaped reflecting pins for the external row in the receiver.

- o Downcomer - The downcomer is the pipe or duct which contains the hot product air as it is drawn to ground level by an induced draft fan.

The arrangement of the primary components of the volumetric receiver is shown schematically in Figure 1.5.

The volumetric receiver has three inherent features which are fundamentally different from other currently proposed solar central receiver designs.

- o Volumetric Absorption - The arrangement of a large number of surfaces in a volume makes the receiver appear to be absorbing insolation in a volume rather than on one surface as with other more conventional designs.
- o Heating Ambient Air - Ambient air is drawn past the absorbing surfaces. This has the advantage of having the lowest air temperature and surface temperatures located

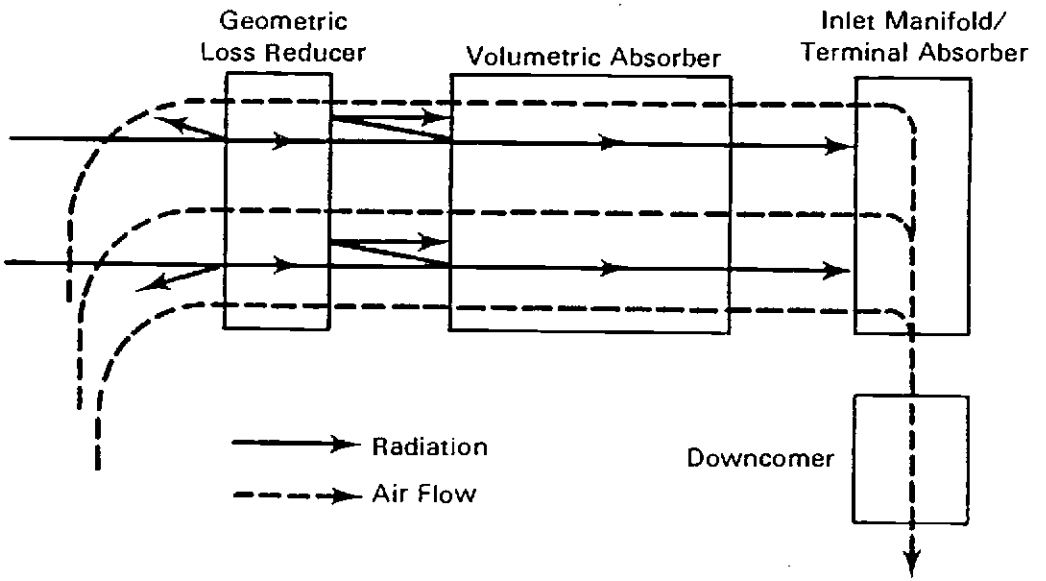


Figure 1.5. Schematic of generic volumetric receiver

at the external surface of the receiver. This results in reduced thermal losses.

- o Reflecting Rows - The reflecting rows are a new type of loss reduction technique which relies on the wedge-shaped specular reflecting pins which allow insolation to enter the receiver while inhibiting reradiation and reflections. A cavity-like shroud was also considered for geometric loss reduction.

A more detailed discussion of the different volumetric receiver designs considered in this study is presented in Section 2.2.

## 1.3 PREVIOUS STUDIES

The volumetric receiver was invented at the Pacific Northwest Laboratory (PNL) and the U.S. Department of Energy (DOE) holds the patent on the concept (U.S. Patent No. 4,394,859). The original evaluation of the volumetric receiver consists of a brief internal review conducted at PNL. The results of this evaluation are documented in Drost and Eyler (Drost and Eyler, 1981). Based on the results reported by Drost and Eyler the volumetric receiver was included in a comparison study with six other high temperature air heating receivers. The results of this study are documented in Bird et al. (Bird et al., 1982). The results of the receiver comparisons were used by Sandia National Laboratory in a cost and performance comparison of complete systems using the seven receivers studied by Bird et al. The results of this study are documented by DeLaqiul et

al. (DeLaquil et al., 1983). These three studies will now be summarized while a more detailed discussion of the analytical models and performance results from these studies are included in Section 2.7.

The preliminary study conducted at PNL consisted of developing a simple performance model for the volumetric receiver and subsequently predicting receiver performance. The receiver was modeled as a series of concentric cylindrical zones. The insolation absorbed in each zone was calculated by modeling a zone as a semi-transparent material with a composite absorptivity, emissivity, and transmissivity. Using a method suggested by Viskanta et al. (Viskanta et al, 1978) the distribution of absorbed insolation was determined. The equilibrium temperature distribution was calculated by assuming that there is no internal radiation heat transfer between zones. With the temperature distribution and view factors calculated for infinite concentric cylinders it was possible to determine the reradiation losses. The results of the study were extremely favorable with projected receiver efficiencies of above 95% for a receiver producing hot air at 1093$^{o}$C. The report indicated that many aspects of the receiver needed further analysis including; air flow distribution, pin to air heat transfer, reflecting zone performance, distribution of absorbed energy and impact of heliostat field characteristics (Drost and Eyler, 1981).

The air heating receiver comparison documented in Bird et al., (Bird et al., 1982) consisted of developing preconceptual designs for

seven advanced air heating receivers, one of which was the volumetric receiver. The designs were developed for a range of facility sizes, product air temperatures and pressures. The performance and cost of each receiver design was estimated and areas of technical concern were identified. The analytical model used in this study was essentially the same as that used in the preliminary evaluations. The main differences were in the correlations used in calculating the convective heat transfer coefficients between the pins and the air and in estimating convective losses from the entire receiver to the surroundings. The areas of technical uncertainty were expanded to include new problems identified during the study. The results of this evaluation showed that the volumetric receiver would have excellent thermal performance but that the receiver was more expensive than several other designs (Bird et al., 1982).

The scope of the air heating receiver comparison was limited to the receiver itself. The results of this study were used by Sandia National Laboratory for a comparison of complete solar process heat power plants. The volumetric receiver was predicted to have the lowest levelized energy cost but all designs were expensive when compared to conventional sources and the report concluded that air heating receivers in general may not be a particularly attractive technology (Delaquil et al., 1983).

In 1983 Sandia National Laboratory decided to fund additional research on the volumetric receiver. The project was conducted at PNL with Oregon State University as a subcontractor. Oregon State

University has been primarily involved in the modeling of thermal processes in the receiver.

## 1.4 PROJECT DESCRIPTION

The PNL project entitled, "Volumetric Receiver Development" consisted of four main tasks.

Task 1. Analytical Model Development - This task consisted of development analytical models for:

- Air Flow Distribution
- Absorbed Insolation Distribution
- Internal Radiation heat Transfer
- Pin/Air Heat Transfer
- Performance Model

Task 2. Design Characterization - This task consisted of screening possible volumetric receiver designs using the analytical model developed in Task 1 and identifying the significant characteristics of the most attractive design.

Task 3. Preconceptual Design - This task consisted of conducting a preconceptual design for the receiver design selected in Task 2.

Task 4. Cost Estimate - Task four involved the development of a cost estimate for the receiver preconceptual design developed in Task 3.

Oregon State University was primarily involved in Tasks 1 and 2.

The analytical model for insolation distribution, internal radiation heat transfer and the performance model were developed at OSU along with a model for the convective heat transfer between ceramic fibers and air. OSU also conducted the Task 2 design characterization. This thesis consists of the development of the analytical models and the design characterization.

## 1.5 OBJECTIVES OF STUDY

The objectives of this thesis can be divided into two categories; Model Development (Task 1) and Design Characterization (Task 2). The specific objectives in each area are described in the next two sections.

### 1.5.1 Model Development

The major activity in this research was the development of analytical models for the analysis of a volumetric receiver. As Section 2.0 will demonstrate, the volumetric receiver includes many unique features which are not easily analyzed. The models had to be sufficiently accurate in order to predict receiver performance and account for all relevant phenomena. In addition, the models had to be sufficiently general to allow the analysis of a wide range of possible designs. The major objectives in this area include:

Insolation Distribution - The objective was to develop a model which predicts the distribution of absorbed insola-

tion in the volumetric receiver for a variety of absorbing media and receiver geometries.

Internal Radiation Heat Transfer - The objective was to predict the radiation heat transfer both between various receiver surfaces and between the receiver surfaces and the surroundings. The model had to be sufficiently general to allow the analysis of a variety of absorbing media and geometries.

Pin/Air Heat Transfer - The objective of this work was to predict the convective heat transfer coefficient for convection between a small fiber and air.

Performance Model - The objective was to combine the radiation heat transfer models, pin/air heat transfer model and the air flow distribution model into a performance model which predicts the receiver temperature distribution, product temperature and receiver performance.

### 1.5.2 Design Characteristics

The objectives associated with Task 2 involve using the models described above to analyze a variety of volumetric receiver configurations and to select the most attractive configurations. The major objectives in this area are:

Configuration Selection - The first objective in Task 2 was to select the general volumetric receiver configuration

to be used in the study. The four general configurations are described in Section 2.2

Design Characterization - The second objective was to conduct parametric and sensitivity studies on the general configurations in order to identify the major characteristics of an attractive design.

# CHAPTER 2

## VOLUMETRIC RECEIVER THERMAL PROCESSES

The volumetric receiver is a unique design and consequently involves thermal processes and applications which are not encountered in more conventional solar receiver designs. This section will provide an overview of the thermal processes associated with the volumetric receiver and will be a starting point for the discussion of the analytical model described later in the report.

The operation of a volumetric receiver includes a variety of thermal processes. Insolation from the heliostat field passes through the geometric loss reducer and strikes the absorbing media with a small fraction of the insolation lost by reflection. Air is drawn into the receiver past the absorbing media. As the absorbing media increases in temperature, incident energy is either convected to the air or radiated away to other sources. As this summary shows, the volumetric receiver thermal processes can be divided into five categories:

- o Insolation reflection and distribution on absorbing surfaces
- o Air flow distribution
- o Absorbing media heat transfer
  - a) convection to air
  - b) radiation to other surfaces or surroundings
- o Absorbing media equilibrium temperature.

Section 2.1 will describe the components of receiver efficiency and establish the terminology used in the subsequent discussion. Section 2.2 will present the generic types of volumetric receivers considered in the study. Section 2.3 includes a discussion of radiation heat transfer in a volumetric receiver, followed by a discussion of the air flow distribution problem in Section 2.4, and the required convective heat transfer analysis in Section 2.5. The thermal processes involved in developing a performance model are described in Section 2.6. Section 2.7 includes a description of the analytical models used in previous studies.

## 2.1 COMPONENTS OF RECEIVER EFFICIENCY

A solar central receiver facility used to produce process heat has a thermal efficiency which is the product of five major subcomponent efficiencies. The subcomponent efficiencies are included in Equation 2.1.

$$\eta_{total} = \eta_{field} \times \eta_{intercept} \times \eta_{absorption} \times \eta_{thermal} \times \eta_{piping} \quad (2.1)$$

Each of the major subcomponent efficiencies will be described in the following sections. The field efficiency will not be discussed in detail because, for a given generic type of receiver, the field efficiency is independent of the specific design characteristics.

### 2.1.1 Field Efficiency

The field efficiency is the ratio of solar energy that is specularly reflected by the heliostat field minus atmospheric attenuation

to the solar energy striking the heliostat field. Field efficiency includes the impact of heliostat absorbitivity, diffuse reflection, and atmospheric attenuation of the resulting beam. Atmospheric attenuation is caused by absorption and scattering of solar radiation as it travels from the heliostat to the receiver. Atmospheric attenuation is occasionally included in the intercept efficiency. (Duffie and Beckman, 1974).

Field efficiency will vary between receiver types. A cavity receiver, which normally will have all heliostats located north of the receiver tower (North Field) will have a different efficiency than an open receiver which has heliostats located all around the receiver (surround field). Once the type of receiver is selected, the field efficiency is relatively insensitive to variations in receiver design features.

### 2.1.2 Intercept Efficiency

Intercept efficiency is the ratio of radiant energy striking the receiver absorbing surface to the energy specularly reflected from the field minus atmospheric attenuation. The intercept factor measures how much of the energy from the field is "intercepted" by the receiver. If we assume that a heliostat image is symetrical about its centerline and the receiver occupies the width from A to B, the intercept factor is defined as:

$$\eta_{intercept} = \frac{\int_{A}^{B} I(w)dw}{\int_{-\infty}^{\infty} I(w)dw} \qquad (2.2)$$

where I(w) is the image intensity as a function of the distance w from the centerline of the image (Duffie and Beckman, 1974). Often, design modifications which reduce thermal losses, such as a reduction in the aperture size of a cavity type geometric loss reducer (bringing A and B closer together) will result in an increase in intercept losses.

### 2.1.3 Receiver Absorpitivity

The receiver absorpitivity is a measure of the reflection losses from the receiver, and is given by the ratio of solar energy absorbed by the receiver to the solar energy striking the receiver absorbing surface. The receiver absorbitivity can be influenced by the optical properties of the absorbing surfaces (absorbitivity) and the geometric arrangement of the receiver (i.e., cavity type receiver).

### 2.1.4 Receiver Thermal Efficiency

The receiver thermal efficiency is given by the ratio of solar energy added to the product to the energy absorbed on the receiver surfaces. Thermal efficiency is also equal to:

$$\eta_{thermal} = \frac{Q_{absorbed} - Q_{reradiation} - Q_{convection} - Q_{conduction}}{Q_{absorbed}}$$

The components of thermal losses are related to different heat transfer mechanisms. Reradiation losses consist of energy that is transferred to the surrounding by radiation heat transfer. As the receiver surfaces increase in temperature they will radiate energy in

all directions. A fraction of this energy will leave the receiver and be lost. Convection losses consist of energy which is lost due to heating air which then leaves the receiver. Conduction losses are losses due to conduction through insulated surfaces. Energy lost by conduction ultimately leaves the receiver by convection to the surroundings. Reradiation and convection losses are much larger than conduction losses which can often be ignored.

### 2.1.5 Piping Losses

Piping losses consist solely of heat loss through the walls of the downcomer. Energy required to overcome pressure drop in the downcomer is not traditionally included in piping efficiency. Normally it is included as a parasitic power requirement which is calculated separately. A solar central receiver could have parasitic power requirements included with thermal efficiency if a Second Law effectiveness was used as the thermodynamic figure-of-merit but, in this report, the more traditional First Law approach will be used.

## 2.2 VOLUMETRIC RECEIVER CONCEPTS

While keeping the essential features of the volumetric receiver, the designer still has a great deal of freedom in selecting a volumetric receiver design. The designs selected for inclusion in this study do not exhaust the possible arrangement but probably are representative of the concept. The discussion of design alternatives is

included at this point in order to facilitate the discussion of thermal processes.

The two key design decisions are the selection of the geometric loss reduction techniques and the absorbing media. Two types of absorbing media were considered, fins and small fibers. Two fin designs were included in the study; radial fins and staggered fins. These designs are shown in Figure 2.1. Two fiber concepts were considered, one with fixed fibers and a second with augmented convection. The convection augmentation can be obtained either by rotating a fraction of the fibers or by inducing tangental air flow with a preswirl. These designs are also shown in Figure 2.1.

Two geometric loss reduction techniques were considered. The first involved using wedge-shaped reflecting pins arranged to form the external surface of the receiver. The second geometric loss reduction technique involved locating the absorbing surfaces in a shroud or cavity. The two geometric loss reduction techniques are shown in Figure 2.2. In addition, there is the option of not including any type of geometric loss reduction.

The combination of four absorbing media options and three geometric loss reduction options results in 12 possible designs. In order to limit the scope of the study, PNL selected five designs for evaluation. These are presented in Table 2.1.

After completion of the convective heat transfer study, it was obvious that the convective heat transfer coefficient between all fin designs and the air was very low, resulting in an extremely large and

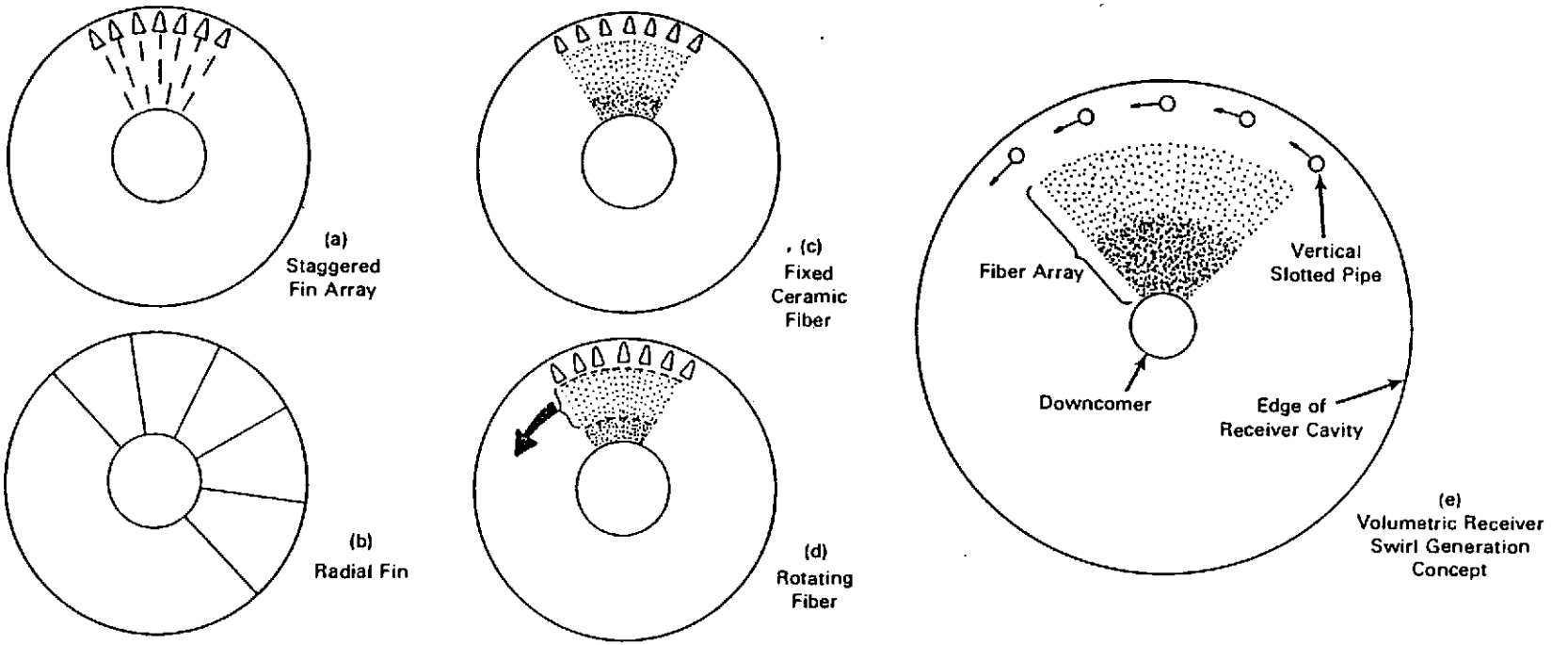


Figure 2.1. Volumetric receiver designs

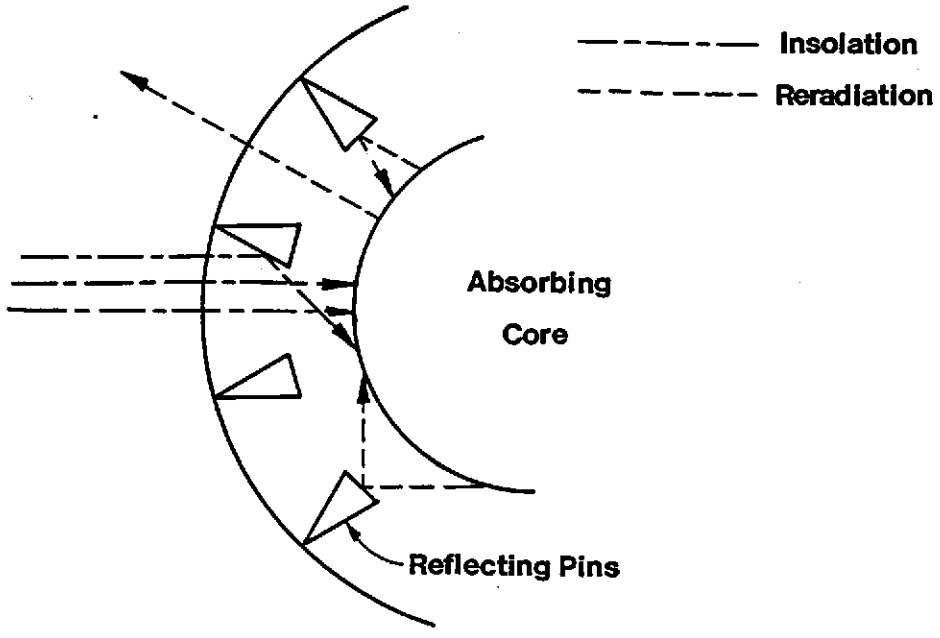


Reflecting Zone Concept

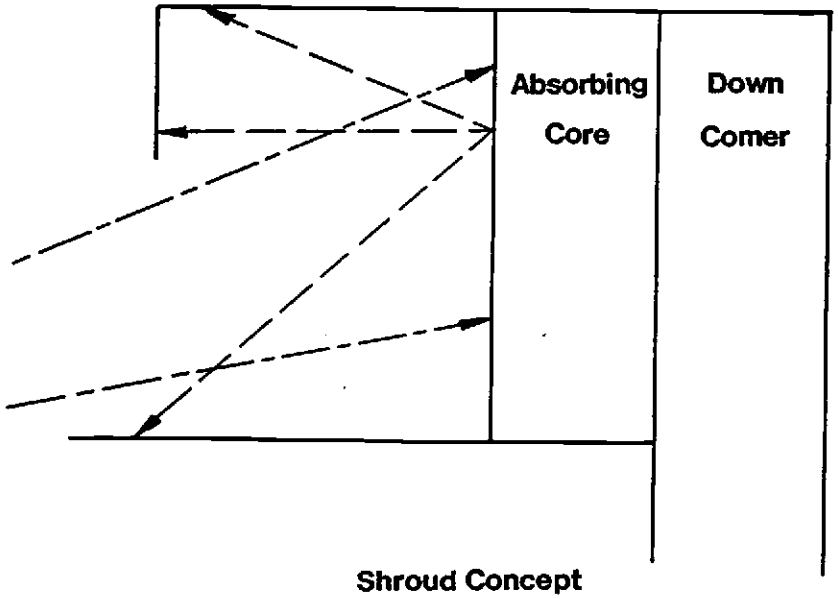


Shroud Concept

Figure 2.2. Geometric loss reducer

Table 2.1.

Volumetric Receiver Design Options

| Case | Geometric Loss Reduction Technique | Absorbing Media |
|---|---|---|
| 1 | Shroud | Radial fin |
| 2 | Shroud | Staggered fin |
| 3 | Shroud | Non augmented fiber |
| 4 | Reflecting zone | Fiber with preswirl |
| 5 | Shroud | Fiber with preswirl |

inefficient receiver, therefore the designs with fins were not studied in the same detail as options 4 and 5 but were included for completeness. The non augmented fiber design also proved to be unattractive and was not evaluated in detail. The development of the analytical model included the requirement that the model must be sufficiently flexible to analyze all five generic concepts.

## 2.3 RADIATION HEAT TRANSFER

Radiation heat transfer is involved in both the distribution of insolation and the internal radiation heat transfer between zones. These are related but distinct problems and will be discussed separately. First, the characteristics of the insolation will be described.

### 2.3.1 Properties of Insolation

The insolation striking the receiver is composed of a large number of heliostat images. Each heliostat redirects the sun's radiation onto the receiver forming an image. The minimum image size is determined by the size of the solar disk, the distance from the heliostat to the receiver and the receiver orientation. The minimum image size (w) for a heliostat with a slant distance from the receiver of r is given in Equation 2.3 (Duffie and Beckman, 1974).

$$w = 2r \tan 16' \tag{2.3}$$

The theoretical image size can be increased by a variety of imperfections in the collector field including small-scale errors in the reflector surface, microscopic errors in the reflecting surface, and beam scattering caused by atmospheric particulate. These combine to cause the actual image to exceed the minimum image size. An approximate estimate of actual image size is given by Equation 2.4 (personal communication with Sandia).

$$w = .012r \tag{2.4}$$

As part of this study PNL investigated the properties of a heliostat image. The results indicated that the image can be considered as a circle and that the distribution of energy in the image can be assumed to be Gaussian relative to the centerline of the image.

If the image is larger than the absorbing surface of the receiver, or if the heliostat is not properly aimed then a fraction of

the energy in the image will miss the receiver's absorbing surface. This intercept loss can be significant, particularly for a shroud design where the aperture area is substantially smaller than the area of the absorber.

Intercept losses can also be increased by aiming strategies which are used to uniformly distribute energy on the receiver. Given that the energy distribution in the heliostat image is Gaussian, the consequence of aiming all heliostats at one point would be a peak flux 230% greater than the average flux, therefore multiple aiming points are often used. This may result in the heliostat image being purposely aimed at a point closer to the edge of the receiver than apparently necessary, causing an increase in intercept losses. The distribution of solar energy on the absorbing surface may be further complicated by a shroud or cavity type enclosure. In these designs the heliostat image must pass through the aperture in addition to satisfying requirements for even flux distribution on the absorbing surface.

In a typical heliostat field, heliostats will be located over a large area. For a facility producing 50 $MW_t$, the closest heliostat to the tower may be 80 m away from the centerline of the tower while the most distance heliostat may be 500 m away, with the typical heliostat being located approximately 400 m away. This produces a wide variation in image sizes and incident angles in the vertical direction on the receiver. Figure 2.3 shows the variations in incident angle and image size for a hypothetical 50 $MW_t$-field.

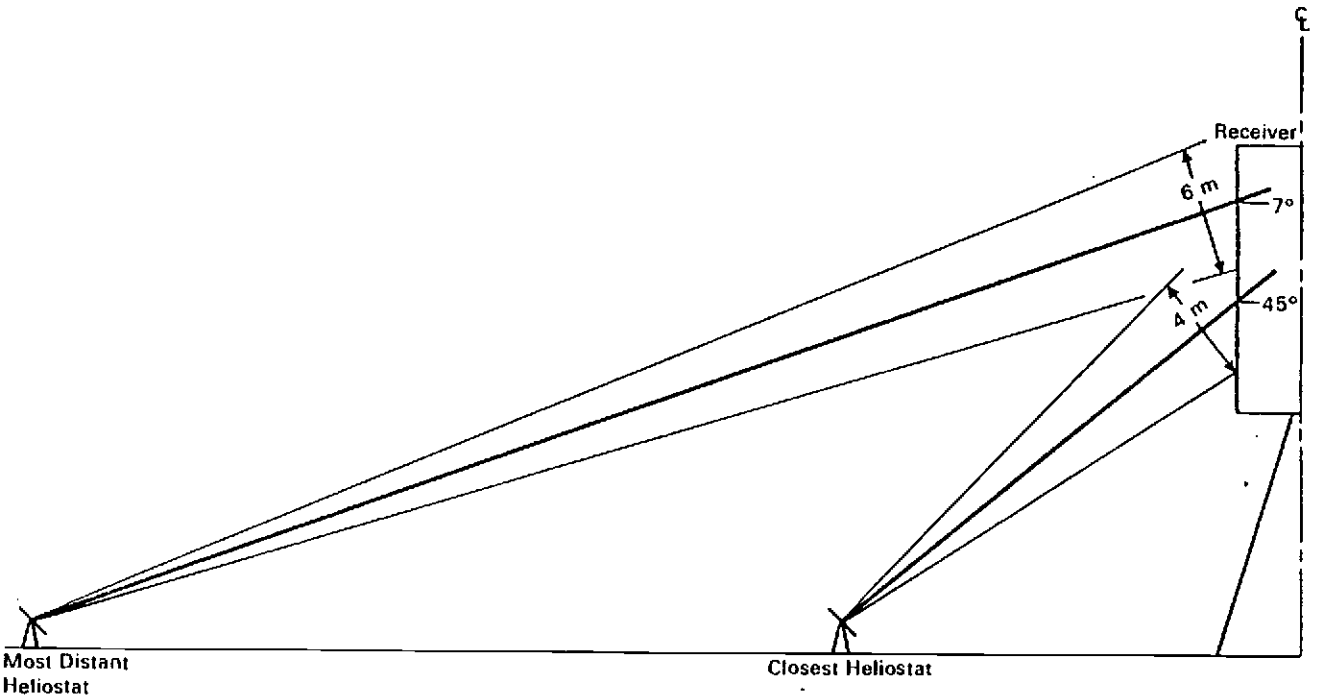


Figure 2.3. Heliostat images

Volumetric receiver performance is sensitive to the incident angle of the insolation in the circumferential direction. The reflecting pin designs are particularly sensitive. As Figure 2.4 shows, radiation entering a typical reflecting pin cell will tend to be absorbed or reflected out to the surroundings if the incident angle is very large. As with the energy distribution in a heliostat image, the incident angle will have a Gaussian distribution. The standard deviation of the incident angle distribution is related to the standard deviation of the heliostat flux distribution. Defining the image width as the image diameter which contains 97% of the energy in the image, one-half of the image width now equals the standard deviation ($\sigma$) of the image distribution. Figure 2.5 shows how the standard deviation of the incident angle distribution depends on receiver radius and image width (2 $\sigma$). The standard deviation for the incident angle distribution is given in Equation 2.5.

$$\sigma_{\alpha} = \sin (\sigma_{image}/R) \tag{2.5}$$

With the standard deviation known, and assuming Gaussian distribution, the incident angle distribution can be calculated.

Insolation is solar radiation and will have a spectral distribution approximated by black body radiation from a surface at 6000K (Seigel and Howell, 1972, Duffie and Beckman, 1974). In general, all receiver surfaces were assumed to be gray so that the spectral distribution of the insolation did not affect the analysis.

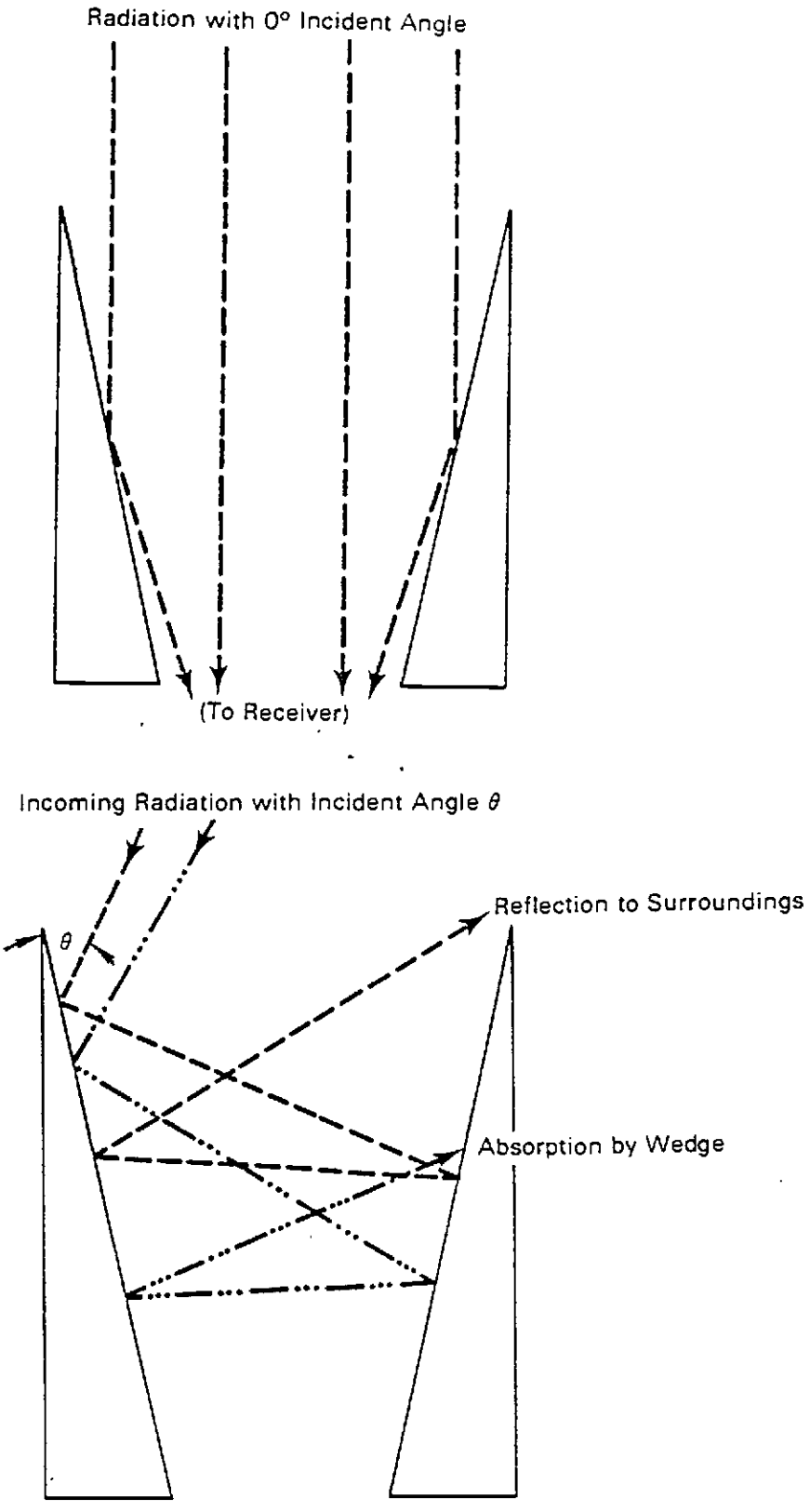


Figure 2.4. Impact of incident angle distribution

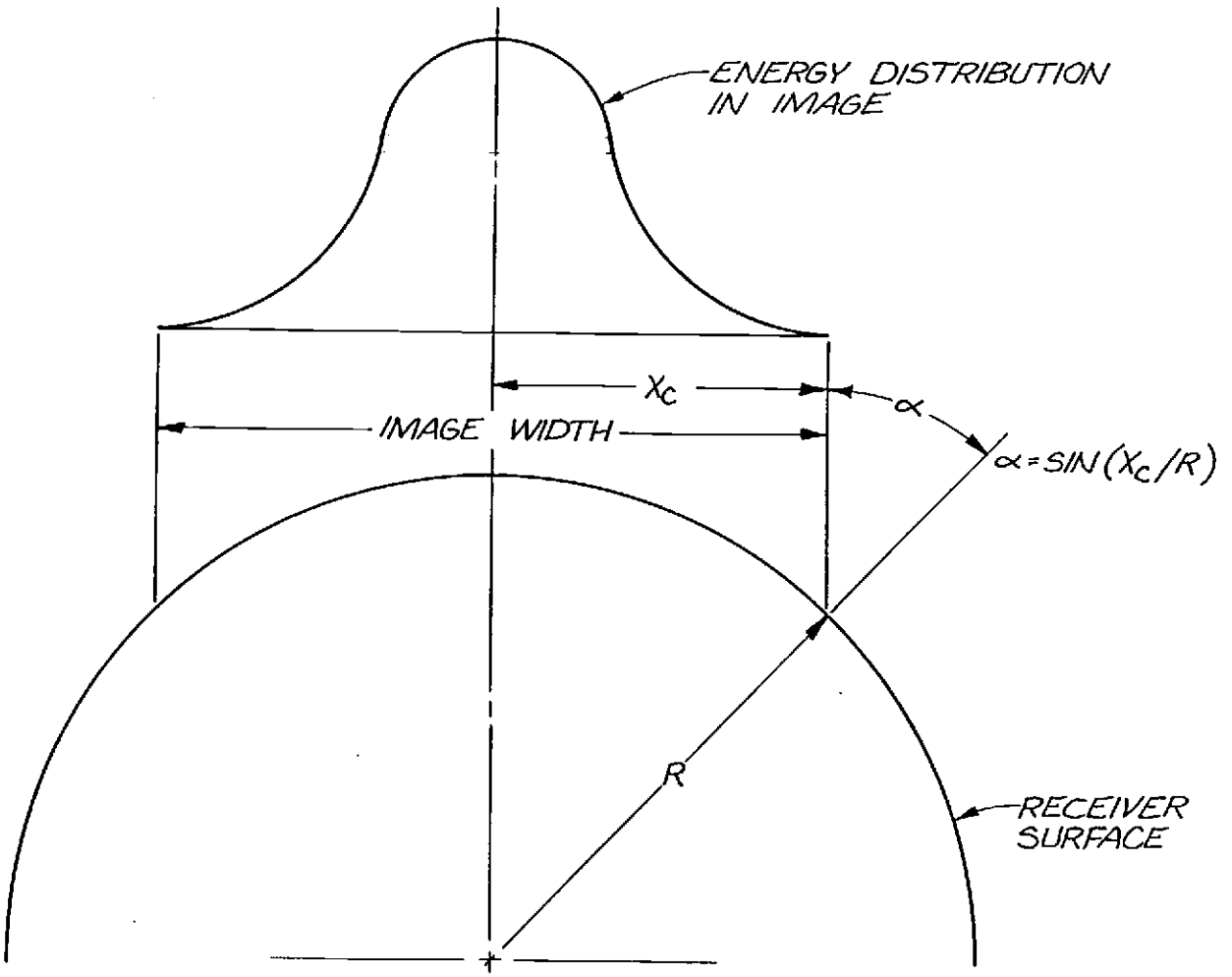


Figure 2.5. Modeling the distribution of incident energy on receiver

### 2.3.2 Insolation Absorption for Reflecting Zone Designs

The factors affecting insolation absorption in a volumetric receiver can best be described by following a hypothetical photon as it interacts with the receiver surfaces. The photon enters the receiver and can either pass through the row of reflecting pins without striking a surface or it may hit a reflecting pin. When the photon strikes the surface of the reflecting pin, there are several possible results, the photon may be absorbed, specularly reflected, or diffusely reflected. The dividing line between diffuse reflection and specular reflection is to some extent arbitrary, but in general a specularly reflected photon will have a reflection angle approaching the incident angle. The reflecting zone surface is selected to have a low absorbitivity and high specularity so we assume that our photon is reflected into the receiver. The photon will move into the receiver until it strikes an absorbing surface, where the photon is most likely absorbed due to the high absorptivity of these surfaces. If the photon is reflected it may move deeper into the receiver or it may move towards the outer surface and may actually leave the receiver, in which case the photon would contribute to reflection losses. The photon will continue striking surfaces and being reflected until it is either absorbed or reflected out of the receiver.

The results of a surface/photon interaction will depend on the optical properties of the surface. In general, the surface properties such as absorpitivity, emissivity, and specularity will depend on characteristics of the surface such as its temperature and surface

conditions; and on the characteristics of the incident radiation, particularly incident angle and spectral distribution (Siegel and Howell, 1972).

In addition to surface interactions, the photon could interact with the air in the receiver. This effect is normally ignored in receiver analysis as was done in this study, but the impact may not be negligible (Clausing, 1981).

The impact of the incident angle distribution is obvious. Any deviation from a normal angle of incidence will reduce the depth of penetration of a photon into the receiver. As the angle of incidence increases, a photon will tend to strike the reflecting pins and be reflected back and forth between the pins until it is absorbed or reflected out of the receiver. At a sufficiently large incident angle insolation will be either completely absorbed on the reflecting pins or reflected out of the receiver with none of the insolation penetrating into the receiver.

### 2.3.3 Insolation Absorption for Shroud Designs

A photon entering a shroud design will experience a slightly different set of interactions. First the photon must enter the receiver through the aperture of the enclosure without actually striking it, in which case it would be an intercept loss. Once inside the receiver the photon must actually strike the absorbing surfaces. There is the possibility that a photon may enter the shroud and miss the absorbing surfaces. There is also the possibili-

ty that a photon may enter the shroud, miss the absorbing surfaces or pass through the absorbing surfaces and leave the receiver. When the photon strikes the first absorbing surface, it will probably be absorbed but, if the photon is reflected in the outward direction, the photon may either leave the receiver or be absorbed on the shroud. The shroud is insulated on the outside therefore the internal surface will be heated by the photons reflected or reradiated from the absorbing core. These interior shroud surfaces will then transfer some energy by convection to the air entering the receiver or may radiate energy back to the absorbing array. In either case energy absorbed on the shroud is not necessarily lost to ambient. Once a photon enters the absorbing array its history will be similar for either a reflecting pin or shroud design.

The selection of aperture size is the critical decision in a shroud design. A large aperture will let most of the insolation enter the receiver and will simplify flux distribution on the absorbing surfaces but it will be relatively ineffective in blocking reflected radiation and reradiation from the absorbing array. A small aperture will have low reflection and reradiation losses but much of the insolation will strike the exterior surface of the shroud and become an intercept loss.

### 2.3.4 Internal Radiation Heat Transfer

As the various surfaces in the receiver absorb energy their temperatures will increase and they will begin to reradiate thermal

energy in all directions. Some of the energy will be absorbed by other receiver surfaces; a fraction will leave the receiver and be a reradiation loss. A given surface will both radiate energy and receive radiated energy from all other surfaces resulting in a net radiant energy loss or gain for the surface. Other phenomena such as convection to the air will be occurring at the same time. The interaction between two surfaces will involve radiation heat transfer by many paths. First, if the surfaces have an unobstructed view of each other, they may interact directly. Also radiation from one surface may reach another by specular or diffuse reflection off of any other or combination of other surfaces. Obviously, the calculation of internal radiation heat transfer is complicated but it can not be ignored because internal radiation heat transfer is a major mechanism whereby energy is transferred from the hot internal surfaces to the external surfaces. This results in a higher temperature for external surfaces and higher losses to the surroundings.

## 2.4 AIR FLOW

One unique feature of the volumetric receiver is that ambient air is drawn directly into the receiver. This has the advantage of making the absorbing array look like a counterflow heat exchanger with external surfaces having the lowest temperatures, but care must be taken to ensure proper air distribution. As the temperature of the various receiver surfaces increase, the major mechanism for removing energy from a surface is convection to the air. If air is

not distributed in a manner approximating the distribution of absorbed insolation, the radiant energy absorbed on a surface will not be removed sufficiently fast to prevent the surface from overheating. Therefore, air flow into the receiver must be distributed in both axial and circumferential directions.

If the receiver were at ambient temperature and an inlet manifold were not included, the air entering the receiver would be concentrated along the bottom of the absorbing array as shown in Figure 2.6. When the receiver is at operating temperature there will be a large variation in air density from the external rows to the internal rows. The buoyancy induced flows will tend to give the air a vertical velocity component. In addition, the inlet manifold will have orifices to distribute air in the desired manner.

The driving force for the air flow is the pressure difference caused by the induced-draft fan. Energy added to the air by the fan will be used to overcome drag caused by the receiver surfaces, inlet manifold, and downcomer, and to accelerate the air.

Air flow distribution in the circumferential direction should be tailored to meet the circumferential distribution of insolation which tends to be greatest on the north side of an open receiver and smallest on the south side. In addition, wind effects may cause circumferential variation in air flow distribution by causing a higher than average pressure at the stagnation point and a lower than average pressure on the downstream side of the receiver.

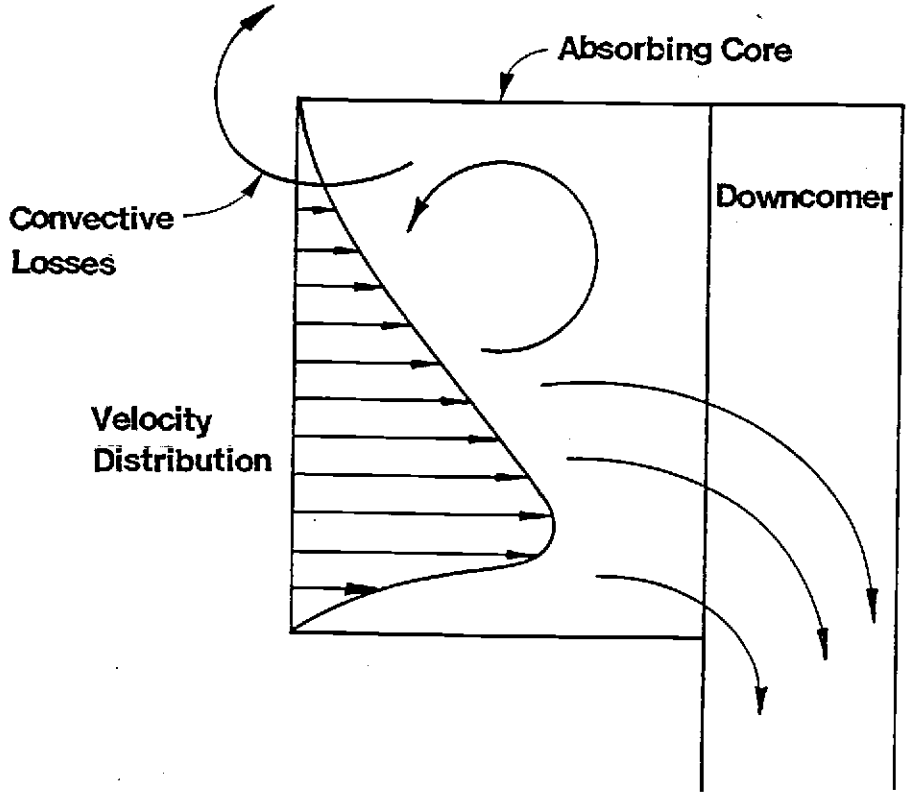


Figure 2.6. Air flow patterns

One aspect of internal air flow is of particular interest. As indicated above, buoyancy affects caused by large air density variation will cause the air to rise in the receiver. When air reaches the receiver roof, most will be drawn into the receiver but some will recirculate and leave the receiver. The energy used to heat the exiting air is considered a convection loss. This process is shown in Figure 2.6.

Two methods for augmenting convection between the fibers and the air were considered in this study, both involved specific air flow problems. The preswirl concept consists of providing the incoming air with tangential momentum and allowing conservation of angular momentum to increase the tangential velocity as the air moves into the receiver. The major air flow problem involves calculating the relative fiber/air velocity as a function of receiver location and in determining the most attractive method of providing the initial angular velocity.

The rotating fiber design adds another complicating factor to the air flow analysis. The purpose of rotating the fibers is to increase the relative velocity between the fibers and the air in order to increase convection but as the fibers rotate through the air the resulting drag will accelerate the air in the circumferential direction. Once the air has a circumferential velocity, density variations and conservation of angular momentum will tend to further accelerate the air in the circumferential direction. Air velocity in the circumferential direction will reduce the relative velocity

between the fibers and air thereby reducing the convective heat transfer.

## 2.5 CONVECTION

As the absorbing surfaces receive insolation they will increase in temperature until the net radiation heat transfer to other surfaces and convection to the air is equal to the insolation absorbed on the surface. Convection to the air is the most significant mechanism for removing heat from the surfaces and, therefore, to a great extent determines the equilibrium temperature of the surfaces. A high convective heat transfer coefficient is desired because this leads to the lowest temperature difference between the absorbing surfaces and the air. Two general types of absorbing surfaces are included in the study, fins and ceramic fibers, and each required a separate set of convective heat transfer correlations.

The fins involve flow past relatively large flat plates. There might be few large plates or many staggered smaller plates. Air flow velocities can range from approximately .1 m/s to 10 m/s. In the low velocity cases, natural convection can be the dominant heat transfer mechanism. With higher velocities, mixed forced and natural convection can be encountered. As the air velocity further increases, forced convection will dominate. In addition, entrance effects and heat transfer enhancement techniques can be significant.

The second type of absorbing surface considered in the study is a small diameter ceramic fiber. Due to the small diameter (1 mm) of

the fibers, the predominant mode of heat transfer is forced convection. In some cases, surface roughening can be significant.

## 2.6 RECEIVER THERMAL PERFORMANCE

The receiver thermal performance is best described by the receiver thermal efficiency which includes the impact of convective losses, conduction losses and reradiation. All of these loss mechanisms are a function of the receiver equilibrium temperature distribution.

If the volumetric receiver is exposed to constant insolation, receiver surfaces will increase in temperature until all surfaces are in thermal equilibrium. The equilibrium temperature of a given surface is that at which the energy absorbed on the surface from insolation and radiation from higher temperature surfaces just equals convection to the air and radiation to both cooler surfaces and ambient. For a given surface in the receiver, its equilibrium temperature is coupled by radiation heat transfer to all other surfaces which interact with the surface, and by convection to the air flowing past the surface whose temperature must be known.

With the receiver at equilibrium each surface will be reradiating to the surrounding (reradiation losses) and some fraction of the heated air will leave the receiver (convection losses). These losses, in addition to the negligible conduction losses will reduce the energy available for heating the air. One major goal of the receiver design is to minimize the thermal losses thereby allowing

more of the energy absorbed on the receiver to be used to heat product air.

A second factor in receiver performance is the parasitic power requirement. Fan power must be used to overcome pressure drop in the receiver absorbing array and inlet manifold. Designs with a rotating fiber array also require power to rotate the array. Parasitic power is used to overcome drag on the fiber and friction associated with the rotating mechanism. Preswirl designs require parasitic power to run the fans that give the air its initial tangential momentum.

In addition to operation at the nominal design point, two special cases are important; emergency conditions and daily flux variations.

With the receiver at its design temperature, equipment malfunctions can cause significant safety problems. The first type of occurrence would be a dramatic increase in the local insolation flux. This would cause an increase in local material temperatures until the new higher rate of absorption of insolation can be balanced by an increase in convection and radiation from the surface. If the resulting temperature is above the maximum material temperature damage to the receiver can result. A second emergency condition would result from a loss of power to induce air flow or rotation, this would result in a decrease in convection from the absorbing surfaces with an accompanying increase in material temperature.

During the day the amount of radiation striking the heliostat field will vary which causes the amount of energy available to the

receiver to change with time. It is normally assumed that the product temperature must remain constant so the receiver equilibrium temperature distribution will remain approximately constant, therefore, the magnitude of receiver losses is relatively constant. This results in efficiency varying throughout the day with the highest efficiency occurring during periods of high insolation and with efficiency dropping as the insolation decreases.

## 2.7 ANALYTICAL MODELS USED IN PREVIOUS STUDIES

The two previous evaluations of receiver performance (Drost and Eyler 1980, Bird et al., 1982) used simple analytical models to evaluate receiver thermal processes. The analytical models described in Sections 3, 4, and 5 were to some extent influenced by the earlier models, therefore, these will be briefly discussed before proceeding with detailed descriptions of the analytical models.

Absorbed insolation distribution and reflection losses were calculated in Drost and Eyler (Drost and Eyler, 1980) and Bird et al. (Bird et al., 1982), using the same optical model. The receiver was divided into cylindrical zones each with specified optical properties. A ray of insolation was followed as it entered the first (external) zone and subsequently passed into the second zone. All possible reflection, absorption and transmission interactions were analyzed. The results were four equations which predicted the absorption of energy in both zones, the reflection losses and the transmission through the two zones. The equations were in the form

of infinite series but calculations showed that only a few terms needed to be evaluated. The equations are presented in Bird et al. (Bird et al., 1982). After analyzing the first two zones, these were then modeled as one zone with composite zone properties and the process was repeated with the first two zones combined together as zone one and the third zone being the second zone for the optical analysis. This was repeated until all zones were analyzed. The results included both reflection losses and the distribution of absorbed energy. While this method was developed independently, subsequent literature review indicated that Viskanta et al. (Viskante et al., 1978) developed a similar method for analyzing multiple cover glass flat plate collectors.

The calculation of a zone's optical properties required several simplifying assumptions, one of which proved to be inaccurate and caused a substantial overestimate of receiver performance. The transmissivity of a zone was assumed to be equal to the fraction of the area of a right circular cylinder which did not contain pin material. The zone absorbitivity was calculated as the product of the surface emissivity and 1.0 minus the zone transmissivity (Bird et al., 1982). These two calculations assume that insolation is radially directed and that the surfaces in a given zone will only absorb insolation on the projected areas as seen from the outside of the receiver. Actual insolation will have a distribution of incoming angles rather than be radially directed. This results in radiation being absorbed more rapidly than was estimated in Drost and Eyler

(Drost and Eyler, 1981) and Bird et al. (Bird et al., 1982). The weakness of this assumption was identified and included in the areas of concern discussed by Bird et al. (Bird et al., 1982).

The impact of internal reradiation was briefly considered in Drost and Eyler (Drost and Eyler, 1981), but was neglected in Bird et al. (Bird et al., 1982). The difficulty in calculating view factors combined with the assumption of negligible internal radiation heat transfer resulted in the deletion of any analysis of internal radiation heat transfer. As indicated in Section 2.3.4 internal radiation heat transfer is a major factor in determining the receiver temperature profile.

Air flow was modeled in Drost and Eyler (Drost and Eyler, 1981) using the TEMPEST computer code developed at PNL. The results indicated that air flow distribution could be a problem and that thought must be given to the design of the inlet manifold.

Material temperatures were calculated by determining the temperature difference between the air and the receiver surfaces required to transfer the energy absorped on the surfaces to the air. This calculation depends on knowing the convective heat transfer coefficient. In Bird et al. (Bird et al., 1982), the convective heat transfer coefficient was modeled as convection between a duct and air with a multiplier to include the impact of mixed forced and natural convection. Subsequent investigations showed that this model overestimated the convective heat transfer coefficient.

Reradiation losses were used in Equation 2.6.

$$Q_{reradiation} = \sum_{j=1}^{n} A\sigma\varepsilon F_{j-0} \left(T_j^4 - T_o^4\right) \qquad (2.6)$$

The question of the proper emission area and view factor was not adequately addressed because of the extreme difficulty in estimating view factors analytically for complicated geometries.

Convection losses from the receiver were estimated by modeling the receiver as a right circular cylinder in cross flow at the external zone temperature. This approach ignored the impact of having air drawn into the receiver.

The early studies of the volumetric receiver were preliminary investigations conducted with limited resources, therefore, simplifying assumptions and uncomplicated models were appropriate. A design study requires a more accurate and justifiable analytical model of the volumetric receiver thermal processes.

# CHAPTER 3

## RADIATION HEAT TRANSFER MODEL

Much of the attractiveness of the volumetric receiver depends on the effect of the unusual geometry on radiation absorption and heat transfer. The receiver absorbing rows are placed so that high-temperature surfaces will be in the interior of the receiver reducing reradiation and reflection losses from the receiver. The reflecting rows or shroud also reduce radiation losses by acting as a "light valve" allowing insolation to enter the receiver but inhibiting reflected or reradiated energy from leaving the receiver interior. These two features can substantially reduce receiver thermal losses, but in order to have any confidence in the predicted results an accurate method of calculating radiation heat transfer must be available. Section 3.1 discusses the details of the problem and the possible solutions. Section 3.2 presents a background overview of Monte Carlo modeling, while Section 3.3 describes the details of the specialized Monte Carlo code developed for volumetric receivers. Section 3.4 discusses the exchange factor model while Section 3.5 presents the absorbed insolation distribution model. The comparison of code results with experimental results is discussed in Section 3.6. A discussion of the impact of sample size on the results is included in Section 3.7. Two computer codes using the Monte Carlo technique were developed, the VORRUM code for calculating absorbed insolation distribution and the VOREFM computer code for calculating

exchange factors. The details of these codes are presented in Appendices B and C.

## 3.1 INTRODUCTION

Radiation heat transfer analysis can be quite challenging, particularly when a large number of surfaces with nonideal optical properties are considered. The analytical techniques available for radiation heat transfer vary widely in required effort, limiting assumptions, and accuracy. This section will describe the particular problem and discuss the reasoning used in selecting Monte Carlo modeling as the preferred approach.

### 3.1.1 Problem

To realize the benefits of a volumetric receiver design the concept must be optimized. This requires that a given receiver arrangement be analyzed for radiative heat transfer with the results then used in a thermal and fluid dynamics analysis to predict receiver performance. With the receiver performance estimated, receiver capital costs and levelized energy costs can be estimated. The procedure will be repeated until an attractive design is identified. The radiation heat transfer analysis is required for all succeeding calculations. In particular, the following information is required:

1. Distribution of Absorbed Insolation - As insolation strikes the receiver it will pass through the reflect-

ing zones or shroud with a fraction being absorbed or reflected and then enter the absorbing zones where the remaining radiation is absorbed. The radiation analysis must be able to predict where insolation is absorbed in the receiver as a function of receiver geometry, surface properties, and insolation characteristics. This analysis should also predict reflection losses from the external surfaces.

2. Thermal Radiation Exchange Factors - The radiation analysis must also predict radiation interaction between different receiver surfaces and interactions between surfaces and the surroundings. Radiation heat transfer between receiver surfaces and the surrounding represents a loss; therefore, this quantity is of particular importance. The actual radiation heat transfer between surfaces cannot be calculated at this state of the design process because surface temperatures are not known. Instead, this analysis will calculate an exchange factor between surfaces which will allow the calculation of radiation heat transfer at the appropriate phase of the design process.

The radiation heat transfer analysis is particularly complicated because of the large number of surfaces involved - approximately 50 for a symmetrical section of a fin type receiver, and many hundreds for a fiber type receiver (each with four surfaces) and the impor-

tance of including directional surface properties and possibly spectral properties.

### 3.1.2 Radiation Heat Transfer Modeling

The efforts of many investigators have resulted in the development of a variety of methods for analyzing radiation heat transfer problems. A literature review identified two generic types of analyses appropriate for modeling the radiation heat transfer in a volumetric receiver. The first method would model the radiation between individual receiver surfaces while the second would model the receiver absorbing surfaces as an emitting or absorbing gas without individual surfaces being identified. The fin-type receiver geometries clearly could not be modeled as an absorbing and emitting gas because this model would not give results with the level of detail required. In addition, a fin array exhibits strongly anisotropic properties which would further complicate any analysis. A fiber receiver could be modeled as an absorbing emitting gas due to the large number of small surfaces.

#### 3.1.2.1 Fin Type Receiver Radiation Modeling

The key problem in modeling discrete surfaces is in predicting the view factor or exchange factor between surfaces. Emery et al. (Emery et al., 1981) identified seven methods for predicting view factors. They concluded that for complicated configurations only numerical methods are appropriate, particularly for cases with

partially obstructed views, which is the case for the volumetric receiver. Of the four numerical approaches, they concluded that a Monte Carlo approach is best suited to the determination of view factors between a single small area and surrounding areas. This is normally the situation encountered in the volumetric receiver where we are interested in radiation heat transfer for either a small fin or a small symmetric section of the receiver exterior boundary. Monte Carlo modeling has the added advantage of allowing the inclusion of non-diffuse non-gray surfaces with relative ease (Siegel and Howell, 1972; Howell, 1968; Toor and Viskanta, 1968).

With the selection of Monte Carlo modeling, there were still two possible approaches; a general Monte Carlo computer code could be acquired, or a specialized Monte Carlo computer code optimized for a volumetric receiver could be developed. A variety of generalized Monte Carlo photon and neutron transport codes (Halbleib, 1979; Los Alamos, 1978) and Monte Carlo radiation heat transfer codes exist (Corlett, 1966). In both cases the general applicability of these codes would be purchased at the price of substantial complexity. The resulting model would require excessive computer time particularly for use as a design tool where many geometric arrangements would have to be considered.

The selected method of modeling radiation heat transfer was to develop a specialized Monte Carlo computer code designed to take advantage of the regular geometry of the volumetric receiver in order

to reduce computer time thereby increasing the scope of possible investigations.

#### 3.1.2.2 Fiber Type Receiver Radiation Modeling

The fiber type receiver could be modeled as an absorbing emitting medium and evaluated using either analytical techniques such as analytic solutions of the equation of transport or zoning methods (Siegel and Howell, 1972), but all analytical methods ultimately depend on having an estimate of the attenuation and scattering caused by the fibers. This information can only be developed by either Monte Carlo modeling or experiment.

Monte Carlo modeling can either use specified surfaces with a fixed location or use a statistical method to determine the location of an event. The first method is similar to the method selected for analyzing the fin designs. The second method has been used by a number of authors to investigate radiation heat transfer in packed beds (Yang, 1981), and participating media (Mishkin and Kowalski, 1983). This approach was attractive but was finally rejected because it would require the development of a second Monte Carlo code, therefore, one Monte Carlo approach, using discrete fixed surfaces was selected for both fin and fiber designs.

## 3.2 MONTE CARLO MODELING

The Monte Carlo approach to radiation heat transfer problems has been widely used and the method is well documented (Siegel and

Howell, 1972; Toor and Viskanta, 1968; Weiner et al., 1965). In this section the Monte Carlo method will be briefly described. The specific model used for analyzing the volumetric receiver will be described in Section 3.3.

The Monte Carlo approach is a statistical method of solving a physical problem which can be modeled as a series of probabilistic and deterministic events. Energy emitted from a surface is simulated by a large number of energy bundles. The emitted bundles are followed as they proceed from one event to another with the results of each event being recorded until the energy bundles either leave the receiver or are absorbed on a surface. A large number of bundles are simulated with the results of all events being totaled. A sufficiently large number of bundles must be considered to insure that variations in the results due to random events are small. The results can then be used to determine the fraction of the emitted energy which has been absorbed on each surface or has left the receiver.

The major problems with Monte Carlo modeling are those associated with geometrical considerations (which surface is struck by a bundle) and surface considerations (what happens when the surface is struck). Methods of modeling the interactions of a bundle with a surface are described by several authors (Siegel and Howell, 1972; Yang, 1981). When a photon strikes a surface the incident angle and wavelength are known. If surface properties such as absorptivity and specularity are known as a function of incident angle and wavelength

then the relevant optical properties can be calculated. If the bundle is totally or partially absorbed the energy reduction due to the interaction is added to the total for the surface. A totally or partly reflected photon bundle must have a reflection angle selected. If the reflection is specular, the angle of reflection equals the angle of incidence. For a diffuse reflection, the reflection angle is selected in such a way as to insure that there is an equal probability for reflection in any direction.

The problem associated with receiver geometry involves determining which surface is struck by a photon bundle once the bundle has been emitted. Many researchers have avoided this problem by selecting simple geometries. When complex geometries are considered (Corlett, 1966; Modest, 1968) the method consists of describing each surface mathematically and determining which surfaces intercept the vector describing the path of the energy bundle. The distance between the emission point and each intercepting surface is calculated. The closest intercepting surface is the surface impacted by the energy bundle. When a large number of surfaces are included the computational time associated with determining impact location becomes substantial.

The volumetric receiver includes an arrangement of pins in concentric cylindrical rows. The regular spacing of the pins and the arrangement into rows suggests that a more efficient method of determining impact location can be used. This approach consists of dividing the receiver into computational cells where the cells are

arranged so that absorbing surfaces are located on cell boundaries. This simplifies the identification of the impact location because one of the four surfaces in a cell is the emitting surface and only the three remaining cell boundaries can be struck by the emitted photon bundle.

## 3.3 ANALYTICAL MODEL

A typical receiver geometric arrangement is shown in Figure 3.1. The outer two rows consist of wedge shaped reflecting pins and the inner surfaces consist of fins or fibers. The receiver is now divided into zones and each zone is divided into cells. The cell boundaries are either the edge of a fin or the center line of a wedge-shaped pin. The photon bundle enters one cell of the external row, bounces around between the cell boundaries until it exits the cell, and moves into the next cell. Zone characteristics such as pin spacing, wedge angle and offset, which affect the movement of a photon bundle, are depicted in Figure 3.1.

The normal procedure is to identify a symmetric section of a receiver design. The boundaries of the section are assumed to be perfect specular reflecting surfaces. Figures 3.2 and 3.3 present this arrangement for both insolation distribution calculations and exchange factor calculations. Any photon bundle reaching the section boundary is reflected back into the receiver with a reflection angle equal to the incident angle. The use of a specular section boundary can be justified by symmetry. For each photon bundle which exits the

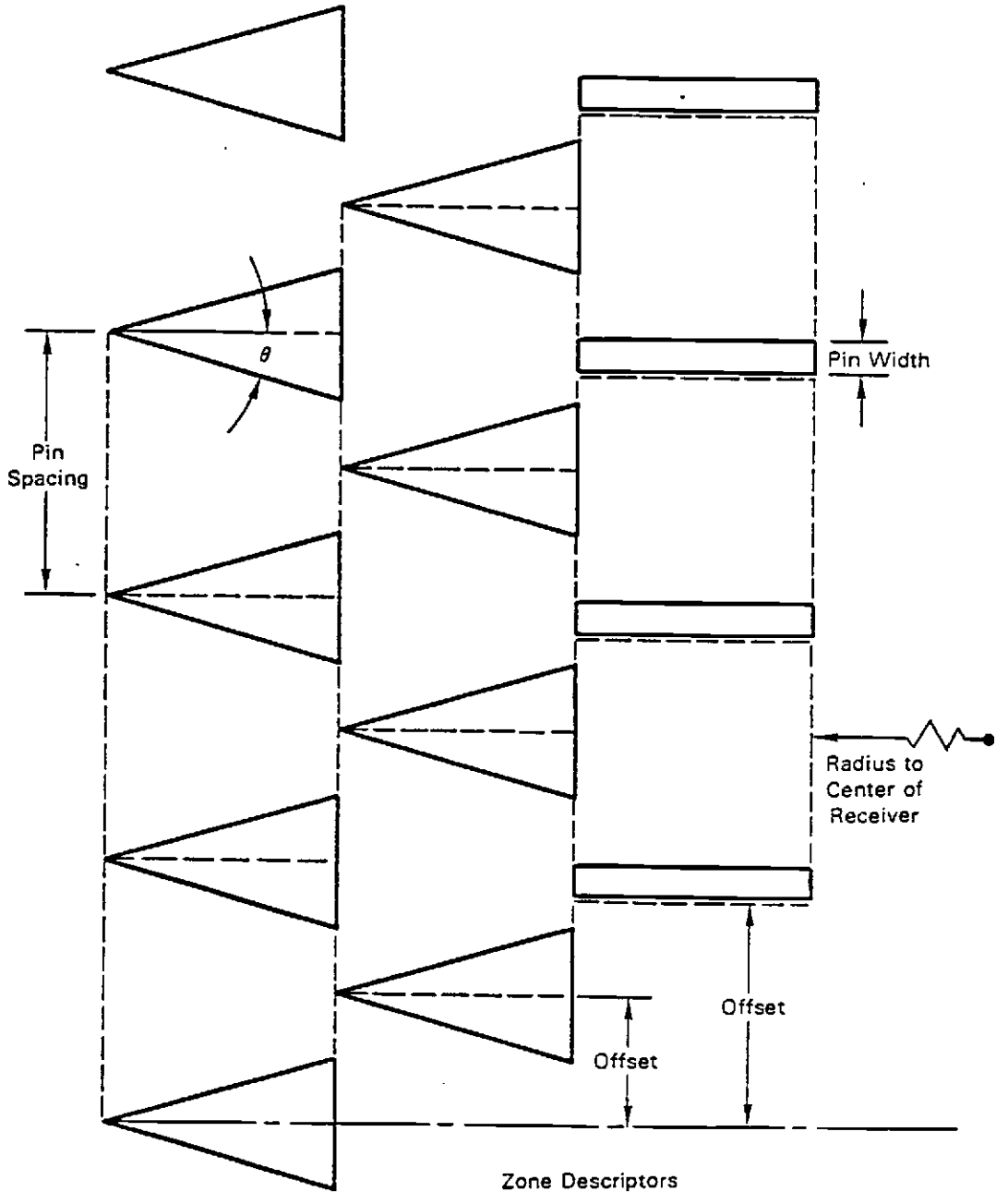


Figure 3.1. Definition of cell parameters

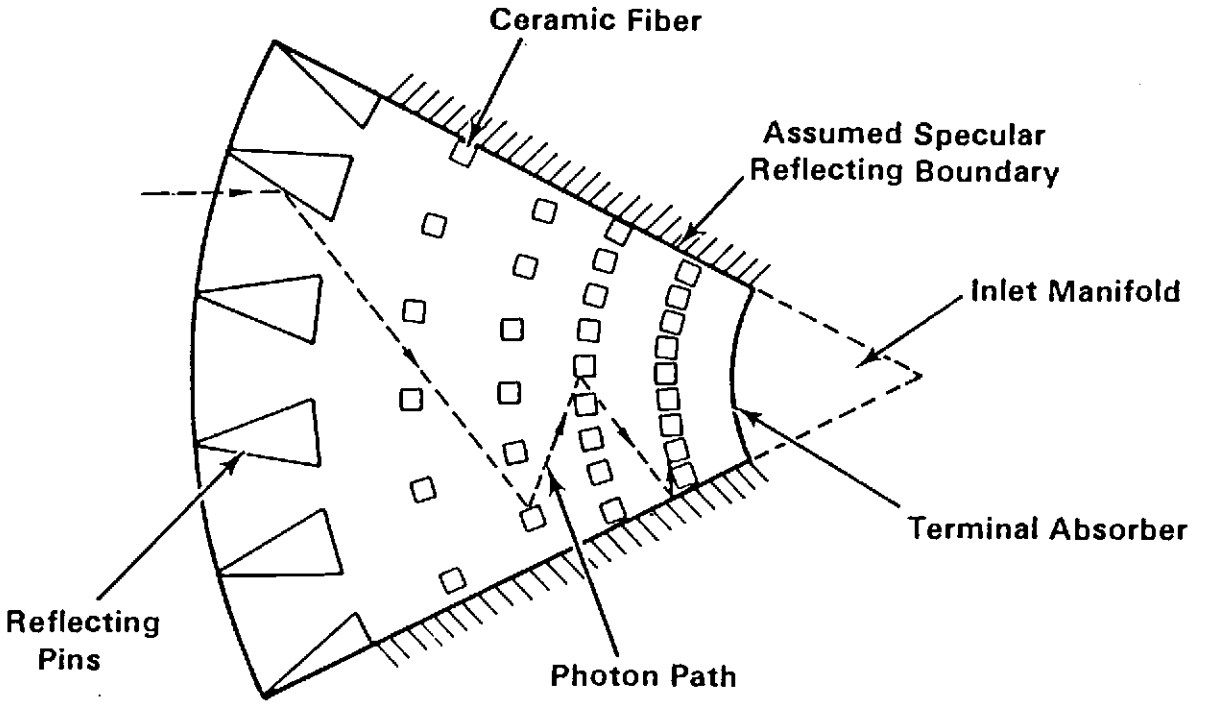


Figure 3.2. Monte Carlo model for insolation distribution

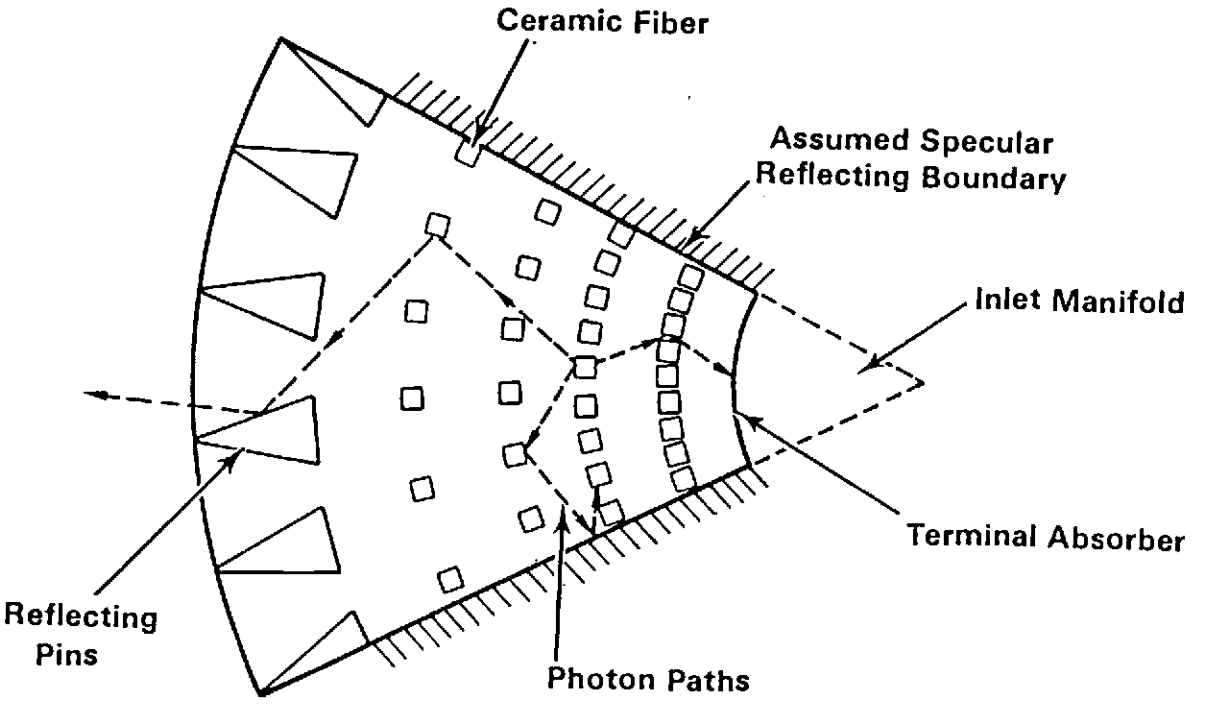


Figure 3.3. Monte Carlo model for exchange factor calculations

computational section, one photon bundle will enter from an adjoining section.

With the computational section defined, the emitting cell surface is identified. This will either be an external cell boundary, if insolation distribution is required or the surfaces of a typical fiber or fin, if exchange factors are required. In either case a large number of photon bundles are emitted from the surface of interest. The photon bundles are divided into NBATC batches each of which contains NPHOT photons bundles. After all batches have been simulated the mean and standard deviation of the NBATC results are calculated. The mean gives the nominal value for insolation distribution or exchange factor, and the standard deviation gives an indication of the statistical uncertainty in the mean value.

The Monte Carlo procedure can now be divided into three tasks; determination of photon original emission location, determination of the results of the interaction of a photon bundle and a cell, and calculation of cell-to-cell movement of a photon bundle.

### 3.3.1 Photon Bundle Emission

Photon bundles can be emitted at a variety of locations depending on the required information. If the distribution of absorbed insolation is desired then the photon bundles are originally emitted from the exterior cell boundary into an exterior cell. If the exchange factor is required from a surface, the photon bundles are emitted from the surface of interest. In either case the photon

bundles are followed until their energy drops below a minimum level or the bundle exits the receiver. Figure 3.2 presents the situation for calculation of insolation distribution while Figure 3.3 shows typical photon bundle histories for exchange factor calculations. Both Figures 3.2 and 3.3 show a typical fiber receiver layout with the fibers modeled as small rectangles. The surface area of the small rectangle equals the surface area of the cylindrical fiber with its specified fiber diameter. This section will discuss photon bundle emission for insolation-distribution calculation. Exchange factor calculations will be discussed in Section 3.4.

As discussed in Section 2.3.1, insolation will have an inlet angle distribution which is assumed to be Gaussian. The standard deviation of the insolation distribution can be calculated based on a heliostat image size and the radius of the receiver. The location of the point of emission is determined by dividing the emitting cell boundary into NICRM increment. NPHOT/NICRM photons are emitted from the center of each increment. The emission angle is determined from Yang. (Yang, 1981)

$$\alpha = \sqrt{2}\,\sigma\ \mathrm{erf}^{-1}\ (2R-1)$$

where $\alpha$ = emission angle

$\sigma$ = standard deviation of incident angle distribution

R = random number from 0.0 to 1.0

$\mathrm{erf}^{-1}$ = inverse error function

This function insures that the distribution of a large number of emission angles will approximate a Gaussian distribution with a standard deviation of $\sigma$.

### 3.3.2 Cell/Photon Interaction

In this section the method of analyzing the path of one photon bundle through a computational cell will be described. The algorithm for analyzing a single cell is applicable to a wide variety of cell shapes but the approach used in the present analysis is limited to:

1. straight line cell boundary
2. $\theta > 0.0$ where $\theta$ is the cell boundary wedge half angle
3. $\theta_{right} = \theta_{left}$
4. Gray surfaces (optical properties are not wavelength dependent)
5. 2 dimensions $(r,\theta)$
6. Regular fin or fiber spacing in a zone.

Once the emission point and angle are selected one photon bundle is emitted with an energy of 1.00 and the photon bundle history is determined until either the photon bundle leaves the cell or it is terminated due to its energy dropping below a minimum level. With the selection of the emission point, two angles are calculated, Beta-right and Beta-left (see Figure 3.4). If the emission angle is less than Beta-left, but greater than Beta-right, the photon bundle exits the cell through the opposing cell surface. If the emission angle

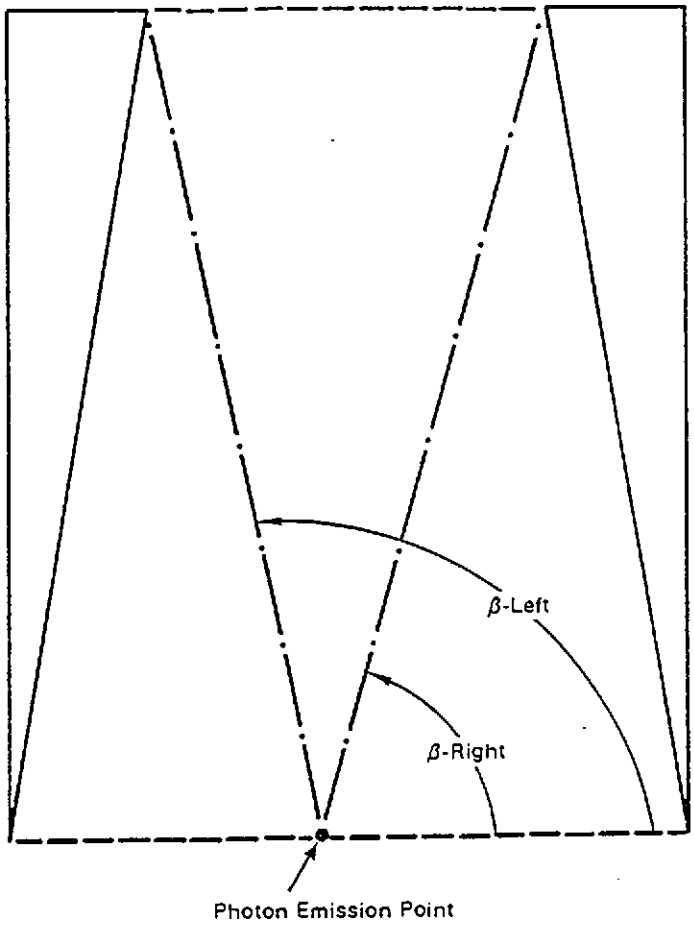


Figure 3.4. Cell Angle.

exceeds Beta-left, the photon bundle strikes the left wall. If the emission angle is less than Beta-right, the photon bundle strikes the right wall. A similar method was used by Howell and Bannerot in an evaluation of surface geometry modifications for the improvement of solar collectors (Howell and Bannerot, 1974).

Once the impacted surface has been determined, the location of the impact and the incident angle is determined by geometry. The energy of the photon is reduced by an amount equal to the product of its current energy level and the surface emissivity. The energy given up by the photon bundle is absorbed on the impacted surface.

At this point, the process is repeated with the impacted surface becoming the emitting surface and Beta-right and Beta-left being calculated based on the impact location. The surface is modeled as having both diffuse and specular reflection components. A random number is selected and, if it is less than the surface specularity, the photon is reflected specularly (emission angle equals reflective angle). Otherwise the photon is reflected diffusely where the emission angle equals cos (-1 + 2R) where R is a random number between 0.0 and 1.00. With the new emission location and angle selected, the procedure is repeated until the photon bundle energy drops below a minimum level or the photon bundle exits the cell. In either case the energy absorbed by each surface is recorded.

### 3.3.3 Cell-to-Cell Photon Transport

Photon bundles are originally emitted into a cell in the external row of pins (row 1). The procedure described in Section 3.3.2 is used to determine the photon history. If the photon history is not terminated due to absorption energy loss, the exiting surface, location, and angle are recorded. This information is used in a procedure which takes the exiting location, angle, and surface for the first cell and calculates in inlet location, angle, and surface for the next cell entered by the photon bundle. This process is repeated as the photon bundle moves from cell to cell through the receiver until the photon bundle either is terminated or exits the receiver (which is recorded as a reflection loss).

A row is described by the cell external pin spacing, the pin type (straight or wedge shaped), pin thickness or wedge angle, offset, and radius of the row based on the center line of the receiver. The offset indicates how the cells of one row are oriented relative to other rows. The significant parameters are shown in Figure 3.1. The location where an incoming bundle enters a cell is calculated from the exiting location of the adjacent donor cell. The total arc length from the datum to the exit location is calculated. This is used along with the appropriate dimension of the receiving cell to determine the inlet location. The inlet angle can be calculated directly from the outlet angle of the donor cell.

If the calculation of the exiting location indicates that the photon bundle strikes a pin tip a procedure similar to that described in Section 3.2 is followed. The photon bundle energy is reduced by an amount equal to the product of current photon bundle energy and the surface emissivity. If the current photon energy is still above the minimum level it will be reflected back into the donor cell. The entering location of the photon bundle will be the same as the previous exiting location but the angle of the photon bundle entering the original donor cell will depend on whether the pin tip was a specular or diffuse surface.

### 3.3.4 Surface Properties

It has been shown by previous investigators that direction-dependent properties can have a significant impact on radiation heat

transfer (Toor, 1967). The volumetric receiver design would be particularly sensitive to direction-dependent properties because many of the interactions take place at large incident angles. If the diffuse assumption is relaxed, it is now necessary to provide information on the incident angle dependence of emissivity, reflectivity, absorptivity, and specularity. Modest (Modest, 1978) makes the following assumptions concerning surface properties.

1. $\alpha'_\lambda, \varepsilon'_\lambda$ and $\rho'_\lambda$ are independent of temperature
2. for solar irradiation wavelengths (.1 μm < λ <2.5 m) spectral values for emissivity and absorptivity are correlated by

$$\varepsilon'_\lambda = \alpha'_\lambda = \varepsilon'_{\lambda,n}\left[1-\left(\frac{2\beta}{\pi}\right)^8\right] + \left[\varepsilon'_{\lambda,msx} - \varepsilon'_{\lambda,n}\right]\exp\left[\left(-\frac{30\beta}{\pi} - 7\right)^2\right] \quad (3.1)$$

3. for infrared wavelengths ($\lambda > 2.5$ μm) spectral values for emissivity and absorptivity can be calculated from

$$\varepsilon'_\lambda = \alpha'_\lambda = \varepsilon'_{\lambda,n}\left[1 - \left(\frac{2\beta}{\pi}\right)^{10}\right] + \left[\varepsilon'_{\lambda,msx} - \varepsilon'_{\lambda,n}\right]\left(\frac{2\beta}{\pi}\right)^2\left[1 - \left(\frac{2\beta}{\pi}\right)^2\right] \quad (3.2)$$

In addition, Modest suggests that the second term in Equation 3.1 can be dropped in order to decrease running time. Modest, in his study, was concerned with metallic specular reflecting surfaces such as silver-teflon which show an increase in emissivity with incident angle.

In this study, dielectric materials predominate, suggesting that the second term in Equation 3.1 can be deleted. As a check on this assumption, two reflecting row cases were was simulated; one using Equation 3.1 for surface properties and a second using Equation 3.1 without the second term. The small variation in results was not significant, therefore the second term in Equation 3.1 was deleted. The VORRUM model which deals with insolation distribution uses Equation 3.1. The VOREFM model which deals with radiation exchange at infrared wavelengths uses Equation 3.2.

## 3.4 EXCHANGE FACTOR CALCULATION

The exchange factors from one zone to all other zones are calculated by selecting a typical fin or fiber in the zone and emitting photon bundles from all four fin or fiber surfaces. The photon bundles are followed and their histories are noted. After a sufficiently large number have been simulated the resulting absorbed energy distribution gives the fraction of energy leaving the emitting surface which is subsequently absorbed on another surface; with this result, the exchange factor can be calculated from Equation 3.3 (Toor and Viskanta, 1968).

$$B_{ij} = \lim_{n_i \to \infty} (N_{i-j}/N_i) \qquad (3.3)$$

The significance of $B_{ij}$ and it's relationship to other radiation properties is discussed in Section 6.

The calculation of exchange factors follows the same procedure used in the determination of insolation distribution. A photon bundle is emitted into a cell and the interactions between the cell and the photon bundle are determined. If the energy level of the photon bundle has not dropped below the minimum energy level, the photon bundle will exit the cell and move into a new cell where it can interact with the cell boundaries. This procedure is continued until the photon bundle either exits the receiver or its energy level drops below the minimum amount.

The main difference between the insolation calculation and the exchange factor calculation is in the location of the initial emission. The point of emission for exchange factor calculations is determined by dividing a typical fin or fiber surface into increments and emitting photon bundles from the mid-point of each increment. The number of photon bundles emitted in each increment is based on the surface area of the increment relative to the total surface of the fin or fiber. The number of photons emitted from increment j is given by Equation 3.4.

$$NPHIM_j = \frac{NPHOT \times Area_j}{\sum_{j=1}^{n} Area_j} \qquad (3.4)$$

where $NPHIM_j$ = number of photon bundles emitted from increment j

$Area_j$ = surface area of increment j

NPHOT = number of photons emitted from fin or fiber

All emitting surface areas are assumed to be diffuse emitters. The selection of emission angle follows the same procedure used for selecting the angle for diffuse reflection described in Section 3.3.2.

This method for calculating exchange factors is based on the assumption that a zone consists of one row of fibers or fins and that there is a regular spacing between the fibers or fins. In addition, the geometric relationship between surfaces in any one row and all other rows must be constant in the circumferential direction. In this case a symmetry argument can be used to justify using one typical fin or fiber as the emitter because all fins or fibers in a given zone "see" the same geometric arrangement in all other zones. Those restrictions are met in all volumetric receiver designs with one exception - the staggered fin array - where the fins are packed more densely in the interior zones. This concept was not an attractive one and did not merit a more detailed evaluation so one "typical" fin was selected as the emitter accepting the fact that other fins in the same zone would "see" different geometric configurations. In fiber designs, simulations have shown that the emitting surfaces are so small compared to the spacing between zones that the relative arrangement of fibers in different zones as indicated by the OFSET parameters had no detectable effect on exchange factor calculations.

The calculation of a complete set of exchange factors for a receiver consists of taking one representative fiber or fin in each

zone and determining the exchange factors to all other zones. For a receiver with n zones this will require n Monte Carlo simulations and will produce an n + 1 by n + 1 matrix of exchange factors where the surroundings are now included as one zone. It is obvious that the calculations of exchange factors can make substantial demands on computing resources.

## 3.5 INSOLATION DISTRIBUTION CALCULATION

The calculation of insolation distribution is related to exchange factor calculations except the results consist of the exchange factors from ambient to the receiver surfaces. As with exchange factor calculations, the use of one typical emitting surface in calculating insolation distribution is based on the assumption of regular spacing between fins and fibers in a zone, and constant geometric relationships between surfaces in one row and all other rows.

The calculations of absorbed insolation distribution involves one Monte Carlo simulation. The results are the fraction of insolation absorbed in each of n zones and the fraction of energy exiting the receiver to the surroundings. The last result is the reflection loss from the receiver.

## 3.6 MODEL VERIFICATION

The Monte Carlo model described above was used as the basis for two computer codes. The VORRUM computer code calculated absorbed

insolation distribution while the VOREFM code calculated exchange factors. In order to develop confidence in the analytical model a variety of tests were conducted to verify the results. The verification of a Monte Carlo code is complicated due to the variation in results caused by the probabilistic processes included in the model, therefore three approaches were pursued: comparison with manual ray tracing, comparison with analytical results, and comparison with experimental results.

The first method consisted of comparing predicted photon bundle impact locations and incident angles with manual calculations and graphic ray tracing. In all cases the predicted results duplicated manual results.

The second approach compared predicted results with analytical results for an enclosure with either black or diffuse-gray surfaces. The enclosure is shown in Figure 3.5 and the results are presented in Table 3.1. In the diffuse-gray case the analytical results are approximate because the diffuse-gray model assumes uniform incident flux on each surface. This is a poor assumption for the case being studied. In order to improve the accuracy of the analytical calculation, surface four was divided into four zones, each assumed to be isothermal and to receive uniform incident flux. The results for the analytical diffuse-gray case are reported in Table 3.1.

The final method of verifying VORRUM involved comparing the predicted results to experimental results. The fraction of radiation

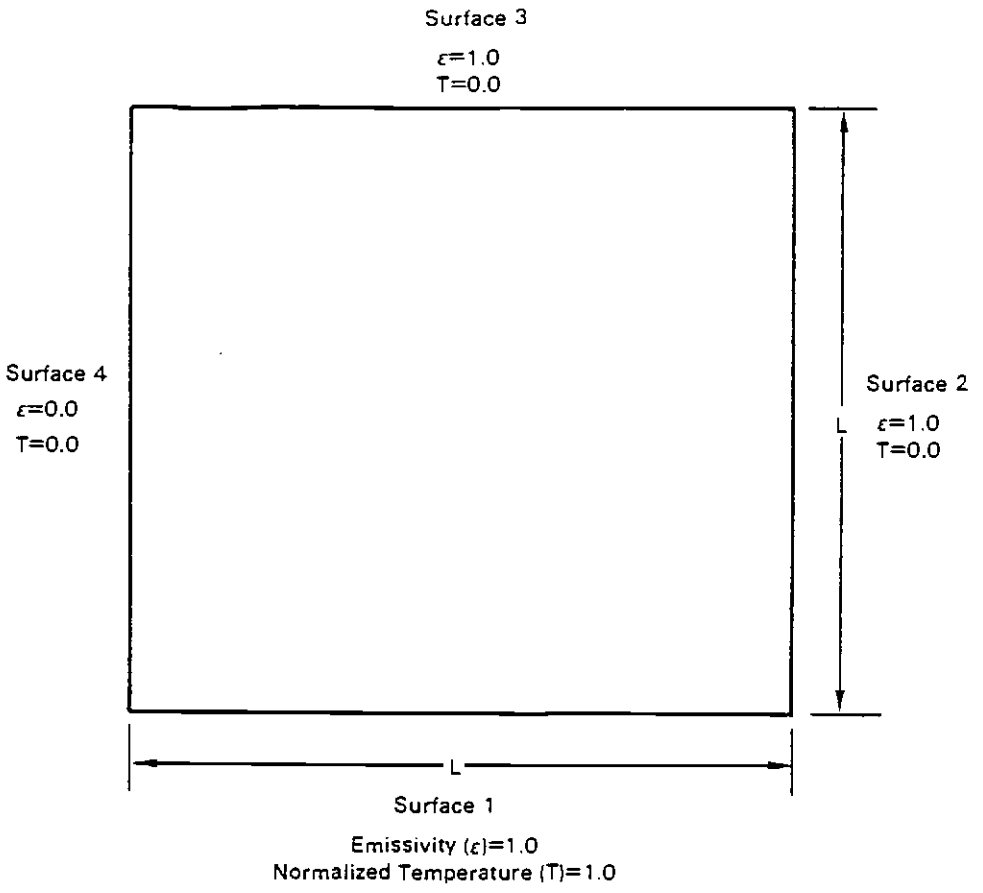


Figure 3.5 Enclosure used for comparison with analytical results.

Table 3.1.

Analytical Results Versus Monte Carlo Model Predictions

| Heat Transfer Path | Analytical | % of Energy Leaving Surface Computer Results | Computed Results Standard Deviation |
|---|---|---|---|
| 1-2 | 41.39 | 41.36 | 0.94 |
| 1-3 | 48.97 | 48.86 | 0.97 |
| 1-4 | 9.64 | 9.78 | 0.50 |

transmitted through both one and two reflecting zones was determined experimentally by PNL for a range of inlet angles. The results for the first row are presented in Figure 3.6. VORRUM was used to simulate the same situation understanding that the uncertainties in dimensions, angles and surface properties in the experimental model would make an accurate comparison difficult. VORRUM assumed a constant emissivity independent of incident angle or wavelength and was modified to emit all photon bundles at the incident angle of interest. The results, presented in Figure 3.5 show that VORRUM duplicates the general trend of decreasing transmittance with increasing angle of incidence. As the angle of incidence increased, VORRUM tended to underestimate the transmittance. Inlet angles off normal produce multiple reflections. This type of situation has been recognized as being the most challenging for a Monte Carlo simulation (Howell and Bannerot, 1974) particularly when uncertainties in dimensions, angles, and surface properties of the physical model are considered. The conclusion, given the uncertainties in the comparison, is that VORRUM successfully predicted experimental results, with predicted results being conservative in that zone transmissivity is underestimated.

A second comparison was made between experimental results and the results predicted by VORRUM. In this case the experimentally determined transmittance of two reflecting zones was compared to the transmittance determined using VORRUM. The comparison is presented in Figure 3.7. As with the one zone case, VORRUM tends to underesti-

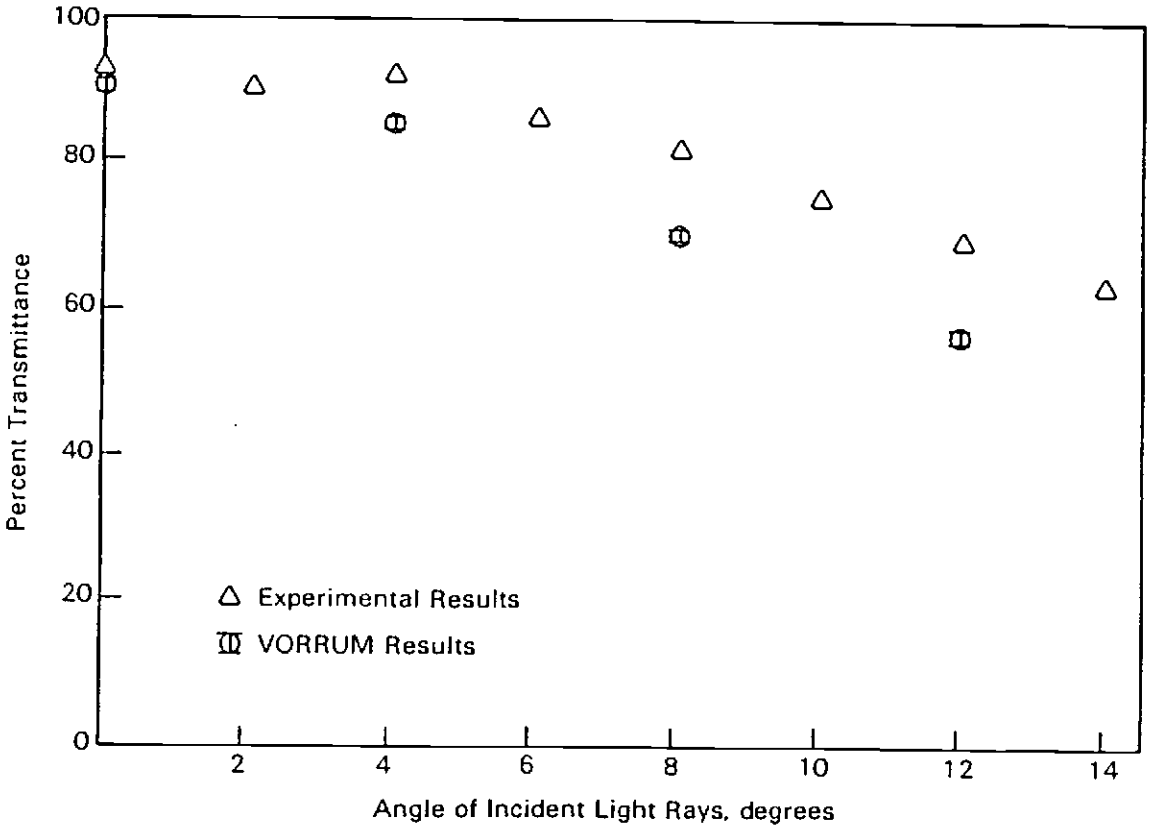


Figure 3.6. Comparison with experimental results for transmission through one reflecting zone

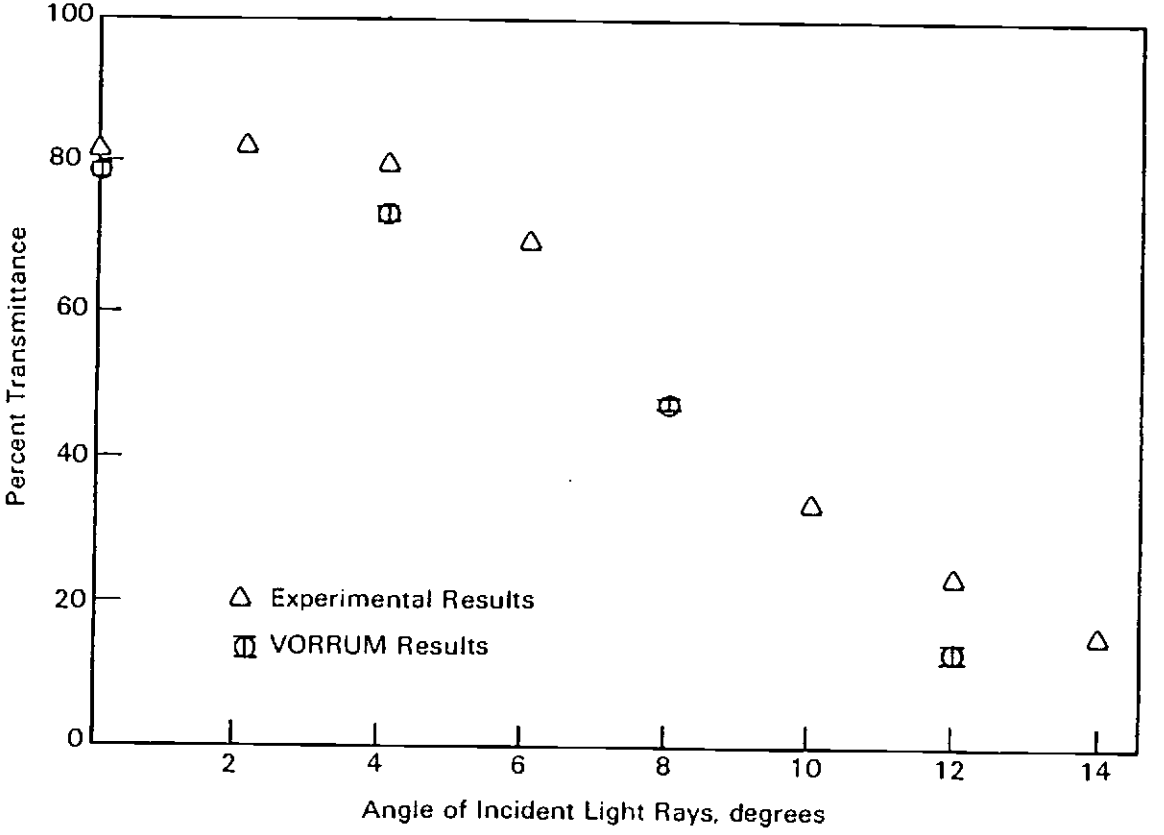


Figure 3.7. Comparison with experimental results for transmission through two reflecting zones

mate the transmittance while duplicating the general trend of decreasing transmittance with increasing angle of incidence. In general, given the uncertainties in the comparison, it appears that results from VORRUM can be successfully correlated with experimental results.

The VOREFM exchange factor code uses the same Monte Carlo technique as VORRUM so that results of the comparisons described above also apply to VOREFM. The main difference between the two codes is in the initial emission of the photon bundles. These calculations have been compared to manual calculation and the two are in agreement.

## 3.7 SAMPLE SIZE CONSIDERATIONS

The uncertainty in the results of a Monte Carlo simulation depends on the number of photon bundles simulated. As the number approaches infinity the uncertainty and the computer budget both approach 0.0. Unfortunately the uncertainty decreases as $1/\sqrt{N}$ where N is the number of photons simulated while the computer budget decreases linearly with N. Therefore, some compromise between uncertainty and running time was required.

Early sensitivity studies indicated that the variance in the results was decreased by using the minimum number of batches consistent with the assumption of a Gaussian distribution for the results. In addition, photon energy was incrementally reduced rather than having the photon either terminated or unaffected by an inter-

action. This allowed more information to be obtained from one photon bundle. Other variance reduction techniques, such as photon bundle splitting and Russian Roulette (Hammersley and Handscomb, 1964) were investigated but these are appropriate where there is one small area of interest in the region being simulated. This was not the case in the volumetric receiver simulation.

The design procedure consisted of using small numbers of photons in survey studies to identify attractive designs and then increasing the sample size once a design had been selected. Survey studies using VORRUM used photon batch sizes of 100 for 20 batches and produced standard deviations which were around 20% of the mean value for most results. Preliminary designs were conducted using batch sizes of 800 for 20 batches which resulted in standard deviations which were around 5% of the mean values. Due to the expense of calculating exchange factors, VOREFM was run with batch sizes of 100 for 20 batches. While the uncertainty experienced in this study was suitable for a survey study, a detailed design would require VORRUM and VOREFM simulations with much larger batch sizes, with perhaps 5000 photons per batch. This would require around 10,000 CPU seconds of computer time on a CDC 3300 computer.

# CHAPTER 4.0

# CONVECTIVE HEAT TRANSFER MODEL

The design study included two generic types of absorbing arrays; the fin array and the ceramic fiber array. Preliminary calculations indicated the decisive importance of convective heat transfer phenomena in predicting receiver performance. Therefore, substantial effort went into the identification of approprite convective heat transfer models. Section 4.1 summarizes the convective heat transfer model for fin surfaces, Section 4.2 discusses the impact of enhancements on convection from fins while Section 4.3 described the model used for convection from a fiber array. The investigations described in Section 4.1 and 4.2 were conducted by PNL and are summarized for completeness. The fiber convective heat transfer model discussed in Section 4.3 was part of this investigation.

## 4.1 CONVECTIVE HEAT TRANSFER FROM FIN SURFACE

The convective heat transfer model for fins consisted of a model for forced convection, natural convection and a method of combining the two effects.

### 4.1.1 Forced Convective Heat Transfer

The closest representation of the absorbing region of the receiver was assumed to be a compact heat exchanger with staggered

plates or cylinders. An empirical expression developed by Weiting (Weiting, 1975) was selected for detailed calculations because it included the greatest sensitivity to configuration parameters. Weiting's correlation consists of

$$\frac{h}{\rho V_\infty C_p} = \beta\left(\frac{L}{D_h}\right)^b (\alpha)^c (Re)^d (Pr)^e \qquad (4.1)$$

where $D_h$ = hydraulic diameter

$\alpha$ = height/width ratio of the free flow area

$L$ = distance from the front of the plate

$V_\infty$ = free-stream velocity

Re = Reynold number

Pr = Prandtl number

The exponents, b, c, d, e and $\beta$ are experimentally determined constants.

The forced convection correlation finally selected by PNL for use in the performance model consisted of a Pohlhausen solution for developing boundary layers (Kays and Crawford, 1980).

$$Nu = .644 \left(\frac{LV_\infty}{\nu}\right)^{1/2} \left(\frac{C_p \mu}{k}\right)^{1/3} \qquad (4.2)$$

where

$L$ = distance from the front of the plate

$V_\infty$ = free stream velocity

$\nu$ = kinemistic viscosity

$C_p$ = constant pressure specific heat

$\mu$ = viscosity

$k$ = conductivity

### 4.1.2 Natural Convective Heat Transfer

The selected correlations for natural convection was proposed by Siebers, Schwird and Moffat (1983). This correlation was based on data collected at temperatures reasonably close to the volumetric receiver operating temperature with air as the convecting fluid. The correlation consists of

$$Nu_{natural} = 0.98 * (Gr)^{1/3} \left(\frac{T_{surface}}{T_{Air\ Bulk}}\right)^{-.14} \qquad (4.3)$$

where the significant length in the Grashof number is the height of a fin.

### 4.1.3 Mixed Mode Heat Transfer

The effects of mixed mode heat transfer were modeled using

$$h_{mixed} = ((h_{forced})^a + (h_{natural})^a)^{1/a} \qquad (4.4)$$

where the values for a was assumed to be 3.2 based upon investigations conducted by Sieber, Schwind and Moffat (1983).

## 4.2 ENHANCED HEAT TRANSFER FROM FINS

The initial calculations of convective heat transfer from the absorbing fins indicated that the convective heat transfer coefficient would be too low to allow a successful design, therefore heat transfer enhancements were considered. A literature review identified a number of enhancements, these are discussed in Drost et al. (Drost et al., 1985).

In general, the enhancement is greatest in the turbulent and transition regimes, with transition typically occurring at a Reynolds number (based on the hydraulic diameter) of about 1,000. The range of Reynolds numbers for flow into the volumetric receiver, based on channel width for the radial-fin configurations, is expected to be on the order of $10^3$ to $10^4$. The effect of accelerating flow, as the air moves inward along a radius, will be to increase stability of the flow and reduce the enhancement effects.

One flow regime of interest is the "second laminar flow" regime which is found to exist for all plate surfaces with fins for interrupting the boundary layer. In this regime, enhancement is caused by the self-sustaining flow oscillations that are produced in the boundary layer. Operations in this regime may be of interest because significant heat transfer enhancement may be obtained while avoiding the vibration and noise in the transition and turbulent regimes.

A rough summary of the conclusions to be drawn from the investigation of convection heat transfer enhancement includes:

1) in the "pure" laminar regime, very little (if any) enhancement is expected;
2) in the "second-laminar" regime, enhancements of 80 to 100% may be obtained;
3) in the turbulent regime, enhancements of 2 to 3 times normal may be expected.

## 4.3 CONVECTION HEAT TRANSFER FROM CERAMIC FIBERS

The ceramic fiber considered in this study consists of a large number of Nextel 312 ceramic strands twisted together. The diameter of a fiber depends on the number of threads in the fiber. A fiber with a diameter of 0.51 mm (0.02 inches) would include 4 strands while a 1.285 mm (0.05 inch) diameter fiber would include 18 strands (3M Company). For the analysis of convective heat transfer, a ceramic fiber was modeled as a single cylinder. This simplified the analysis because the convection from smooth circular cylinders has been the subject of many investigations. Studies of convection associated with hot wire anemometry are particularly relevant due to the similar conditions and cylinder diameters.

Morgan (Morgan, 1975) reviewed a large number of investigations of overall convective heat transfer from smooth circular cylinders and has proposed correlations for natural and forced convection. For natural convection from horizontal cylinders Morgan suggests the following correlation.

$$(Nu)_D = B_1 \, (Gr \cdot Pr)_D^{m1}$$

where $B_1$ and $m_1$, are given in Table 4.1. Morgan believes that the proposed correlation has a maximum uncertainty of $\pm$ 5% over the whole given range of $(GrPr)_D$ except possibly for four transition regions at $(GrPr)_D$ values of $10^{-2}$, $10^2$, $10^4$, and $10^7$. For vertical cylinders Morgan suggests that the correlations given in Table 4.1 may be used if the diameter is replaced by height and if $(GrPr)_H$ is between $10^4$

and $10^{12}$. Morgan does not estimate maximum uncertainty for a vertical wire.

For forced convection, Morgan suggests the following correlations for a cylinder in crossflow in air.

$$(Nu)_D = D_2(Re)^n \qquad (4.6)$$

Table 4.1

Natural Convection Correlation Constants for Fibers

| Ranges of Gr · Pr | | | |
|---|---|---|---|
| From | To | $B_1$ | $m_1$ |
| $10^{-10}$ | $10^{-2}$ | 0.675 | 0.058 |
| $10^{-2}$ | $10^{2}$ | 1.02 | 0.148 |
| $10^{2}$ | $10^{4}$ | 0.850 | 0.188 |
| $10^{4}$ | $10^{7}$ | 0.480 | 0.1250 |
| $10^{7}$ | $10^{12}$ | 0.125 | 0.333 |

where the values of D and n are given in Table 4.2 Morgan states that the proposed correlation has a maximum uncertainty of $\pm$ 5% except possibly in the vicinity of transition points.

The impact of the temperature difference between the fiber and the air can also be significant. Morgan presents the results of experimental investigations and concludes that this area is not adequately understood. Morgan proposes that the free convection

correlation be adjusted with the following multipler where q may range between 0.1 and 0.29

$$\left(\frac{T_f}{T_a}\right)^q$$ where $T_f$ is the film temperature

For this study, q is assumed to be 0.2.

Table 4.2

Forced Convection Correlation Constants for Fibers

| Ranges of ReD | | | |
|---|---|---|---|
| From | To | $D_2$ | $N_2$ |
| $10^{-4}$ | $4 \times 10^{-3}$ | 0.437 | 0.0895 |
| $4 \times 10^{-3}$ | $9 \times 10^{-2}$ | 0.565 | 0.136 |
| $9 \times 10^{-2}$ | 1 | 0.800 | 0.280 |
| 1 | 35 | 0.795 | 0.384 |
| 35 | $5 \times 10^{3}$ | 0.583 | 0.471 |
| $5 \times 10^{3}$ | $5 \times 10^{4}$ | 0.148 | 0.633 |
| $5 \times 10^{4}$ | $2 \times 10^{5}$ | 0.0208 | 0.814 |

Combined natural and forced convection can be significant at low Reynolds numbers. Morgans suggested method of combining natural and forced convective components consists of calculating the resultant velocity which is the velocity of the free stream plus the velocity caused by natural convection. The resultant velocity is then used with the forced convection correlations.

Surface roughness in the form of twisted strands can have a significant impact on the convection from a cylinder. Morgan investigated this topic in a second paper (Morgan, 1973). Morgan concluded that stranding has little if any effect on the overall heat transfer from a cylinder if $Re_D$ < 2000. Morgan observes that in this range the increased heat transfer area due to stranding does not contribute to heat transfer, implying that boundary layer separation occurs at the crest of one strand and laminar re-attachment occurs at the crest of the next strand. Above $Re_D$ = 2000 stranding can have a significant effect. $Re_D$ encountered in this study are well below 2000 therefore the impact of stranding is neglected.

The impact of fiber diameter on the convective heat transfer coefficient is shown in Table 4.3. The results on Table 4.3 were calculated using equation 4.7. The results show that the convective heat transfer coefficient increases with decreasing fiber diameter. At fiber diameters of interest the natural convection coefficient is between 5 $W/m^2 \cdot K$ and 10 $W/m^2 \cdot K$. As Table 4.3 shows, the forced convection component dominates the natural convection component of the convective heat transfer coefficient. Based on these results, small diameter fibers were selected and the impact of natural convection was neglected. This resulted in the following correlation for convection from a ceramic fiber.

$$Nu_D = D\ (Re_D)^n\ \left(\frac{T_f}{T_a}\right)^{.2} \qquad (4.7)$$

where D and n are given in Table 4.2.

Table 4.3

Convective Heat Transfer vs. Fiber Diameter
(Velocity - 5 m/s, Air Temperature = 500 K)

| Fiber Diameter | $Re_D$ | $NU_D$ | $\underline{h}$ ($W/m^2 \cdot K$) |
|---|---|---|---|
| 0.01 | 1316 | 17.2 | 94.4 |
| 0.005 | 658 | 12.4 | 136.4 |
| 0.001 | 131 | 5.8 | 318.4 |
| 0.0005 | 66 | 4.2 | 460.1 |
| 0.0001 | 13 | 2.1 | 1171.5 |

# CHAPTER 5.0

# AIR FLOW MODELING

The air flow analysis task concentrated on predicting air flow distribution, receiver pressure drop and convective losses. Section 5.1 deals with performance modeling of the inlet manifold. Section 5.2 discusses air flow distribution for receiver designs with induced rotational air flow. Section 5.3 describes the procedure for calculating convective losses from the receiver. The air flow modeling was conducted by PNL and is included for completeness.

## 5.I Manifold Orificing and Receiver Pressure Drop

### 5.1.1 Orifice Distribution Calculation Method

It was clear that an orifice distribution scheme for the inlet manifold would have to be adopted to obtain the desired axial distribution of air inflow into the receiver. In the initial receiver design, where an orifice distribution scheme was not employed, the air flow was grossly maldistributed with most of the flow occurring in the bottom of the receiver. Adding orifices to the manifold would choke off the large flow near the receiver bottom and force more air to flow through the upper portions of the manifold. One problem with implementing this idea was in determining the required orifice configuration.

Heat generation in the receiver is assumed to be axially uniform, therefore the desired air inflow distribution should also be

axially uniform. A uniform orifice distribution along the manifold would produce a uniform pressure drop across the manifold and there would be no pressure drop along the manifold. However, a pressure drop along the manifold does exist because air is constantly being added to the down-flow in the manifold. This accelerating flow in the manifold will create a pressure drop along its length. Therefore, a non-uniform orifice distribution is required. The correct distribution will result in a balance between the presure drop across the orifices and the pressure drop along the manifold.

Based on the requirement for a balance between pressure drop the orifices and the pressure drop along the manifold, the following relationship was developed (Drost et al., 1985).

$$\frac{d\bar{f}}{dx} - \frac{16(L-X)}{D^2} c^2 \bar{f}^3 = 0 \qquad \bar{f} = \frac{a}{\pi D} \qquad (5.1)$$

where a = total orifice area per unit length (m)

c = orifice coefficient for a single orifice

d = manifold diameter (m)

X = coordinate direction of manifold axis (m)

L = manifold length (m)

This equation can be solved numerically for $\bar{f}$ which gives the required orifice distribution.

### 5.1.2 Air Flow Distribution TEMPEST Model

To verify the computed orifice configuration and also determine receiver pressure drop, the receiver was modeled using the PNL-developed code, TEMPEST. TEMPEST is a hydrothemal computer program

designed to analyze a broad range of coupled fluid dynamic and heat transfer problems. TEMPEST uses the full three-dimensional, time-dependent equations of continuity, motion, and heat transport to calculate the velocity, pressure, and temperature fields for either laminar or turbulent fluid-flow situations.

TEMPEST was used to model an isothermal receives. Air was drawn through the receiver isothermally at a temperature of 1093 C. This was done for three reasons. First, isothermal flow at 1093 C maximizes the air flow velocity in the receiver and results in a conservative estimation of the receiver pressure drop. Secondly, it has no effect on the function of the manifold because in the real case the air has already been heated to this temperature before it reaches the manifold. Finally, this assumption minimized the demands on computing resources.

The distribution of air flow in the receiver predicted by the model with the calculated manifold orifices still was not uniform. The reason for this variation appears to be the difference between the orifice distribution calculation and the calculation performed by TEMPEST. While the orifice distribution calculation is essentially a one-dimensional treatment of receiver flow, the TEMPEST simulation is a full three-dimensional model. Upgrading the orifice distribution calculations to account for multi-dimensional effects was impractical. The selected approach consisted of using the manifold interior pressure distribution calculated in the first model to back-calculate a new loss coefficient distribution. On incorporation of this

revised distribution into the model, the calculated inflow distribution becomes uniform to within $\pm$ 3%.

Receiver pressure drop is determined from the same TEMPEST simulation by subtracting the interior pressure at the bottom of the manifold from the atmospheric pressure.

## 5.2 Tangential Air Flow Analysis

In most receiver designs, the radial inflow of air by itself is not sufficient to cool the receiver interior. Therefore, additional cooling is provided by establishing a relative velocity between the air and the absorbing array in the circumferential direction. This can be done in two ways. The first design creates this relative velocity by rotating the fiber array through the inflowing air. In the second design the fiber array is stationary and the incoming air is given a rotational component (preswirl) which creates the relative velocity as the air is drawn into the receiver.

In both designs, the presence of the fiber bed acts to reduce the relative velocity and, consequently, the convective heat transfer coefficient. Rotating fibers tend to drag air along with them, creating a rotational air velocity in the same direction as the fibers are traveling. Similarly, the drag of fixed fibers acts to slow down the rotational component of the inflowing air. Two other effects, the thermal expansion of the air as it is heated and the conservation of angular momentum, act to speed up the rotation of the air as it is drawn into the receiver.

In analyzing the air flow in these designs, it is important to insure that the relative velocity between the air and fibers is large enough throughout the receiver to maintain an adequate heat transfer coefficient. For rotating fiber design, this requires the rotational component of the air flow to be small in relation to the fiber rotation. Conversely, it is desirable to have the rotational velocity of the air as large as possible in the fixed fiber designs with preswirl. At the same time, however, it is necessary to show that the combined effects of thermal expansion and conservation of angular momentum do not create a maelstrom in the interior of the receiver. This could result in excessive stresses on the internal ceramic fibers.

TEMPEST does not have the capability for modeling this kind of flow situation. A new computer routine, VORTEX, was created to analize of this type of air flow. VORTEX makes use of the cylindrical form of the Navier-Stokes equations to describe the flow in the receiver. Some simplifying assumptions were made.

- o Uniform axial inflow-this allows a two-dimensional treatment of the flow in the r-$\theta$ plane.
- o Flow is steady-state.
- o Flow is inviscid.
- o There is no pressure gradient in the tangential direction; the only driving or retarding force is the drag of fibers.

- o Fiber drag is considered a body force (distributed uniformly over given volume).
- o Radial or tangential flow velocities do not vary in tangential direction (axisymmetric flow).

The details of the model development and its embodyment in the VORTEX computer code is described in Drost et al. (1985).

The receiver is divided into a number of radial zones that can represent an area of the fiber absorbing array a reflecting row, or a dead zone (free space). Within each zone, the distribution of heat generation and fiber distribution (if any) is considered uniform. VORTEX divides each zone into a number of nodes. VORTEX requires specification of receiver characteristics, zone characteristics, and boundary conditions to complete the calculation.

VORTEX first makes use of continuity and a steady-state heat balance to calculate the radial flow velocity, temperature, and density of the air at each point in the receiver. Using this information along with the input conditions, VORTEX then repeatedly solves the governing equation of motion at each point in the receiver, starting at the receiver periphery and marching inwards, to give the distribution of relative velocity.

## 5.3 Receiver Convective Loss

Calculations of the convective losses from the volumetric receiver are also accomplished using TEMPEST. Only the reflecting

zone designs were analyzed for convective losses. No convective loss calculations were performed for the shrouded designs.

The "reflecting row" concept is used to reduce reradiation losses. Since the wedges are not perfect reflectors, they will absorb a portion of the incoming energy flux and have a temperature greater than the incoming air. The temperature difference between the reflecting wedges and the air will induce natural convection. If air velocities due to natural convection are large compared to the inflow velocity, a significant precentage of the energy absorbed by the wedges could be lost to the surroundings. TEMPEST was employed to estimate thermal energy loss caused by natural convection over the reflecting wedges.

The TEMPEST model used to perform the analysis consists of a three-dimensional cartesian representation of one-half of a single reflecting wedge, the dead zone between it and the fiber bed, and the atmosphere outside it. The wedge nodes generate heat at a uniform volumetric rate determined from the results of a receiver performance simulation.

Convective loss from the receiver is determined from the simulation by examining the air velocity distribution crossing the plane representing the receiver surface (plane normal to wedge tip). The cells with a negative flow velocity normal to this plane represent regions where convective loss is occurring. The net heat transport into the ambient is calculated from these outflow velocities and the corresponding air temperature. This value is then multiplied by the

total number of half-wedges (twice the total number of wedges) to determine the total receiver convective loss. The details of the convective loss calculations are presented in Drost et al. (1985).

# CHAPTER 6.0

# PERFORMANCE MODEL

The performance model combines the results of the radiation heat transfer study, the convective heat transfer study and the air flow study together into a model which determines the performance of a volumetric receiver design. The primary results of the performance model are the equilibrium temperatures of the receiver surfaces. This information can then be used to calculate important performance parameters such as air temperature, reradiation losses and flux ratio. Section 6.1 described the receiver arrangement model and other key assumptions. Section 6.2 discusses the selection of a transient model while Section 6.3 describes the details of the transient model. The subsequent three sections describe models for specific features used in the transient model; these include radiation heat transfer, drag and convection and shroud performance. Section 6.7 discusses the type of results obtained and Section 6.8 describes verification.

## 6.1 RECEIVER ARRANGEMENT AND ASSUMPTIONS

In order to simplify the analysis of a volumetric receiver, the receiver is divided into a number of concentric cylindrical zones. Each zone is assumed to be isothermal with all surfaces having the same temperature. The zone arrangement and indexing scheme is shown

in Figure 6.1. For a receiver with n zones, the surroundings are considered to be zone 0 with the first receiver zone being zone 1. The terminal absorber is zone n. When either a reflecting zone or shroud is included it would be designated zone 1 with the first absorbing zone being zone 2. Previous investigations (Drost and Eyler, 1981) indicated that increasing the number of zones improves receiver performance but that the effect decreases as more zones are considered until there is negligible benefit for adding any more zones. This point occurs at about ten zones. Therefore, all designs were modeled as having at least ten zones.

The arrangement of the receiver in concentric cylindrical zones is based on the assumption that insolation and air flow do not vary in the vertical and circumferential directions. Consideration of radiation flux variations in either the circumferential or vertical directions would have involved a large number of zones with a very large number of exchange factors. The assumption of uniform air flow is reasonable because the air flow analysis has shown that there is substantial flexibility in distributing air flow. The assumption of uniform flux is less accurate particularly because surrounding fields have a distinct asymmetry with the largest number of mirrors being north of the receiver. The argument for assuming uniform flux is that an actual zone would not be cylindrically shaped but would also be asymmetric as shown in Figure 6.2. This would result in something approaching uniform flux. In addition, the performance model calculates a flux ratio which predicts the maximum flux maldistribution

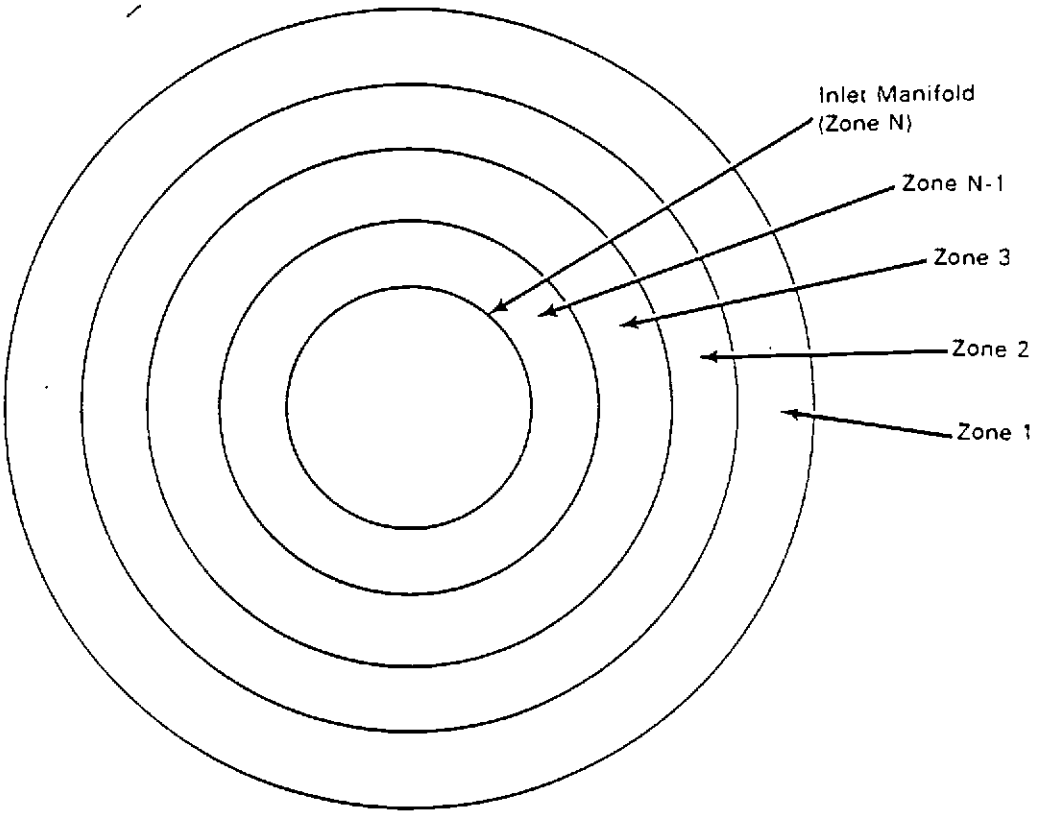


Figure 6.1. Zone arrangement

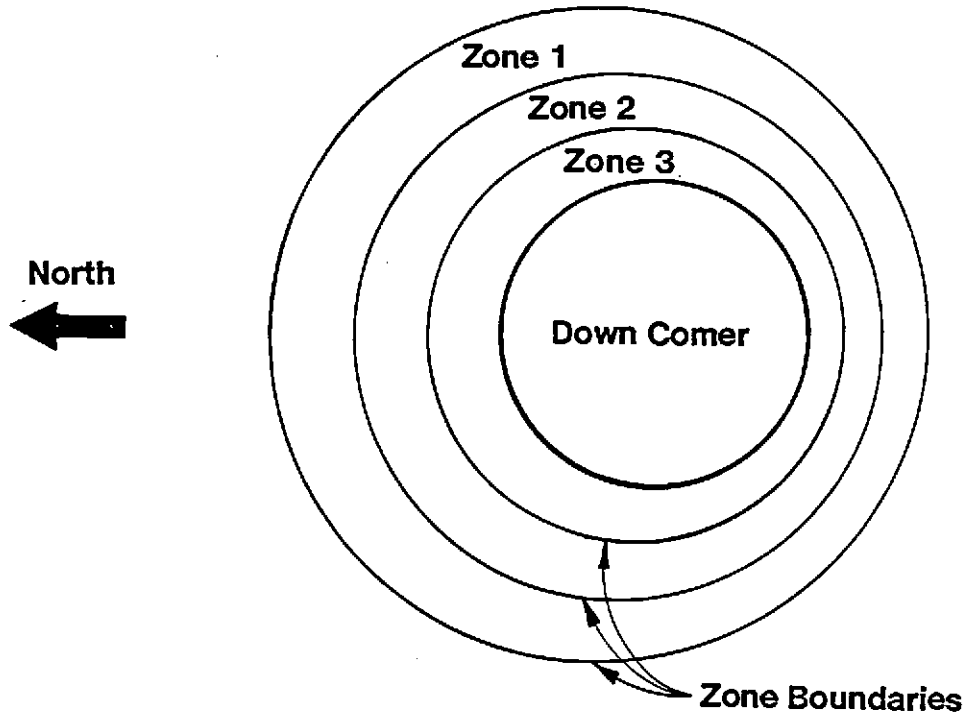


Figure 6.2. Zone shapes

which can be tolerated without exceeding material temperature limits. In most cases, the local flux could be 2 to 3 times the average flux without exceeding the material temperatures.

A second set of assumptions involves material properties, particularly surface emissivity. Emissivity is used in determining exchange factor reciprocity, and maximum material temperature which is in turn used for calculating the flux ratio. The assumed material properties are given in Table 6.1.

Table 6.1

Material Properties

| Zone Type | Material | Emissivity and Absorptivity | Maximum Temperature (K) |
|---|---|---|---|
| Reflecting zone | Aluminum | 0.2 | 645 |
| Shroud | Insulated refractory | 1.0 | 1800 |
| Fiber zone | Nextel 312 | 0.9 | 1480 |
| Fin zone | Silicone carbide | 0.8 | 1590 |
| Terminal absorber | Silicone carbide | 0.8 | 1590 |

## 6.2 GENERAL APPROACH

The main problem in modeling volumetric receiver performance consists of determining the equilibrium temperatures of the various receiver surfaces while they are interacting by radiation heat

transfer with other receiver surfaces and the surroundings, and interacting by convection with the air flowing past the surfaces. Two numerical approaches were considered, a steady state approach and a transient approach. The steady state approach was similar to an "iterative" method of solving second order partial differential equations. Zone material temperatures were assumed and the convective and radiation heat transfer were determined, allowing the calculation of a new zone temperature. This procedure was continued until the zone temperatures converged. Unfortunately this approach proved to be unstable for many cases of interest so a second "transient" approach was considered. The transient approach consisted of having the receiver start at an initial temperature. As insolation is absorbed on various surfaces, the surface temperature will increase until the insolation absorbed on a surface just equals the net radiation heat transfer and convection from the surface. By including a variable fictitious thermal inertia or variable time step the stability of the transient approach could be insured. Due to the stability problems with the steady state approach, the transient approach was selected.

## 6.3 TRANSIENT MODEL

The transient approach consists of letting a receiver at some initial temperature increase in temperature until the receiver reaches an equilibrium steady state temperature distribution. By conducting an energy balance on zone i we get

$$\frac{dT_i}{dt} = \frac{Q_i(T)}{\dot{m}_i Cp_i} \tag{6.1}$$

where $Q_i$ consists of both a convection and radiation component in addition to insolation and is given by Equation 6.2

$$Q_i = A_i \epsilon_i \left( \sigma T_i^4 - \sum_{j=0}^{n} B_{ij} \sigma T_j^4 \right) - h_i A_i (T_i - T_{ai}) + Q_{ins_i} \tag{6.2}$$

Equation 6.1 was solved numerically using Euler's method, resulting in Equation 6.3 (Carnahan et al., 1969)

$$T_{i_j} = \frac{Q_i \Delta T}{\dot{m}_i Cp_i} + T_{i_{j-1}} \tag{6.3}$$

Unlike most transient solutions, we are not interested in the time dependent solution but in the steady state solution, therefore the actual values used for $t$ and $m_i C_{pi}$ are not important as long as the numerical scheme is stable and does not require an excessive amount of computer time. The quantity $t$ was thus assumed to be 1 and was not explicitly included in the calculation. The product $mC_p$ was included and represented the variable which could be adjusted to insure convergence of zone temperatures. Increasing the thermal mass improves stability but increases the computer time required for convergence.

The performance analysis is conducted for a receiver producing hot air with a specified exit temperature. The convergence of zone

temperatures does not insure that the actual product temperature will equal the design temperature, therefore the zone temperature convergence procedure must be nested in a procedure that converges on the design product temperature. This approach starts with an assumed amount of energy incident on the receiver (receiver power level). The transient simulation is continued until steady state temperature conditions are reached and the product temperature is compared to the design temperature. A new value for incident energy on the receiver is selected if the calculated and design temperatures are not equal and the process is repeated.

With an assumed power level and initial temperature, the computation proceeds over a large number of time steps until receiver temperature converges. The calculations for time step j starts with the zone and air temperatures known from time step j-1. The numerical scheme consists of five steps:

Step 1 - The insolation added to each zone and reflection losses are calculated based on the insolation distribution from the Monte Carlo radiation model and the current power level.

Step 2 - Based on the j-1 zone temperatures, the net radiation heat transfer between zones is calculated (see Section 6.3).

Step 3 - Based on the j-1 zone and air temperatures, the air temperature at time step j is calculated using Equation 6.4.

$$T_{Air_j} = T_j + (T_{a_{j-1}} - T_j)e^{\left(\frac{-h_{j-1}A}{\dot{m}_a Cp_a}\right)} \qquad (6.4)$$

Step 4 - With the zone and air temperatures known the energy convected from the zone to the air can be calculated by an energy balance on the air.

Step 5 - The new zone temperature is determined using Equation 6.3.

Step 6 - The zone temperature convergence is checked and iteration is terminated if the zone temperatures converge, otherwise steps 1 through 6 are repeated until convergence is obtained.

The receiver is initially assumed to be at the temperature of the surroundings. The surroundings are assumed to be at 297 K; this value is used for air inlet temperature and "sky" temperature used for calculating reradiation losses.

The performance model is embodied in the RATS (Radiation And Thermal Simulation) computer code. The code is described in more detail in Appendix A.

## 6.4 RADIATION HEAT TRANSFER

The performance model uses zone temperatures to determine the radiation heat transfer between zones. This is done using exchange factors supplied by the Monte Carlo radiation simulations.

### 6.4.1 Definition of Exchange Factors

The Monte Carlo radiation heat transfer model gives an exchange factor between various surfaces. The exchange factor is equal to the fraction of total emitted energy bundles leaving one surface that is incident on a second surface (Howell, 1968). Toor and Viskanta define an absorption factor between finite surfaces i and j. The absorption factor is given in Equation 6.5 (Toor and Viskanta, 1967).

$$B_{ij} = \lim_{N_i \to \infty} N_{i-j}/N_i \tag{6.5}$$

$N_{i-j}$ represents the number of energy bundles emitted by surface i which are absorbed at surface j. Based on a comparison of the Monte Carlo algorithms used by Howell and Toor and Viskanta, it appears that Howell's "exchange factor" is the same quantity as Toor and Viskanta's "absorption factor". In this paper the term "exchange factor" will refer to $B_{ij}$ as defined in Equation 6.5. It should be noted that the exchange factor is related to the "Hottel Script F" by Equation 6.6 (Toor and Viskanta, 1967).

$$\mathcal{F} = \varepsilon_j B_{ij} \tag{6.6}$$

The net radiation heat transfer rate on a given surface can be calculated by conducting an energy balance on the surface as presented in Equation 6.7 (Toor and Viskanta, 1967).

$$Q_i = A_j \varepsilon_j \left( \sigma T_i^4 - \sum_{j=1}^{n} B_{ij} \sigma T_j^4 \right) \tag{6.7}$$

Toor and Viskanta gives the reciprocity conditions for the exchange factors as (Toor and Viskanta, 1967).

$$A_i \varepsilon_i B_{ij} = A_j \varepsilon_j B_{ji} \tag{6.8}$$

### 6.4.2 Exchange Factor Processing

The exchange factors calculated in the Monte Carlo models are statistical and only approximate the true result. The stability of the transient solution for the equilibrium temperature distribution depends on reciprocity being maintained between surfaces and on the summation of exchange factors equaling 1.00. Due to the statistical nature of the Monte Carlo results, random variations may result in reciprocity, as defined in equation 6.8, not being maintained.

In order to insure that reciprocity is maintained, the exchange factors are processed. Processing consists of assuming that the exchange factors in the outward direction are valid. An exchange factor in the outward direction is an exchange factor between an interior zone and a zone located closer to the external surface of the receiver. The reciprocity relationship, Equation 6.8, is then used to calculate the exchange factors in the interior direction. The exchange factor from a zone to itself is calculated by summing the exchange factors to all other zones and subtracting from 1.0.

The processed exchange factors were compared to the unprocessed exchange factors for several cases and the results indicated that processing had a negligible effect on the exchange factors.

### 6.4.3 Radiation Heat Transfer

With the processed exchange factors known, the radiation heat transfer between zones can be calculated for each time step. At the start of a time step, the zone temperatures are known. Using Equation 6.7 for each zone, the net radiation heat transfer to each zone can be calculated. The net radiation heat transfer to the surrounding is the reradiation loss.

Some care must be taken in calculating the proper zone area for each zone. In general the area is the surface area of either all the fins or all the fibers in a zone. The interior zone, or terminal absorber, is modeled as only emitting in the outward direction, therefore the surface area should only be the area of the external surface of the terminal absorber.

The key assumptions in the radiation heat transfer calculation have been discussed in Chapter 3, but one additional assumption relates to the performance modeling, that the exchange factors are independent of surface temperatures. The exchange factors are a function of surface geometry and optical properties. Optical properties such as emissivity, absorptivity and reflectivity are, in general, a function of temperature, therefore the exchange factors should be a function of temperature but computational resources were not sufficient to run the Monte Carlo simulation for each time step. In addition, all except the reflecting zone surfaces were already high emissivity surfaces and any increase in emissivity due to a tempera-

ture rise would result in a small percentage change in the emissivity. Also, an increase in surface emissivity is desirable because the reduction in reflection losses normally exceeds the increased reradiation, therefore, by using a constant emissivity based on low temperature data, the results should be conservative. The reflecting zone values are a major exception because the attractiveness of the concepts depended on maintaining a low emissivity in the reflecting zone. Reflecting zone designs were unattractive, even using optimistic optical properties, therefore considering temperature dependent optical properties would only increase the unattractiveness of the reflecting zone concept.

## 6.5 CONVECTION AND DRAG

The performance model includes algorithms for determining the convective heat transfer coefficient between the receiver surfaces and air. In addition the performance model predicts the power required to turn the rotating section of rotating fiber designs.

### 6.5.1 Relative Velocity

The determination of both the convective heat transfer coefficient and drag depends on the relative velocity between the receiver surface and the air. For fins the relative velocity has only one component which is in the radial direction. The radial velocity is given as

$$V_r = \frac{\dot{m}}{\rho A} \tag{6.9}$$

where air density is calculated assuming air is an ideal gas at the zone bulk-air-temperature. The flow area is the area available for air flow in a given zone. This is a function of the zone radius and the fraction of area that is blocked by solid surfaces.

Designs with rotating fibers involve two components of relative velocity, the radial component, $V_r$, given in Equation 6.9 and a tangential component, $V_\theta$, caused by the rotation of the fiber through the air. As air moves into the receiver the drag of the air on the moving fibers will tend to accelerate the air in the tangential direction, reducing the relative velocity. This effect is accounted for by including a drag factor DF which is the ratio of the actual relative velocity to tangential velocity of the fibers. The drag factor was calculated as part of the air flow analysis described in Section 5. The relative tangential velocity for zone i is

$$V_\theta = (\dot{\omega})\ (2\pi r_i)\ (DF)/60 \qquad (6.10)$$

The combined relative velocity is given by

$$V_{rel} = \sqrt{V_r^2 + V_\theta^2} \qquad (6.11)$$

### 6.5.2 Convection From Fins

Convection from zones with fins or wedge-shaped pins is assumed to consist of a forced and natural convection component. The natural convection component Nusselt number is given as

$$Nu_{N,L} = 0.098 Gr_L^{1/3} \left(\frac{T_{zone(j)}}{T_{Air_B(j)}}\right)^{-0.14} \quad (6.12)$$

where the significant length is the vertical height of the fin or wedge shaped pin. This is normally the height of the zone. The forced convection component is given as

$$Nu_{F,Z} = 0.654 \, (Re_Z)^{0.5} \quad (6.13)$$

where the significant length Z is the horizontal length of the fin or reflecting zone. This is normally the thickness of a zone. Air properties are calculated at the film temperature, which is the average of the zone and bulk air temperatures. The convective heat transfer coefficient includes both natural and forced convection and is given by

$$h = \left((h_N)^{3.2} + (h_F)^{3.2}\right)^{1/3.2} \quad (6.14)$$

The terminal absorber is a special fin-shaped surface which includes the orificed inlet manifold. Due to the difficulty in predicting the convection from the terminal absorber, particularly for designs which include a substantial tangential air velocity, it was decided to arbitrarily fix the heat transfer coefficient from the terminal absorber as 30 $W/m^2 \cdot K$.

### 6.5.3 Convection From Fibers

Convection from fibers for either fixed or rotating fiber designs is dominated by forced convection. The Nusselt number based on fiber diameter for forced convection is given as (Morgan, 1975):

$$\text{Re} < 35$$

$$Nu_{F,D} = 0.583\ (Re_D)^{0.471} \qquad (6.15)$$

$$\text{Re} > 35$$

$$Nu_{F,D} = 0.795\ (Re_D)^{0.384}$$

where air properties are calculated at the fiber temperature. Inclusion of a shroud involves a separate convection model which is presented in Section 6.6.

### 6.5.4 Drag

For designs with rotating absorbing zones, the parasite power required to actually rotate the zones is of interest. Parasitic power requirements are calculated by estimating the power required to overcome drag on the rotating surfaces and then dividing by an efficiency which accounts for motor and speed reducer losses and rolling friction.

The drag force on a given zone is equal to the number of fibers in the zone times the drag per fiber. The number of fibers can be calculated from the average zone radius, the fraction of the zone surface area blocked by fibers and the fiber diameter. The drag on an individual fiber is given by Equation 6.16 where the fiber is

modeled as a cylinder in cross flow. The Reynold number in Equation 6.16 is based on cylinder diameter and the area is the projected area of the fiber (Welty, Wicks, Wilson, 1976).

$$F = \frac{A_p C_D \rho V_\infty^2}{2} \tag{6.16}$$

The drag coefficient is calculated from Equation 6.17 (Bejan, 1982).

$$\text{Re} < 4.0$$

$$C_D = 10.0\ \text{Re}^{-0.6} \tag{6.17}$$

$$\text{Re} > 4.0$$

$$C_D = 5.484\ \text{Re}^{-0.246}$$

The power to overcome drag in zone i is given by Equation 6.18.

$$P_I = \frac{(\text{Number of fibers}_i) A_{pi} C_{Di}\ {}_i V_i^3}{2} \tag{6.18}$$

The total parasite power used to rotate all rotating zones is given by Equation 6.19.

$$P_T = \sum_{I=1}^{n} P_I \tag{6.19}$$

## 6.6 SHROUD MODEL

The inclusion of a shroud involves a separate model for determining the exchange factors between the shroud, ambient and all other receiver surfaces. In addition, a separate convective heat transfer model is required to predict the convection between the shroud and the incoming air. Otherwise, the shroud is treated as any other receiver zone.

The Monte Carlo computer codes do not model the impact of the shroud on either insolation distribution or internal exchange factors. The prediction of exchange factors, involving the shroud or ambient, required the combination of a method for predicting view factors between cylinders of finite length and the results of the Monte Carlo simulations.

A volumetric receiver with a shroud is modeled as an absorbing cylindrical core surrounded by a cylindrical shroud. Figure 6.3 shows the assumed arrangement of the receiver and the numbering scheme for the various surfaces. The view factors between the various surfaces shown in Figure 6.3 can be calculated using the equations for view factors between nested cylinders of finite length (Siegel and Howell, 1972) and view factor algebra. The view factors between the surfaces in Figure 6.3 will equal the exchange factor if all surfaces are considered to be black. This is a good assumption for ambient and not necessary for the core because we know the exchange factors for the core from the Monte Carlo model. In order to determine the impact of the shroud emissivity on receiver performance a transient simulation of the receiver shown in Figure 6.3 was developed using a diffuse-gray model for shroud surfaces. The core was modeled as being a black body at a temperature which radiated energy at a rate equal to reflection and reradiation from a typical core. The results are shown on Table 6.2. These indicate that the emissivity of the shroud surfaces has little impact on either shroud temperature or reradiation losses.

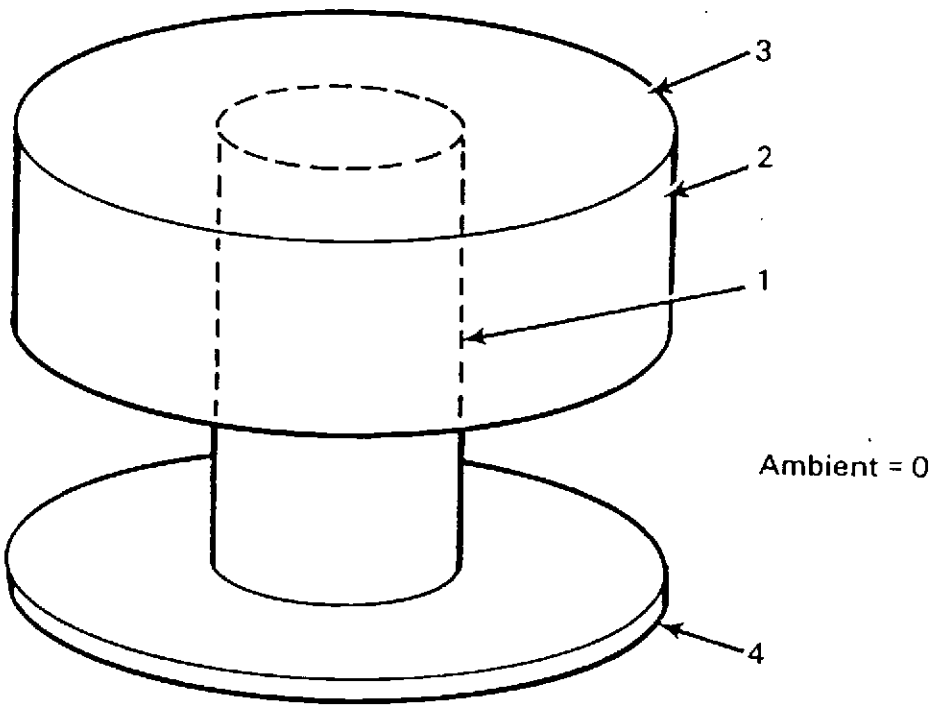


Figure 6.3. Shroud arrangement

Table 6.2

Impact of Shroud Emissivity on Receiver Performance

| | | | | |
|---|---|---|---|---|
| Receiver height | | | | 7 m |
| Core radius | | | | 5 m |
| Shroud radius | | | | 8.5 m |
| Aperature height | | | | 3.5 m |
| Shroud Emissivity | Surface Temperature 2 | 3 | 4 | Reradiation Losses (MW) |
| 0.2 | 990.5 | 951.9 | 891.2 | 10.17 |
| 0.4 | 991.8 | 956.4 | 901.4 | 10.17 |
| 0.6 | 992.2 | 957.7 | 904.3 | 10.16 |
| 0.8 | 992.2 | 958.0 | 905.4 | 10.15 |
| 1.0 | 992.4 | 958.6 | 906.3 | 10.14 |

The shroud can also have the size of the aperture reduced by blocking a fraction of the circumference as shown in Figure 6.4. This type of reduction of aperture area may be necessary to allow structure support of the receiver or in order to reduce thermal losses. The area of surface 2 is increased to include the area of the blocked portion of the aperture while the area of surface 0 is decreased by the same amount. The exchange factors are modified to account for the reduced aperture area. The details of the calculation of various exchange factors are presented in Appendix D.

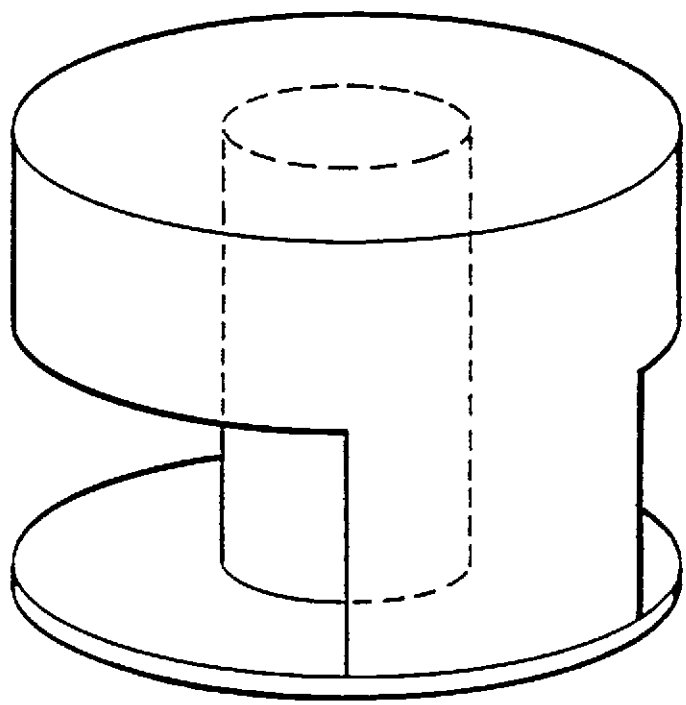

FIGURE 6.4. Shroud with Aperature Blocking

The general approach used in the performance model is similar for both a shrouded and nonshrouded receiver. All surfaces are initially assumed to be at ambient temperature. Insolation is added to the receiver and the temperature of the receiver surface increases until the equilibrium temperature is reached. The shroud can absorb insolation directly from the heliostat field or as reflected energy from the absorbing core. Reflected energy from the core is calculated by the Monte Carlo model. The reflected energy is assumed to be diffuse so that the fraction of reflected energy reaching the shroud is determined by the exchange factor from the core to the shroud. The remaining fraction of reflected energy exits the receiver to the surroundings and is considered a reflection loss. Otherwise the shroud behaves exactly as any other zone in the receiver.

Convection from the shroud surfaces to the incoming air can be an important factor in reducing thermal losses. The nature of convection differs from the other surfaces and a separate convection model was required. Two cases were considered; the first case consisted of considering convection from the bare walls of the shroud. The second case consisted of filling the shroud with a fiber fill to add heat transfer area as shown in Figure 6.5. In both cases the conservative assumption of including only natural convection from these surfaces was made.

Heat transfer from the bare shroud can be divided into natural convection from the shroud floor, roof and side. Equation 6.19 gives the Nusselt number for natural convection from the shroud wall. In

this case the significant length is the height of the shroud (Welty, Wicks, Wilson, 1976).

$$Ra < 1.0 \times 10^9$$

$$Nu_{N},x = .555\ Ra^{.25}$$

$$Ra > 1.0 \times 10^9$$

$$Nu_{N},x = .0210\ Ra^{.4}$$

Natural convection from the receiver floor is given by Equation 6.20 and natural convection from the receiver roof is given by Equation 6.21. In both cases the significant length is the area of the annular region between the shroud and the core divided by the perimeter of the annular region (Welty, Wicks, Wilson, 1976).

$$Ra < 2.0 \times 10^7$$

$$Nu_{N,x} = 0.54\ Ra^{0.25}$$

$$Ra > 2.0 \times 10^7 \qquad (6.20)$$

$$Nu_{N,x} = 0.14\ Ra^{0.333}$$

$$Nu_{N,x} = 0.27\ Ra^{0.25} \qquad (6.21)$$

Natural convection from a single strand in the fiber fill is given by Equation 6.22 where the significant length is the fiber diameter (Morgan, 1978).

$$Ra < 100$$

$$Nu_{N,x} = 1.02\ Ra^{0.148}$$

$$100 > Ra > 10{,}000 \qquad (6.22)$$

$$Nu_{N,x} = .85\ Ra^{0.188}$$

$$Ra < 10{,}000$$

$$Nu_{N,x} = .480\ Ra^{0.250}$$

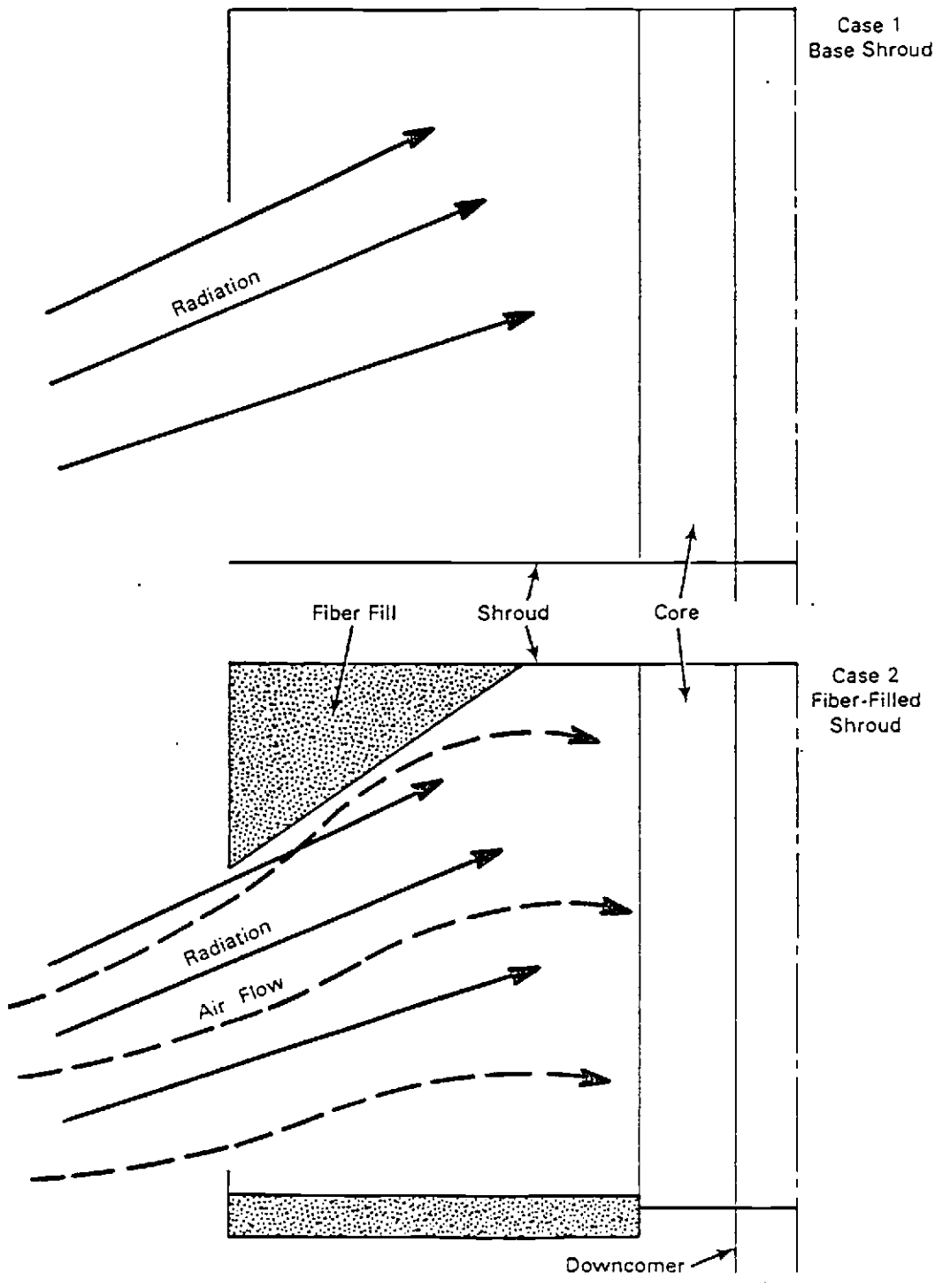


FIGURE 6.5. Shroud Convection

Due to the nature of the performance model the entire shroud is assumed to be isothermal. As Table 6.2 shows there can be significant temperature variation between surfaces when convection is neglected. The inclusion of convection from shroud surfaces may further increase the temperature variations but the analysis of this effect was beyond the scope of the study.

## 6.7 RESULTS

The performance model is embodied in the RATS6 computer code. The details of the code are presented in the Users Manual included in Appendix A. This section presents a discussion of the results which are typically produced by the performance model included in RATS6.

The primary results of the performance model is the receiver equilibrium temperature distribution, including the zone material temperature, zone air exit temperature, and zone bulk air temperature. With the receiver equilibrium temperature distribution know the performance model determines the reradiation losses and the flux ratio for each zone. The flux ratio is the ratio of maximum allowable flux (flux which would cause the zone material to exceed its maximum temperature limits) to the calculated flux based on average flux distribution. This number indicates how much flux maldistribution can be tolerated without exceeding material temperature limits. The RATS6 computer code also generates a variety of secondary results such as zone convective heat transfer coefficients, exchange factors, and net zone radiation heat transfer.

The computer code calculates several performance figures of merit including receiver absorptivity, thermal efficiency, and total efficiency. Receiver absorptivity is calculated from the reflection loss provided by the Monte Carlo radiation model. The code does not independently calculate reflection loss but, where necessary, modifies it to include the impact of a shroud. The receiver thermal efficiency includes a convective loss component which is not calculated by the performance model but must be included as an input variable. The performance model does not consider optical effects related to spillage or intercept losses; receiver total efficiency only includes the product of receiver absorptivity and thermal efficiency.

The results include a gross receiver energy balance which totals convection, reflection, and reradiation losses, useful energy (energy added to the product air) and unaccounted energy (energy not accounted for due to equilibrium temperature distribution not exactly converging to steady state). The results also include the reradiation loss from each zone. These data proved useful in selecting designs which minimize reradiation losses.

## 6.8 VERIFICATION

Verification of the performance code could not be based on comparison with experimental observations, therefore two approaches were used to give some indication that the performance model was working as intended. First, all significant algorithms such as for heat

transfer coefficients and view factors were compared to manual calculations. Secondly, the equilibrium temperature distribution was checked to insure that the net receiver energy balance, net zone energy balance and net internal radiation heat transfer all equal 0.0 as required by the first law of thermodynamics. The computer code which embodies the performance model also calculates the unaccounted-for energy which gives an indication of how close the computer solution is to the steady state solution. The convergence criterion for zone temperature can be adjusted to obtain the desired level of agreement between the calculated equilibrium temperature distribution and the true steady state solution.

# CHAPTER 7

# VOLUMETRIC RECEIVER DESIGN STUDY

This section reports the results of the volumetric receiver design study. Sections 7.1 and 7.2 give an overview of the study and discuss the general ground rules and assumptions. Discussed in sections 7.3 and 7.4 are the results of the performance analysis for radial-fin and staggered-fin designs and the reasons why these were not pursued. Section 7.5 presents the results for a non-augmented fiber design and highlights the reasons for investigating augmentation. Section 7.6 reports the results of the analysis of a fiber design with reflecting pins and shows why the reflecting pin concept was rejected. Section 7.7 reports the results of the analysis of a fiber design with a shroud.

## 7.1 OVERVIEW OF DESIGN PROCESS

A variety of volumetric receiver designs were considered in the study. The two general types either used fin-shaped ceramic absorbing surfaces or small ceramic fibers. Two fin designs were considered; the radial fin array and the staggered fin array. There were also two fiber designs; the augmented designs, where a relative velocity between the fibers and the air was induced, and a nonaugmented design where the air velocity consists solely of a radial component. Two augmentation techniques were considered, rotation of fibers through the air and inducing a swirl in the air and allowing

conservation of angular momentum to accelerate the air as it spirals into the interior of the receiver. Finally a given receiver could be uncovered, enclosed in reflecting pins, or enclosed in a shroud. The relationship between the various designs is shown schematically in Figure 7.1. This section describing the procedure used to evaluate the various designs and the logic used in deciding on the ultimate choice of a fiber receiver with preswirl and enclosed in a shroud.

The selection of the preferred design was based on four major design decisions which include:

- o Fins or Fibers - the selection of a fiber design over fin designs was based on a preliminary calculation of the required heat transfer area for either a staggered fin or radial fin concept. The results indicated that a very large receiver would be required. This suggested that fiber designs should be investigated in more depth. Later in the study, several fin designs were analyzed in more detail (Section 7.3 and 7.4) and the results confirmed the conclusions of the preliminary comparison.
- o Augmented Fiber vs. Nonaugmented Fiber - the selection of an augmented fiber design over a nonaugmented design was also based on a preliminary calculation of the required heat transfer area for a nonaugmented design. The results also indicated that a very large receiver would be required suggesting that augmentation by increasing the relative velocity between the fibers and the air in the tangential direction should be considered. Later in the study, several nonaugmented designs were analyzed in more

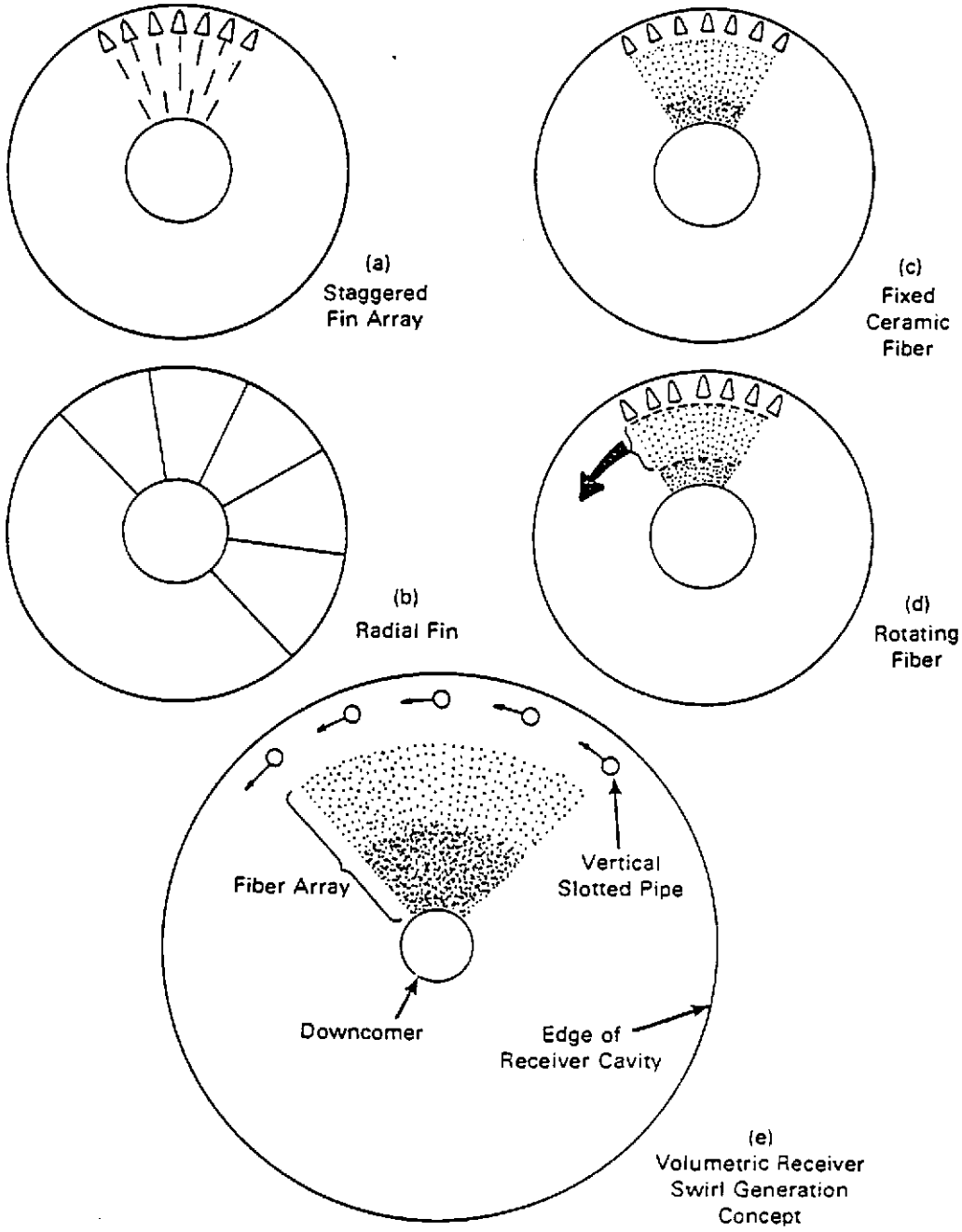


FIGURE 7.1 Solar Thermal Concepts

detail (Section 7.5) and the results confirmed the conclusions of the preliminary comparison.

- o Rotation vs. Preswirl - the selection of preswirl as the preferred method of providing a relative velocity between the fibers and the air was based on two factors; the perceived technical difficulties of rotating a fraction of the fiber-filled zones and the approximately equal performance of a preswirl design and a rotating design.
- o Reflecting Zones vs. Shroud - the selection of a shroud as compared to reflecting zones for geometric loss-reduction was based on an exhaustive evaluation of reflecting zones (Section 7.6) which indicated that, even using optimistic assumptions for optical properties, the reflecting zones would experience excessive material temperatures under normal operating conditions. This suggested that a shroud was the preferred geometric loss-reduction technique.

The procedure used for evaluating a given design consisted of determining the radiation and convection heat transfer rates, and air flow distribution. These results were then combined in the performance model which calculated the design performance. The procedure normally would consist of four steps.

1) Radiation Evaluation - the receiver geometric and optical characteristics is used as input to the VORRUM and VOREFM computer codes which predicted the distribu-

tion of absorbed insolation and the exchange factors between various zones.

2) Convection Analysis - the appropriate convection model is selected from those described in Section 4.0.

3) Air Flow Analysis - for augmented fiber designs, the VORTEX computer code is used to predict the relative velocities between the fibers and the air for the various receiver surfaces.

4) Performance Analysis - using the design features of the receiver, the insolation distribution and exchange factors from the radiation evaluation, the convection model from the convection analysis and the relative velocities from the air flow analysis, the RATS computer code is used to predict receiver performance parameters, temperature distribution, and flux ratios.

The performance analysis of a generic design usually consisted of selecting a base-case design and then investigating the impact of varying significant performance parameters in a series of sensitivity studies. The selection of a base case depended on the generic design being considered. Designs such as the radial fin, staggered fin, and nonaugmented fiber concepts were not attractive and did not merit a detailed investigation to identify an attractive base case design. For these concepts, one reasonable design was selected as the base case. The reflecting zone and shroud designs for the augmented fiber concepts were analyzed in more depth with a range of geometric

configurations being considered and the most attractive being selected as the base case. With the selection of a base case, a series of sensitivity studies was conducted to consider the impact of variables such as product temperature, shroud packing, fiber diameter and air velocities.

In addition to the receiver study, an investigation of the balance-of-plant components was conducted by PNL. Components such as fans, downcomer, heat exchangers or stoves were sized and possible arrangements were investigated. The results of this investigation is discussed in Drost et al. (Drost el al., 1985).

## 7.2 GROUND RULES AND ASSUMPTIONS

In order to compare the various designs on a consistent basis a number of ground rules and assumptions were identified and used throughout the study. In addition, certain technical constraints were imposed on the designs in order to limit the scope of the study.

### 7.2.1 Ground Rules

All base case designs were developed for one set of ground rules. These include:

Plant useful output - 50 $MW_{th}$

Product - high temperature air

Product temperature - 1367 K

Product pressure - 1 ATM

Inlet air temperature - 297 K

Inlet air pressure - 1 ATM

Receiver performance was calculated at one point which corresponded to a 50 $MW_{th}$ output. In an actual plant, daily and annual variations in the heliostat field output will cause variations in the receiver performance and output. The calculation of an average annual output was beyond the scope of this study.

The end use for the product was not specified. The receiver was to provide product at the design temperature delivered to ground level. Drost el al. includes an investigation of the components required at ground level in order to produce a product other than atmospheric pressure high temperature air (Drost et al., 1985).

Convective losses from the receiver were not estimated for most concepts and there was no advantage in selecting arbitrary value for convection losses, therefore convective losses were not included. It should be remembered that total receiver efficiency only included reflection and reradiation losses. Convection and intercept losses are not included. Convective losses should be small because ambient air is being drawn into the receiver preventing heated air from leaving the receiver.

The results reported in the following sections will include a minimum flux ratio. This is the lowest flux ratio for any zone in the receiver. Minimum flux ratios are only caluclate for zones exposed to direct radiation. The flux ratio is not caluclated for a shroud because the shroud does not receive direct insolation and

local maldistributions of flux on the absorbing core will result in a similar but less extreme flux maldistribution on the shroud.

### 7.2.2 Technical Constraints

The designs considered in this study were all assumed to use a surround field. This eliminated downward-facing cavities and cavity receivers with a north field. Both designs have advantages, but the existing radiation heat transfer and performance model did not allow an accurate evaluation of these concepts.

### 7.2.3 Radiation Analysis Assumptions

Several major assumptions in the radiation heat transfer model were discussed in Section 3. Assumptions specific to particular designs are presented here.

The distribution of incident angles for insolation is based on an average image diameter of 4.0 meters. The distribution of energy in the image is assumed to be Gaussian with the image width corresponding to two standard deviations. This resulted in one standard deviation being equal to 1.0 meter. Several reflecting row designs were based on a hypothetical heliostat with an image size of 2.0 meters. These designs were rejected because it is not possible to produce a heliostat which would have such a small image size. All other designs were assumed to use a heliostat field with an average image size of 4.0 meters.

The modeling of fin-shaped rows for radiation heat transfer was straight forward but the fiber designs included several additional simplifying assumptions. All the fibers in a zone were assumed to be in one row; an actual zone might include many rows with the fibers being more sparsely spaced. Secondly, the fibers were modeled as small squares with a surface area equal to that of a cylinder of the specified diameter. This assumption was required because the radiation model in its current form cannot simulate curved surfaces. Due to the small size of the fiber, they may consist of three or four strands wrapped together. The best method for modeling such a surface is unclear but a square model may very well be superior to a cylindrical model. In any case the impact is small because the radiation tends to be quite diffuse, thus the square and cylindrical models have similar performance.

The optical properties assumed for all surfaces are listed in Table 7.1. Temperature dependent variations in optical properties were not considered. The absorptivity and emissivity of aluminum were optimistically assumed to be 0.2. Even with such an assumption, the reflecting row concepts, which depend on specular reflection from aluminum, tended to overheat, this was the major reason for rejecting the reflecting row concept.

### 7.2.4 Performance Model Assumptions

In addition to the assumptions associated with the convection and air flow analysis discussed in Sections 4.0 and 5.0 there are

Table 7.1.

Optical Properties

| Material | Emissivity | Absorptivity | Specularity | Maximum Temperature (K) |
|---|---|---|---|---|
| Aluminum | 0.2 | 0.2 | 0.99 | 645.0 |
| Ceramic fiber[a] Nextel 312 | 0.9 | 0.9 | 0.0 | 1480.0 |
| Silicone Carbide | 0.8 | 0.8 | 0.0 | 1590.0 |
| Shroud | 1.0 | 1.0 | 0.0 | 1800.0 |

[a]From "Properties of Nextel 312".

other design-specific assumptions. These deal with the surface areas to be used in various calculations, flow areas, terminal absorber calculations, air flow assumptions and other constants.

The zone surface area for convective heat transfer is the surface area of the various surfaces in a zone. In general the surface area for convection equals the surface area for radiation heat transfer; there are two exceptions: the terminal abosrber and the shroud with packing. A detailed design of the terminal absorber/inlet manifold was not included in the performance analysis. The radiation model assumes that any radiation passing through to the terminal absorber is absorbed. The exchange factor calculations assume that the terminal absorber has a surface area equal to a right circular cylinder with the radius and height of the terminal absorber. In the performance model the area for radiation heat transfer was also

assumed to be equal to the area of the right circular cylinder with the radius and height of the terminal absorber. It was assumed that the terminal absorber would consist of ceramic fins and the surface area for convection was arbitrarily assumed to be four times larger than the radiation area.

The addition of packing in the shroud was assumed to increase convective heat transfer area without increasing the radiation heat transfer area. The shroud surfaces are already assumed to be black and it can be shown that adding packing cannot increase the emissive power of the shroud above that for a black body.

For fins, the surface area for convection and radiation heat transfer is equal to the surface area of the fins. In fiber designs, the surface area for convection and radiation heat transfer is based on the surface area for all the fibers in the zone with the fiber surface area being based on the design fiber diameter.

When radial air velocity is calculated, the flow area will depend on the amount of possible flow area blocked by solid surfaces. For fin designs, the blocked area equals the sum of the cross sectional areas of the fins in the zone. Fiber designs are more complicated because many rows of sparsely spaced fibers are aggregated into one densely packed row. Basing air velocity on the flow area for the aggregated zone would over estimate the air velocity, therefore the flow area is assumed to be 95% of the potential flow area for any fiber zone.

Two other assumptions are related to air flow. First, the maximum relative air velocity between fibers and the air was arbitrarily limited to 30 meters/sec for both rotating fiber and preswirl designs. Second, for rotating designs a motor/rolling friction efficiency of 50% was assumed. Therefore, installed motor power would be twice that required to overcome drag on the receiver fibers.

## 7.3 RADIAL FIN DESIGN STUDIES

The radial fin concept consists of large ceramic fins arranged radially to form the absorbing section of the volumetric receiver. Preliminary calculations showed that this concept would not be attractive, therefore the scope of the investigation of the radial fin design is limited. Section 7.3.1 will discuss the base case design. Section 7.3.2 will present the performance results for both the base case evaluation and sensitivity studies.

### 7.3.1 Base Case Design

Based on preliminary calculations it was clear that a radial fin receiver would be large. In this study the receiver height was assumed to be 15 m with the fins extending 10 m out from the center line of the receiver. The selection of the fin spacing was based on a series of insolation distribution calculations using the VORRUM computer code. The results are presented in Table 7.2 where each zone represents a 0.75 m long segment of one radial fin. Based on these calculations the design with 72 fins was selected. The results

Table 7.2.

Energy Absorbed in Zone (%) Assuming
4 m Image Size

| Zone | 12 fins ($30^0$ between) | 24 fins ($15^0$ between) | 36 fins ($10^0$ between) | 72 fins ($5^0$ between) | 120 fins ($3^0$ between) | 360 fins ($1^0$ between) |
|---|---|---|---|---|---|---|
| 1<br>10.0 m - 9.25 m | 4.2 | 5.6 | 6.8 | 9.4 | 13.1 | 35.1 |
| 2<br>9.25 m - 8.5 m | 9.1 | 6.6 | 6.9 | 10.4 | 15.6 | 24.4 |
| 3<br>8.5 m - 7.75 m | 5.5 | 6.6 | 7.8 | 11.0 | 15.6 | 14.3 |
| 4<br>7.75 m - 7.00 m | 6.8 | 7.8 | 7.7 | 11.8 | 11.4 | 7.2 |
| 5<br>7.00 m - 6.25 m | 7.4 | 7.0 | 7.2 | 11.0 | 9.5 | 4.2 |
| 6<br>6.25 m - 5.50 m | 6.2 | 7.9 | 9.1 | 8.1 | 8.0 | 3.4 |
| 7<br>5.50m - 4.75 m | 7.4 | 7.8 | 7.6 | 7.4 | 5.9 | 2.4 |
| 8<br>4.75 m - 4.00 m | 6.8 | 7.0 | 8.0 | 6.5 | 5.0 | 1.8 |
| 9<br>4.00 m - 3.25 m | 6.6 | 8.3 | 7.7 | 5.4 | 3.6 | 1.5 |
| 10<br>3.25 m - 2.5 m | 7.1 | 7.1 | 6.8 | 5.0 | 3.2 | 0.9 |
| 11 | 25.5 | 22.2 | 19.7 | 10.5 | 6.3 | 2.5 |
| Reflection Loss | 7.4 | 6.1 | 4.8 | 3.4 | 2.9 | 2.2 |

shown in Table 7.2 are based on Monte Carlo simulations with a relatively small number of photon bundles, therefore the standard deviation is around 25% of the mean value. In addition, these results assume a surface emissivity of 0.9 when 0.8 would be more reasonable. The actual results are not as important as the trends which show that as more fins are added, the insolation is absorbed on the exterior portions of the fins. In addition, reflection losses decrease with increasing number of fins. Convection considerations suggest a large number of fins but the $1^{o}$ and $3^{o}$ designs have an unacceptable fraction of the energy absorbed in the exterior four zones therefore the $5^{o}$ (72 fin) design was selected.

With the design of the absorbing media selected the base case design was specified. Table 7.3 presents the characteristics of the base case design. It was assumed that the base case design would include a shroud with an aperture height of 6 m. The base case did not include fiber packing of the shroud.

### 7.3.2 Results

The results for the base case design are presented in Table 7.4. The radial fin design was predicted to have a total receiver efficiency of 45.55% and a minimum flux ratio of 0.9 for the interior zone. A flux ratio less than 1.0 indicates that the material temperature limit has been exceeded, therefore this design is unacceptable. The design could be modified to increase the flux ratio either by increasing the receiver radius or diameter. This would increase the

Table 7.3.

Radial Fin Base Case Design

Zone Characteristics

| Zone No. | Type | Height (m) | Depth (m) | Fin Spacing (m) | Convection Area ($m^2$) | Radiation Area ($m^2$) | Emissivity |
|---|---|---|---|---|---|---|---|
| 1 | Shroud | 15.0 m | 9.0 m | N/A | 2714 | 2714 | 1.00 |
| 2 | 0.001 m Thick fin | 15.0 m | 0.75 m | 0.8627 | 1638 | 1638 | 0.8 |
| 3 | " | 15.0 m | 0.75 m | 0.7978 | 1638 | 1638 | 0.8 |
| 4 | " | 15.0 m | 0.75 m | 0.7331 | 1638 | 1638 | 0.8 |
| 5 | " | 15.0 m | 0.75 m | 0.6684 | 1638 | 1638 | 0.8 |
| 6 | " | 15.0 m | 0.75 m | 0.6038 | 1638 | 1638 | 0.8 |
| 7 | " | 15.0 m | 0.75 m | 0.5391 | 1638 | 1638 | 0.8 |
| 8 | " | 15.0 m | 0.75 m | 0.4744 | 1638 | 1638 | 0.8 |
| 9 | " | 15.0 m | 0.75 m | 0.4097 | 1638 | 1638 | 0.8 |
| 10 | " | 15.0 m | 0.75 m | 0.3450 | 1638 | 1638 | 0.8 |
| 11 | " | 15.0 m | 0.75 m | 0.2803 | 1638 | 1638 | 0.8 |
| 12 | Thermal Absorber | 15.0 m | N/A | N/A | 3759 | 236 | 0.8 |

Receiver Height = 15.0 m
Receiver Radius = 19.0 m
Air Flow Rate = 42.8 kg/s
Product Design Temperature = 1367K

Aperture Height = 6.0 m
Blocking Factor = 0.05
Shroud Fill = No

Table 7.4.

Radial Fin Base Case Performance

| Zone | Zone Convective Heat Transfer Coefficient ($w/m^2 \cdot K$) | Zone Material Temperature (K) | Zone Air Exit Temperature (K) | Zone Flux Ratio | Zone Insolation (%) |
|---|---|---|---|---|---|
| 1 | 9.08 | 1080 | 632 | 2.1 | 2.90 |
| 2 | 6.08 | 1167 | 737 | 1.8 | 8.48 |
| 3 | 5.50 | 1248 | 826 | 1.6 | 10.29 |
| 4 | 5.08 | 1316 | 905 | 1.5 | 10.81 |
| 5 | 4.74 | 1369 | 974 | 1.4 | 10.50 |
| 6 | 4.45 | 1410 | 1034 | 1.4 | 9.88 |
| 7 | 4.22 | 1445 | 1088 | 1.3 | 8.71 |
| 8 | 4.01 | 1474 | 1136 | 1.3 | 8.33 |
| 9 | 3.85 | 1502 | 1179 | 1.2 | 6.05 |
| 10 | 3.73 | 1534 | 1219 | 1.1 | 6.46 |
| 11 | 3.62 | 1563 | 1257 | 1.0 | 5.53 |
| 12 | 5.00 | 1598 | 1362 | 0.9 | 11.20 |

Energy Balance

| | |
|---|---|
| Reflection Losses (w) | 941,197 |
| Convection Losses (w) | 0 |
| Reradiation Losses (w) | 59,246,245 |
| Useful Power (w) | 50,347,454 |
| Unaccounted Power (w) | 253,921 |
| Total | 110,788,818 |

Receiver Efficiency

- Receiver Absorptivity = 0.991
- Receiver Thermal Efficiency = 0.459
- Receiver Total Efficiency = 0.455

size and weight of a design which is already too large and heavy. Based on the low efficiency and unacceptable flux ratio the radial fin design was rejected.

The major problem with the radial fin design was the low convective heat transfer coefficient between the fins and the air. It is possible that methods of enhancing heat transfer could be developed. One sensitivity study investigated the impact of a five fold increase in the convective heat transfer coefficient and the results show that the total efficiency is still unacceptably low (67.2%) but that the minimum flux ratio is a reasonable 3.4. It appears that even with a major increase in the convective heat transfer coefficient the radial fin design is not competitive with other air heating receiver concepts.

Several other sensitivity studies were conducted and the results are summarized in Table 7.5. The impact of varying the product temperature was investigated and shows that reducing product temperature will improve receiver efficiency and flux ratio. The inclusion of fiber packing in the shroud improves thermal efficiency by 15% while deleting the shroud decreases the thermal efficiency by 20%.

## 7.4 STAGGERED FIN DESIGN STUDIES

The staggered fin concept consists of a volumetric receiver with an absorbing media of a large number of short fins arranged in annular-shaped zones. The fins in one zone are offset from the fins in

Table 7.5.

Radial Fin Sensitivity Studies

| Base Case | Thermal Effeciency | Total[(a)] Efficiency | Minimum Flux Ratio |
|---|---|---|---|
| Unpacked Shroud T = 1367 K | 45.9 | 45.5 | 0.9 |
| Unpacked Shroud T = 1089 K | 65.6 | 65.1 | 1.8 |
| Unpacked Shroud T = 811 K | 83.4 | 82.6 | 2.6 |
| Packed Shroud T = 1367 K | 52.1 | 51.7 | 1.1 |
| Uncovered T = 1367 K | 36.5 | 35.2 | 0.9 |
| Unpacked Shroud T = 1367 K Augmented Convection | 67.8 | 67.2 | 3.4 |

(a) Does not include convective losses or intercept losses.

other adjacent zones. The staggered fin design has the advantage of allowing more dense packing towards the interior of the receiver and it was originally throught that the staggered fin design would have superior pin-to-air heat transfer. The investigation of convective heat transfer between the fins and the air indicated that there was little difference between the convective heat transfer for a staggered fin or a radial fin design. Preliminary calculations showed

that this concept would not be attractive, therefore the scope of the investigation of the radial fin design is limited. Section 7.4.1 will discuss the base case designs. Section 7.4.2 will present the performance results for both the base case evaluation and sensitivity studies.

### 7.4.1 Base Case Design

Based on preliminary calculations it was clear that a staggered fin receiver would be large. In this study the receiver height was assumed to be 15 m. The absorbing array consisted of 0.75 m long fins. The external radius of the absorbing array was 10 m. The selection of the fin spacing was based on a series of insolation distribution calculations using the VORRUM computer code. The goal was to have a large fraction of the insolation absorbed on the interior zones where the heat transfer area was large and the exchange factor to ambient for reradiation was small. This type of distribution was obtained by having the fins in the exterior rows widely spread with the packing becoming more dense in the interior zones. The absorbing array was not extensively studied and performance can probably be improved but the poor overall performance of this concept indicated that a detailed evaluation was not appropriate.

It was assumed that the base case design would include a shroud with an aperture height of 6.0 m. The base case design did not include shroud fiber packing. The characteristics of the base case design are presented in Table 7.6.

Table 7.6.

Stagger Fin Base Case Design

Zone Characteristics

| Zone No. | Type | Height (m) | Depth (m) | Fin Spacing (m) | Convection Area ($m^2$) | Radiation Area ($m^2$) | Emissivity |
|---|---|---|---|---|---|---|---|
| 1 | Shroud | 15.0 m | 9.0 m | N/A | 2714 | 2714 | 1.00 |
| 2 | 0.001 m Thick Fin | 15.0 m | 0.75 m | 5.18 m | 270 | 270 | 0.80 |
| 3 | " | 15.0 m | 0.75 m | 4.79 m | 270 | 270 | 0.80 |
| 4 | " | 15.0 m | 0.75 m | 4.40 m | 270 | 270 | 0.80 |
| 5 | " | 15.0 m | 0.75 m | 4.01 m | 270 | 270 | 0.80 |
| 6 | " | 15.0 m | 0.75 m | 1.81 m | 540 | 540 | 0.80 |
| 7 | " | 15.0 m | 0.75 m | 1.62 m | 540 | 540 | 0.80 |
| 8 | " | 15.0 m | 0.75 m | 0.71 m | 1080 | 1080 | 0.80 |
| 9 | " | 15.0 m | 0.75 m | 0.31 m | 2160 | 2160 | 0.80 |
| 10 | " | 15.0 m | 0.75 m | 0.13 m | 4320 | 4320 | 0.80 |
| 11 | " | 15.0 m | 0.75 m | 0.05 m | 8640 | 8640 | 0.80 |
| 12 | Terminal Absorber | 15.0 m | N/A | N/A | 8759 | 3759 | 0.80 |

Receiver Height = 15.0 m
Receiver Radius = 19.0 m
Air Flow Rate = 42.8 kg/s
Product Design Temperature = 1367K

Aperture Height = 6.0 m
Blocking Factor = 0.05
Shroud Fill = No

### 7.4.2 Results

The results for the base case design are presented in Table 7.7. The staggered fin design is predicted to have a total receiver efficiency of 39.3% and a minimum flux ratio of 1.2. While the flux ratio of 1.2 implies that an average material temperature limit would not be exceeded, the allowable peak flux is only 20% greater than the average flux. This is an unacceptable safety factor. Based on the low efficiency and unacceptable flux ratio, the staggered fin design was rejected.

As with the radial fin design, the major problem with the staggered fin design is the low convective heat transfer coefficient between the fins and the air. It is possible that methods of enhancing heat transfer could be developed. One sensitivity study investigates the impact of a five-fold increase in the convective heat transfer coefficient and the results show that the total efficiency is still unacceptably low (55.1%) but that the minimum flux ratio has significantly improved to 2.1. It appears that even with a major increase in the convective heat transfer coefficient, the staggered fin design is not competitive with other air heating receiver concepts.

Several other sensitivity studies were conducted and the results are summarized in Table 7.8. The impact of different product temperatures was investigated. Product temperatures of 1089 K ($1500^{o}F$) and 811 K ($1000^{o}F$) were considered and the results show that the receiver efficiency and flux ratios are improved but that the concept

Table 7.7.

Staggered Fin Base Case Performance

| Zone | Zone Convective Heat Transfer Coefficient ($w/m^2 \cdot K$) | Zone Material Temperature (K) | Zone Air Exit Temperature (K) | Zone Flux Ratio | Zone Insolation (%) |
|---|---|---|---|---|---|
| 1 | 9.19 | 1160 | 669 | 1.8 | 5.7 |
| 2 | 6.42 | 1231 | 690 | 1.6 | 3.7 |
| 3 | 6.48 | 1298 | 713 | 1.4 | 7.8 |
| 4 | 6.24 | 1294 | 734 | 1.4 | 6.2 |
| 5 | 6.07 | 1302 | 753 | 1.4 | 5.7 |
| 6 | 5.90 | 1325 | 791 | 1.4 | 7.2 |
| 7 | 5.71 | 1360 | 827 | 1.3 | 8.5 |
| 8 | 5.41 | 1387 | 891 | 1.3 | 9.9 |
| 9 | 4.94 | 1432 | 998 | 1.3 | 14.2 |
| 10 | 4.24 | 1469 | 1145 | 1.2 | 14.4 |
| 11 | 3.43 | 1489 | 1297 | 1.3 | 10.3 |
| 12 | 5.00 | 1508 | 1362 | 1.4 | 4.8 |

Energy Balance

| | |
|---|---|
| Reflection Losses (w) | 2,137,770 |
| Convection Losses (w) | 0 |
| Reradiation Losses (w) | 75,566.536 |
| Useful Power (w) | 50,317,066 |
| Unaccounted Power (w) | 207,801 |
| Total | 128,229,254 |

Receiver Efficiency

Receiver Absorptivity = 0.982
Receiver Thermal Efficiency = 0.400
Receiver Total Efficiency = 0.393

is still not competitive with other air heating receivers at these operating temperatures. The inclusion of fiber packing in the shroud improved receiver efficiency by 15% while the deletion of a shroud decreases thermal performance by 30%.

Table 7.8.

Staggered Fin Sensitivity Studies

| Base Case | Thermal Effeciency | Total[(a)] Efficiency | Minimum Flux Ratio |
|---|---|---|---|
| Unpacked Shroud T = 1367 K | 0.400 | 0.393 | 1.2 |
| Unpacked Shroud T = 1089 K | 0.565 | 0.555 | 1.7 |
| Unpacked Shroud T = 811 K | 0.722 | 0.710 | 2.1 |
| Packed Shroud T = 1367 K | 0.473 | 0.466 | 1.5 |
| Uncovered T = 1368 K | 0.305 | 0.284 | 1.3 |
| Unpacked Shroud T = 1367 K Augmented Convection | 0.560 | 0.551 | 2.1 |

(a) Does not include convection losses or intercept losses.

## 7.5 NONAUGMENTED FIBER DESIGN STUDIES

The nonaugmented fiber concept consists of a volumetric receiver where the absorbing medium is made up of a large number of ceramic fibers. This design does not include augmentation which would supply a relative tangential velocity between the fiber and the air. Convection is based on the radial air velocity caused by air being down into the terminal absorber/inlet manifold. Giving the air a preswirl or rotating the fibers are considered by the augmented designs discussed in Sections 7.6 and 7.7. Preliminary calculations showed that this concept would not be attractive, therefore the scope of the investigation of design is limited. Section 7.5.1 will discuss the base case design. Section 7.5.2 will present the performance results for both the base case evaluation and sensitivity studies.

### 7.5.1 Base Case Design

Based on estimates of receiver heat transfer area and convective heat transfer coefficients it was clear that a nonaugmented fiber design would be very large. The performance of such a receiver was estimated by taking a design for an absorbing fiber core developed for the reflecting zone fiber concept (Section 7.6) and considering only radial air velocity. The resulting absorbing core was 20 m high and had a radius of 7.9 m. The inclusion of a shroud with a 6 m aperture height resulted in a total receiver diameter of 21.9 m. The base case did not include shroud packing. The design of the fiber absorbing core was investigated in the studies described in Sections

7.6 and 7.7 and little improvement in the thermal performance of the fiber absorbing core can be expected. The characteristics of the base case design are presented in Table 7.9.

### 7.5.2 Results

The results for the base case design are presented in Table 7.10. The nonaugmented fiber design would have a total receiver efficiency of 56.7% and a minimum flux ratio of 1.8. The performance of the nonaugmented fiber receiver was superior to the fin designs. When compared to augmented concepts, the large size and low thermal efficiency made the nonaugmented design unattractive. Therefore, the design was not pursued.

Several other sensitivity studies were conducted and the results are summarized in Table 7.11. The impact of different product temperatures was investigated. Product temperatures of 1089 K (1500$^{o}$F) and 811 K (1000 $^{o}$F) were considered and the results show that the receiver efficiency and flux ratios are improved with the 811 K design showing good efficiency and a flux ratio of 3.1. The inclusion of shroud packing shows a relatively small improvement (5%) in receiver performance. This is because the shroud surface of the unpacked design is already quite large and the addition of more surface area by packing doesn't significantly improve performance, but it does improve the flux ratio because a smaller fraction of the energy convected to the air is handled by the interior fiber zones.

Table 7.9.

Non Augmented Fiber Design

Zone Characteristics

| Zone No. | Type | Height (m) | Depth (m) | Fin Spacing (m) | Convection Area ($m^2$) | Radiation Area ($m^2$) | Emissivity |
|---|---|---|---|---|---|---|---|
| 1 | Shroud | 20.0 | 14.0 | N/A | 4152 | 4152 | 1.00 |
| 2 | 0.0006 m dia fiber | 20.0 | 0.6 | 0.012 | 124 | 124 | 0.90 |
| 3 | 0.0006 m dia fiber | 20.0 | 0.6 | 0.009 | 151 | 151 | 0.90 |
| 4 | 0.0006 m dia fiber | 20.0 | 0.6 | 0.0075 | 165 | 165 | 0.90 |
| 5 | 0.0006 m dia fiber | 20.0 | 0.6 | 0.0045 | 240 | 240 | 0.90 |
| 6 | 0.0006 m dia fiber | 20.0 | 0.6 | 0.0033 | 285 | 285 | 0.90 |
| 7 | 0.0006 m dia fiber | 20.0 | 0.6 | 0.0020 | 387 | 387 | 0.90 |
| 8 | 0.0006 m dia fiber | 20.0 | 0.6 | 0.0010 | 566 | 566 | 0.90 |
| 9 | 0.0006 m dia fiber | 20.0 | 0.6 | 0.0005 | 730 | 730 | 0.90 |
| 10 | 0.0006 m dia fiber | 20.0 | 0.6 | 0.0001 | 1016 | 1016 | 0.90 |
| 11 | Terminal Absorber | 20.0 | N/A | N/A | 3759 | 3759 | 0.80 |

Receiver Height = 20.0 m
Receiver Radius = 21.9 m
Air Flow Rate = 42.8 Kg/s
Product Design Temperature = 1367K

Aperture Height = 6.0 m
Blocking Factor = 0.05
Shroud Fill = No

Table 7.10.

Nonaugmented Fiber Design Performance

| Zone | Zone Convective Heat Transfer Coefficient ($w/m^2 \cdot K$) | Zone Material Temperature (K) | Zone Air Exit Temperature (K) | Zone Flux Ratio | Zone Insolation (%) |
|---|---|---|---|---|---|
| 1 | 11.44 | 953 | 728 | 2.8 | 4.7 |
| 2 | 53.16 | 1132 | 781 | 1.8 | 6.2 |
| 3 | 55.70 | 1109 | 835 | 2.1 | 5.1 |
| 4 | 59.23 | 1131 | 890 | 2.2 | 5.6 |
| 5 | 63.47 | 1160 | 963 | 2.3 | 8.2 |
| 6 | 68.44 | 1188 | 1038 | 2.4 | 8.9 |
| 7 | 74.65 | 1237 | 1126 | 2.4 | 13.2 |
| 8 | 82.08 | 1280 | 1219 | 2.7 | 16.9 |
| 9 | 91.13 | 1328 | 1299 | 3.0 | 16.5 |
| 10 | 102.02 | 1365 | 1356 | 3.8 | 12.9 |
| 11 | 5.00 | 1376 | 1362 | 13.3 | 0.9 |

Energy Balance

| | |
|---|---|
| Reflection Losses | 761,415 |
| Convection Losses (w) | 0 |
| Reradiation Losses (w) | 37,650,082 |
| Useful Power (w) | 50,322,276 |
| Unaccounted Power (w) | 189,708 |
| Total | 88,923,483 |

Receiver Efficiency

Receiver Absorptivity = 0.991
Receiver Thermal Efficiency = 0.572
Receiver Total Efficiency = 0.567

Table 7.11.

Nonaugmented Fiber Sensitivity Study

| Base Case | Thermal Effeciency | Total[(a)] Efficiency | Minimum Flux Ratio |
|---|---|---|---|
| Unpacked Shroud T = 1367 K | 0.572 | 0.567 | 1.8 |
| Unpacked Shroud T = 1089 K | 0.802 | 0.795 | 2.5 |
| Unpacked Shroud T = 811 K | 0.934 | 0.926 | 3.1 |
| Packed Shroud T = 1367 K | 0.594 | 0.589 | 2.4 |
| Uncovered T = 1367 K | 0.446 | 0.422 | 1.7 |

(a) Does not include convection losses or intercept losses.

The uncovered design with no shroud has a 20% reduction in receiver efficiency.

## 7.6 REFLECTING ROW FIBER DESIGN STUDIES

The combination of a fiber filled absorbing core and reflecting rows for geometric loss reduction originally appeared attractive and the inclusion of reflecting rows was felt to be an important feature of any volumetric receiver design. Therefore, the reflecting zone

concept was studied in detail. Section 7.6.1 discusses the investigation of the reflecting zone concept by means of a generic study of the reflecting zones. The selection of the base case design is presented in Section 7.6.2. Section 7.6.3 presented the results for the base case and sensitivity studies.

### 7.6.1. Analysis of Reflecting Zones

The reflecting rows represent a the unique feature of this design and were the subject of a generic study to identify the most attractive reflecting row configuration. The study was generic and not associated with a specific design. The inclusion of an absorbing core would have substantially increased the computer time required for one simulation and this would have limited the scope of the study.

#### 7.6.1.1 Model

The generic reflecting zone study was conducted using a modified version of the VORRUM computer code. This variant, the VORRRM (Volumetric Receiver Reflecting Row Model) simulated both the interaction of the reflecting row with insolation and with reradiated or reflected energy. First, the model simulated the interaction of insolation with the reflecting zone determining the amount of energy absorbed in the reflecting zone, the energy reflected back to ambient and the energy passing through the core into the interior. Any radiation passing through the reflecting zones was assumed to be

absorbed in the interior of the receiver. After determining the zone performance with insolation the VORRRM code then simulated the emission of reradiated or reflected photon bundles from an idealized core. The history of the photon bundles was observed and the results for a large number of photon bundles determined the fraction of reradiated or reflected photon bundles which were either absorbed in the reflecting zone, or were lost to ambient.

The analysis of the reflecting zone design for the volumetric receiver consisted of using the VORRRM computer code to simulate a large number of possible designs followed by identification of the most attractive designs based on a performance figure of merit. The significant figure of merit is associated with the minimum combined receiver losses for a given design. The combined receiver losses for the generic study included reflection and reradiation from the interior receiver surfaces and reflection from the reflection zone. The combined reflection and reradiation coming from the absorbing core was assumed to be 30% of the incident energy on the receiver. Based on this estimate the receiver losses are given by

Receiver loss = Reflection loss from reflecting zone + Reflecting zone transmissivity for reradiation x 0.30%

The most attractive reflecting zone design had the lowest losses while not exceeding material temperature limitations. In general, low-loss designs also have large amounts of incident energy and reradiation absorbed in the reflecting zones resulting in high material temperatures. For the generic study, it was assumed that the

reflecting zones are fabricated from aluminum which limits the zone temperature to 650 K. Any safety factor to account for maldistribution of insolation or air flow will further reduce the maximum allowable zone temperature.

The reflecting zone temperature was calculated by estimating the energy absorbed in the zone and then determining the zone temperature necessary to transfer the energy from the pin to the air. The pin-to-air convective heat transfer coefficient was assumed to be 5.0 $W/m^2.K$.

7.6.1.2 Results

The reflecting zone analysis consisted of three stages. In the first stage, the design of a single reflecting zone was investigated for four receiver geometries. Characteristics of the four receiver geometries are:

| Case | Receiver Radius (m) | Receiver Height | Image Size |
|---|---|---|---|
| 1 | 5 | 10 | 4.0 m |
| 2 | 5 | 10 | 2.0 m |
| 3 | 10 | 5 | 4.0 m |
| 4 | 10 | 5 | 2.0 m |

The significant parameters which characterize a reflecting zone design were the cell aspect ratio, cell width, and wedge angle. These parameters are shown in Figure 7.2. The normal surface emissivity was assumed to be 0.2 for the aluminum reflecting rows. This

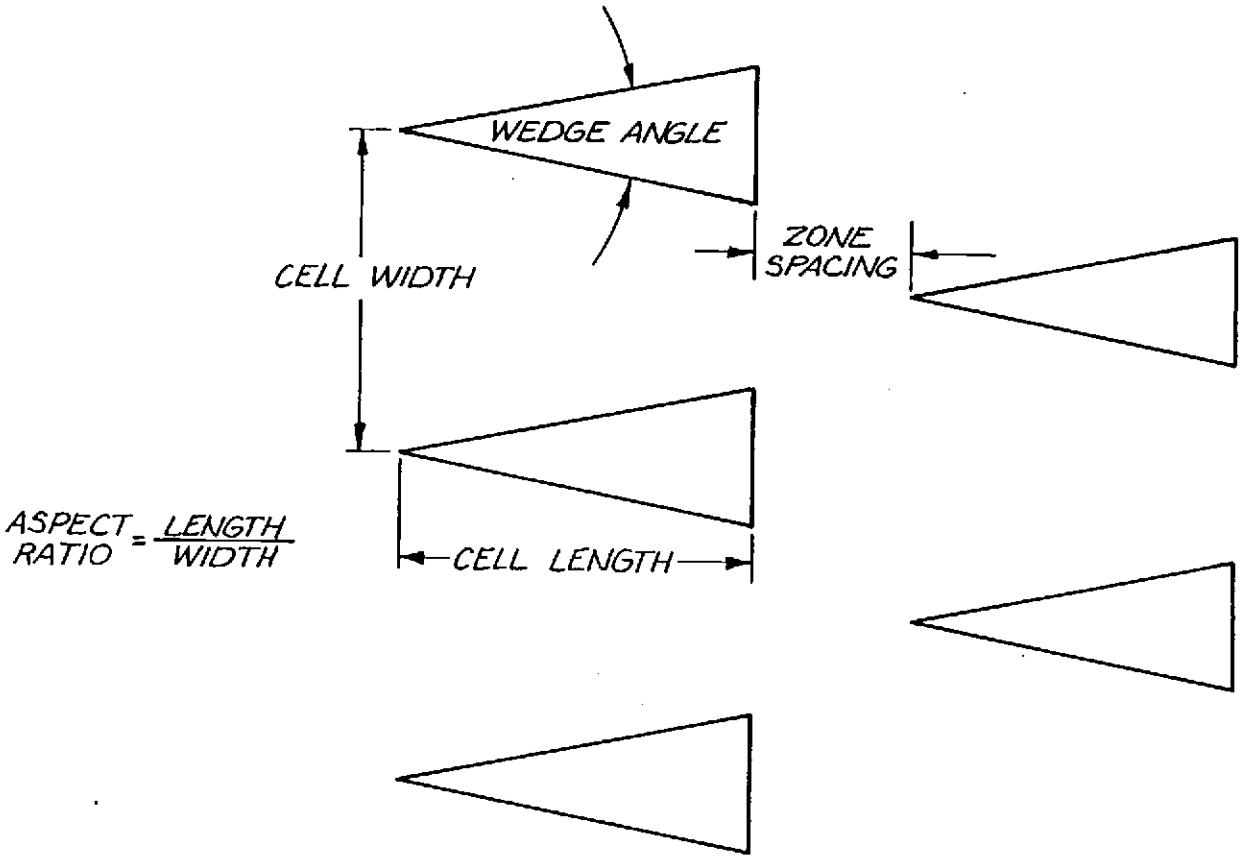


Figure 7.2. Reflecting zone cell parameters

assumption was optimistic-particularly considering that the operating temperature of the reflecting zone was normally around 600 K.

Following the first stage analysis, one of the single-reflecting-zone designs was selected as the first zone in a two-reflecting-zone design, subsequently another single-reflecting-zone design was selected as the first of a three-reflecting-zone design. The results for the case 1 evaluations indicated that all case 1 designs were infeasible because material temperatures exceeding the maximum allowable temperatur for aluminum. Therefore, multiple-zone designs were not considered for this case.

Stage two consisted of simulating a number of two-zone designs. The design of the first zone was fixed while that of the second zone was varied. The aspect ratio, cell width and wedge angle of the second row were the significant variables. The results indicated that the spacing between the two zones was not an important factor in determining the performance, thus this variable was not included in the sensitivity study.

The results of the stage two analysis indicated that the two-zone designs were not competitive with the one-zone design, but in order to determine the impact of adding successive reflecting zones, one three-zone case was investigated. The results of the two zone analysis for case 4 were reviewed and one two zone configuration was selected for the first two zones of a three-zone design. The geometry of the first two zones was fixed while the aspect ratio and wedge

angle of the third zone was varied. The results indicated that the three-zone case was even less attractive than a two-zone case.

The results of the various simulations indicated that the best performance was obtained with a large radius or a small image size. Either resulted in a reduction in the average incident angle of the insolation. Case 1 was rejected because much of the insolation had a large incident angle which resulted in the insolation being either absorbed in the reflecting zone or reflected back to ambient. Based on these results, the base design was determined to have a radius of 10 m and a height of 5 m. The base case design was assumed to operate with a heliostat field which produced a 2.0 m image.

With the selection of the case dimensions, the reflecting row design was identified by reviewing the results of the various simulations described above. Due to assumptions in calculating the zone temperature, the actual value of the zone temperature is less important than the trends indicated by the results.

The impact of successive reflecting zones on reflecting zone performance is shown in Figure 7.3. The results for the best one-two-and three-zone designs are plotted. Adding successive zones has a small effect on receiver losses but a dramatic impact on zone material temperature where only the one zone case has a maximum zone material temperature below 650 K, the assumed maximum allowable material temperature. Based on these results only one reflecting zone design was considered.

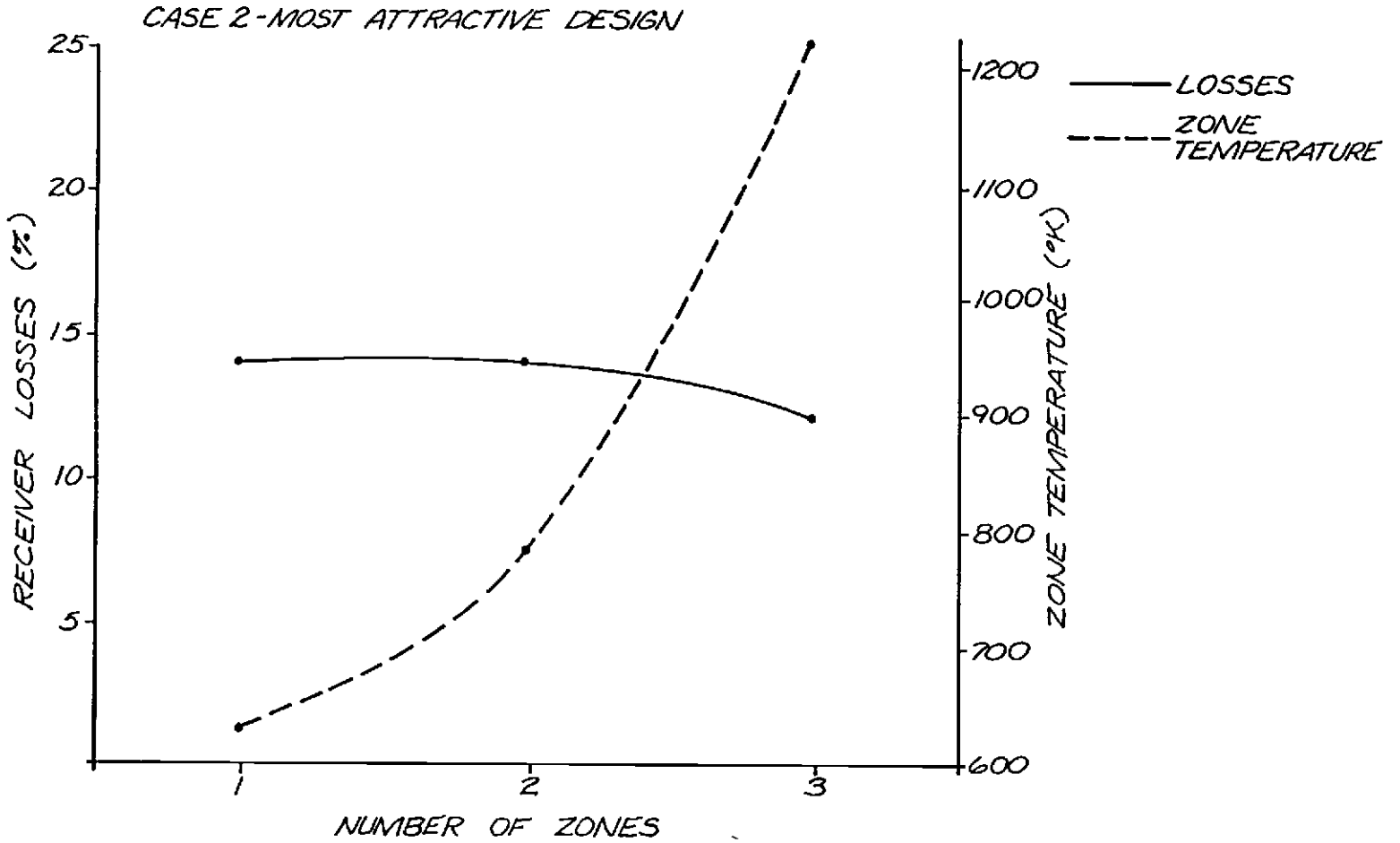


Figure 7.3. Impact of successive reflecting zones on performance

The impact of aspect ratio and wedge angle on losses and zone temperature is shown graphically in Figure 7.4. The influence of cell width on reflecting zone performance is shown in Figure 7.5. Both graphs are for the base case design but, again, the specific values are less important than the general trends.

7.6.1.3 Conclusions

The following conclusions were reached after evaluating the results of the various reflecting row designs considered in this study.

- o The most attractive receiver consisted of a 10 m radius, 5 m height receiver used with a heliostat field which produces a 2 m wide image. The 5 m radius receiver is not feasible with existing heliostats.
- o Multiple reflecting zones are not desirable. One reflecting zone is superior to two zones which are in turn superior to three zones, therefore the base case design will have one row.
- o Increasing aspect ratio will result in a decreased zone temperature because the amount of absorbed energy does not increase as rapidly as does heat transfer area.
- o Increasing wedge angle increases zone temperature and decreases reradiation. The increase in zone temperature is caused by increased absorption of incident radiation

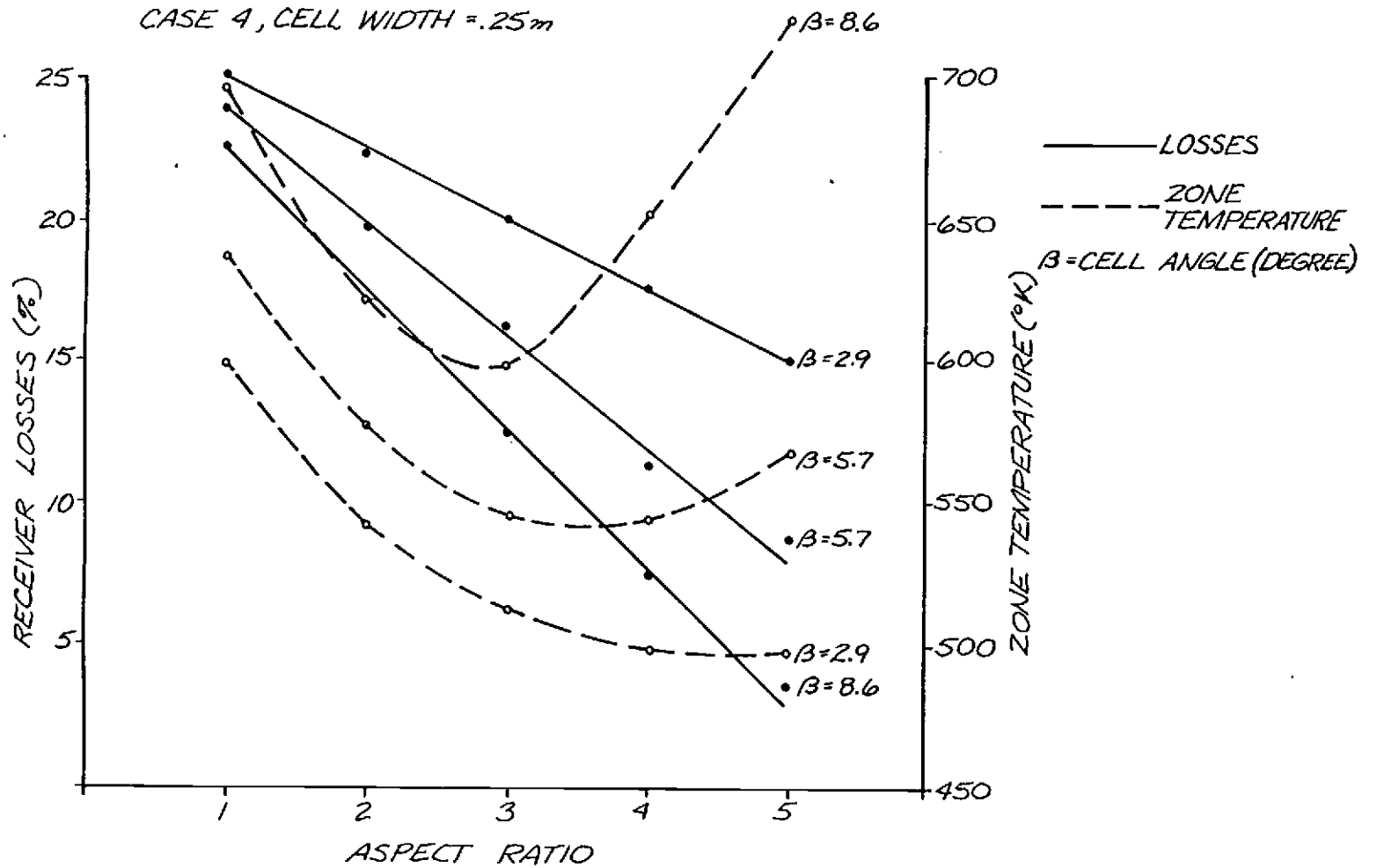


Figure 7.4. Impact of aspect ratio and wedge angle on performance

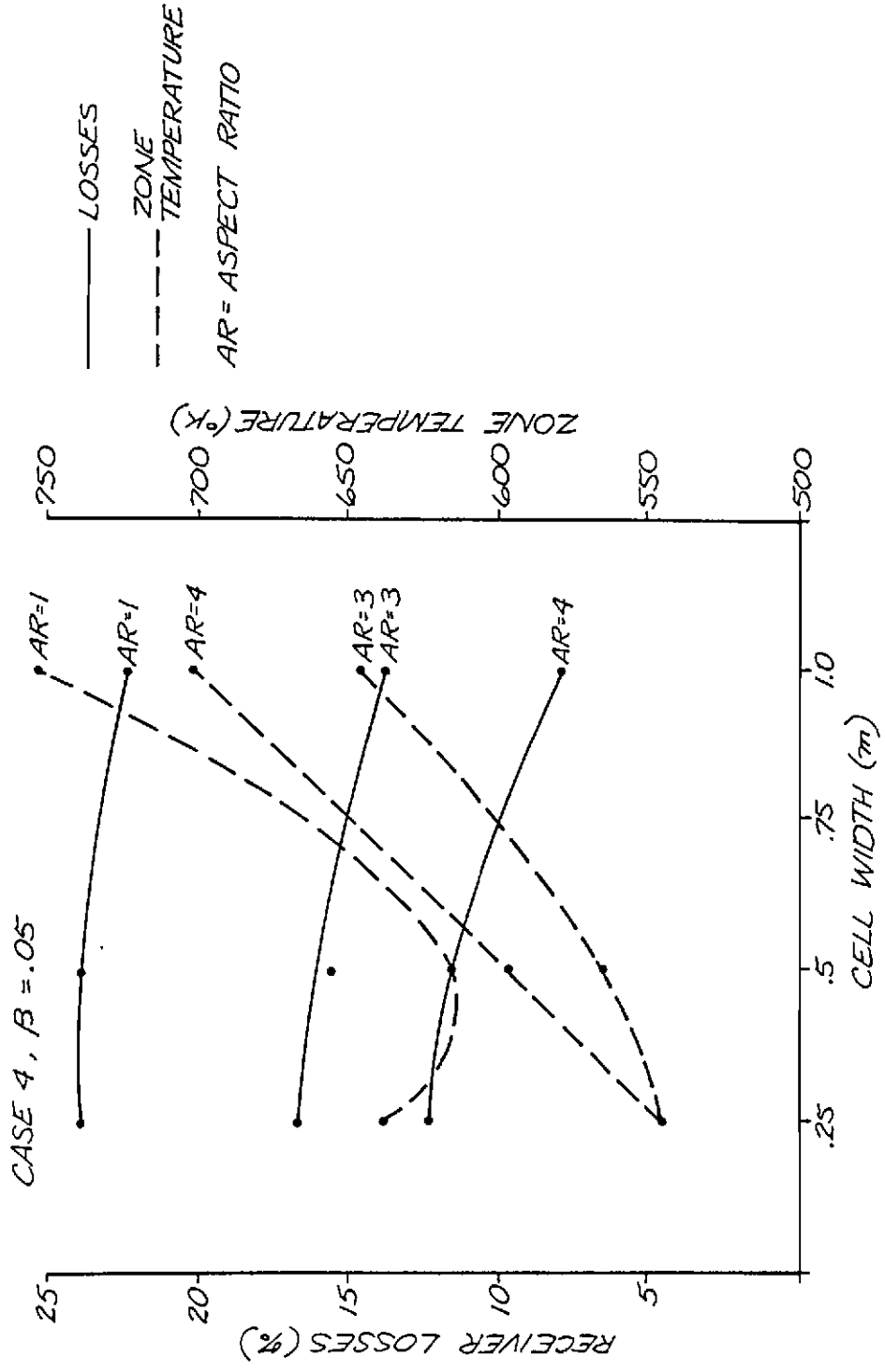


FIGURE 7.5 Impact of Cell Width on Performance

whereas the absorption of reradiated energy is almost constant with wedge angle.

- o While keeping the aspect ratio constant, zone temperature decreases and reradiation losses increase by decreasing the pin spacing (a larger number of shorter pins).
- o Based on the generic study the most attractive reflecting row design consists of 1 m long pins separated by 0.125 m with a wedge angle of $3.5^{o}$.

### 7.6.2 Base Case Design

Using the results of the generic study of reflecting rows, the base case reflecting row fiber design was specified. The characteristics of this concept are presented in Table 7.12. The absorbing zone was selected after simulating several fiber arrays and selecting the design that resulted in the bulk of the energy being absorbed in the interior zones.

### 7.6.3 Results

The results for the base case design are presented in Table 7.13. The reflecting row fiber receiver will have a total receiver efficiency of 86.8% and reflecting row flux ratio of 1.4 and a minimum fiber zone flux ratio of 3.9. The efficiency of this design is excellent as is the fiber zone minimum flux ratio but the reflecting row flux ratio is unacceptably low. These results are based on a

Table 7.12.

Reflecting Row Fiber Design

| Zone Characteristics | | | | | | | |
|---|---|---|---|---|---|---|---|
| Zone No. | Type | Height (m) | Depth (m) | Fin Spacing (m) | Convection Area ($m^2$) | Radiation Area ($m^2$) | Emissivity |
| 1 | Reflecting Fins[a] | 5.0 | 1.0 | 0.125 | 5027 | 5027 | 0.2 |
| 2 | 0.0006 m dia fiber | 5.0 | 1.7 | 0.013 | 37 | 37 | 0.9 |
| 3 | 0.0006 m dia fiber | 5.0 | 0.6 | 0.010 | 44 | 44 | 0.9 |
| 4 | 0.0006 m dia fiber | 5.0 | 0.6 | 0.008 | 50 | 50 | 0.9 |
| 5 | 0.0006 m dia fiber | 5.0 | 0.6 | 0.0051 | 68 | 68 | 0.9 |
| 6 | 0.0006 m dia fiber | 5.0 | 0.6 | 0.0037 | 82 | 82 | 0.9 |
| 7 | 0.0006 m dia fiber | 5.0 | 0.6 | 0.0024 | 106 | 106 | 0.9 |
| 8 | 0.0006 m dia fiber | 5.0 | 0.6 | 0.0011 | 169 | 169 | 0.9 |
| 9 | 0.0006 m dia fiber | 5.0 | 0.6 | 0.0006 | 211 | 211 | 0.9 |
| 10 | 0.0006 m dia fiber | 5.0 | 0.6 | 0.0002 | 278 | 278 | 0.9 |
| 11 | Terminal Absorber | 5.0 | N/A | N/A | 289 | 72 | 0.8 |

(a) 1 m long with wedge half angle of 0.025 radius.

Receiver Height = 5.0
Receiver Radius = 10.0
Air Flow Rate = 42.8
Product Design Temperature = 1367

Table 7.13.

Reflecting Row Fiber Design Performance Results

| Zone | Zone Convective Heat Transfer Coefficient ($w/m^2 \cdot K$) | Zone Material Temperature (K) | Zone Air Exit Temperature (K) | Zone Flux Ratio | Zone Insolation (%) |
|---|---|---|---|---|---|
| 1 | 6.89 | 567 | 444 | 1.4 | 7.5 |
| 2 | 357.46 | 695 | 509 | 4.6 | 3.8 |
| 3 | 377.88 | 765 | 588 | 4.3 | 5.0 |
| 4 | 413.90 | 810 | 669 | 4.7 | 5.1 |
| 5 | 451.42 | 882 | 772 | 4.7 | 7.0 |
| 6 | 497.10 | 977 | 891 | 4.5 | 8.9 |
| 7 | 551.60 | 1087 | 1028 | 4.1 | 12.3 |
| 8 | 605.96 | 1199 | 1177 | 3.9 | 17.1 |
| 9 | 665.48 | 1293 | 1286 | 4.1 | 16.3 |
| 10 | 717.17 | 1361 | 1359 | 4.1 | 12.1 |
| 11 | 5.00 | 1462 | 1362 | 2.3 | 3.0 |

Energy Balance

| | |
|---|---|
| Reflection Losses (w) | 1,104,273 |
| Convection Losses (w) | 0 |
| Reradiation Losses (w) | 6,544,765 |
| Useful Power (w) | 50,406,165 |
| Unaccounted Power (w) | 17,367 |
| Total | 58,072,572 |

Receiver Efficiency

| | |
|---|---|
| Receiver Absorptivity | 0.981 |
| Receiver Thermal Efficiency | 0.885 |
| Receiver Total Efficiency | 0.868 |

reflecting row emissivity of 0.2 and an image size of 2 m; both assumptions are extremely optimistic. Even for this unrealistic case, the reflecting zone temperature as represented in the flux ratio is unacceptably high, therefore the reflecting row concept was dropped from further consideration. The exhaustive investigation of row design as described in 7.6.1 suggests that little improvement can be expected by further optimization of the reflecting row concept. Based on these results, the shrouded fiber receiver was selected as the most attractive concept.

Several sensitivity studies were conducted and the results are reported in Table 7.14. The impact of different product temperatures on receiver performance was investigated. Product temperatures of 1089 K (1500 F) and 811 K (1000 F) were considered and the results showed a substantial improvement in receiver efficiency, but the flux ratio for the reflecting row is only acceptable with a product temperature of 811 K and these results are still based on the unreasonable emissivity and image size assumptions described above. It is unlikely, even at 811 K (1000 F), that a successful reflecting zone design can be obtained.

The impact of the image size assumption was investigated by assuming an image size of 4 m. The base case design radiation distribution and exchange factors were reevaluated using the VORRUM and VOREFM computer codes. The design also includes a new reflecting zone design with 0.625 m-long fins spaced 0.25 m apart. The performance

calculations demonstrate that using an image size of 4 m reduces the reflection row flux ratio to a disastrous 1.1.

Table 7.14.

Reflecting Row Fiber Design Sensitivity Studies

| Base Case | Thermal Efficiency | Total Efficiency | Minimum Flux Ratio for Fiber Zones | Reflecting Zone Flux Ratio |
|---|---|---|---|---|
| Preswirl = 0.05 T = 1367 K | 0.885 | 0.868 | 3.9 | 1.4 |
| T = 1189 K = 0.05 | 0.952 | 0.934 | 6.3 | 2.2 |
| T = 811 K = 0.05 | 0.979 | 0.960 | 6.7 | 2.8 |
| T = 1367 K = 0.10 | 0.861 | 0.836 | 3.1 | 1.1 |
| T = 1367 K = 0.05 rotation | 0.876 | 0.859 | 2.8 | 1.3 |

The impact of rotation as compared to preswirl was investigated and the results indicate that there is little impact on receiver efficiency but a substantial drop in the minimum fiber zone flux ratio. This is caused by the velocity distribution for preswirl more nearly approximating the distribution of incident energy. The preswirl vs. rotation sensitivity study for the shrouded concept did not yield the same result. The difference is that the core radius for

the reflecting zone is 9.0 m with a downcomer radius of 2.3 m, so limiting the maximum fiber velocity to 30 m/s produces low relative air velocities in the receiver interior. The shrouded design has a core radius of 5.0 m with a downcomer radius of 2.3 m, so the reduction in velocity is not as severe and rotation is more competitive with preswirl from the point of view of performance and minimum flux ratio.

## 7.7 SHROUDED FIBER DESIGN STUDIES

The unattractiveness of the fiber receiver with reflecting zones suggested that an alternate geometric loss reducer should be considered. A second method for reducing reradiation and reflection losses involves installing a shroud around the fiber core. This section describes the results of the evaluation of the shrouded fiber receiver. Section 7.7.1 describes the selection of the base case design. Section 7.7.2 presents the results of the performance analysis for the base case design and Section 7.7.3 discusses the results of a series of sensitivity studies conducted on the base case design.

### 7.7.1 Selection of Base Case Design

The base case for a shrouded receiver with a fiber core was selected by considering a variety of fiber core designs and shroud configurations. Three fiber core designs were evaluated; a fiber core with a radius of 2.5 m, a fiber core with a 3.75 m radius and a 5.00 m radius fiber core. Each design was analyzed using the VORRUM

computer code to predict the distribution of absorbed insolation and the VOREFM computer code to predict the exchange factors between zones. Three core heights were considered for each core design and each of these were combined with either two or four shrouds. This resulted in 11 designs for each fiber core. All designs were analyzed using the RATS performance code and the results are presented in Tables 7.15, 7.16 and 7.17.

The base case was selected by reviewing the results and picking the most attractive design. Two restrictions were imposed on the selection. First the aperture height had to be at least 6.0 meters. This aperture height exceeds the size of the largest heliostat image which, it was felt, would result in low intercept losses. Secondly, the base case minimum flux ratio was assumed to be at least 3.0. The impact of a lower minimum flux ratio was considered in the sensitivity study. Using these restrictions the base case design consisted of a receiver with a 5 m radius core, a height of 10 meters and an aperture height of 6 meters. The base case was assumed to include a shroud without packing, but including preswirl convection augmentation. The characteristics of the base case design are presented in Table 7.18.

The shroud design used with all shroud concepts is shown in Figure 7.6. The design is based on several simplifying assumptions. First, the aperture was assumed to be located solely on the side of the shroud. The distance between the core and the shroud was selected based on the 4-meter-aperture design and the design of the

Table 7.15.

2.5 m Meter Radius Core Designs

| Design | Receiver Radius (m) | Receiver Height (m) | Aperture Height (m) | Receiver Efficiency | Flux Ratio |
|---|---|---|---|---|---|
| 1 | 3.5 | 5.0 | 4.0 | 84. | 1.3 |
| 2 | 3.5 | 5.0 | 5.0 | 82. | 1.3 |
| 3 | 7.5 | 10.0 | 4.0 | 87. | 2.1 |
| 4 | 7.5 | 10.0 | 6.0 | 83. | 2.1 |
| 5 | 7.5 | 10.0 | 7.0 | 80. | 2.1 |
| 6 | 7.5 | 10.0 | 10.0 | 79. | 2.1 |
| 7 | 13.5 | 15.0 | 4.0 | 87. | 2.7 |
| 8 | 13.5 | 15.0 | 6.0 | 85. | 2.7 |
| 9 | 13.5 | 15.0 | 7.0 | 82. | 2.7 |
| 10 | 13.5 | 15.0 | 10.0 | 77. | 2.7 |
| 11 | 13.5 | 15.0 | 15.0 | 74. | 2.6 |

Table 7.16.

3.75 Meter Radius Core Designs

| Design | Receiver Radius (m) | Receiver Height (m) | Aperture Height (m) | Receiver Efficiency | Flux Ratio |
|---|---|---|---|---|---|
| 1 | 4.75 | 5.0 | 4.0 | 85. | 2.0 |
| 2 | 4.75 | 5.0 | 5.0 | 83. | 2.0 |
| 3 | 9.75 | 10.0 | 4.0 | 86. | 2.9 |
| 4 | 9.75 | 10.0 | 6.0 | 82. | 2.8 |
| 5 | 9.75 | 10.0 | 7.0 | 79. | 2.9 |
| 6 | 9.75 | 10.0 | 10.0 | 77. | 2.9 |
| 7 | 14.75 | 15.0 | 4.0 | 83. | 3.6 |
| 8 | 14.75 | 15.0 | 6.0 | 80. | 3.5 |
| 9 | 14.75 | 15.0 | 7.0 | 77. | 3.5 |
| 10 | 14.75 | 15.0 | 10.0 | 73. | 3.4 |
| 11 | 14.75 | 15.0 | 15.0 | 70. | 3.4 |

Table 7.17.

5.0 Meter Radius Core Designs

| Design | Receiver Radius (m) | Receiver Height (m) | Aperture Height (m) | Receiver Efficiency | Flux Ratio | |
|---|---|---|---|---|---|---|
| 1 | 6.0 | 5.0 | 4.0 | 85. | 2.4 | |
| 2 | 6.0 | 5.0 | 5.0 | 83. | 2.4 | |
| 3 | 7.5 | 7.5 | 4.0 | 85. | 3.0 | |
| 4 | 7.5 | 7.5 | 5.0 | 83. | 3.0 | |
| 5 | 7.5 | 7.5 | 6.0 | 81. | 3.0 | |
| 6 | 7.5 | 7.5 | 7.5 | 80. | 3.1 | |
| 7 | 11.0 | 10.0 | 4.0 | 83. | 3.6 | |
| 8 | 11.0 | 10.0 | 6.0 | 80. | 3.6 | Base Case |
| 9 | 11.0 | 10.0 | 7.0 | 77. | 3.6 | |
| 10 | 11.0 | 10.0 | 10.0 | 76. | 3.6 | |

(a) Does not include convective losses or intercept losses.

heliostat field. The image from the closest heliostat will strike the plane of the aperture with an angle of approximately $45^{o}$. The image from the most distant heliostat will strike the plane of the aperture with an angle of approximately $7^{o}$. In order to insure that some insolation would impinge on the top of the receiver core the

Table 7.18.

Shrouded Fiber Design

| Zone Characteristics | | | | | | | |
|---|---|---|---|---|---|---|---|
| Zone No. | Type | Height (m) | Depth (m) | Fin Spacing (m) | Convection Area ($m^2$) | Radiation Area ($m^2$) | Emissivity |
| 1 | Shroud | 10.0 | 6.0 | N/A | 879 | 879 | 1.0 |
| 2 | 0.0006 m dia fiber | 10.0 | 0.3 | 0.016 | 34 | 34 | 0.9 |
| 3 | 0.0006 m dia fiber | 10.0 | 0.3 | 0.012 | 43 | 43 | 0.9 |
| 4 | 0.0006 m dia fiber | 10.0 | 0.3 | 0.009 | 52 | 52 | 0.9 |
| 5 | 0.0006 m dia fiber | 10.0 | 0.3 | 0.0055 | 76 | 76 | 0.9 |
| 6 | 0.0006 m dia fiber | 10.0 | 0.3 | 0.0039 | 96 | 96 | 0.9 |
| 7 | 0.0006 m dia fiber | 10.0 | 0.3 | 0.0024 | 132 | 132 | 0.9 |
| 8 | 0.0006 m dia fiber | 10.0 | 0.3 | 0.0011 | 212 | 212 | 0.9 |
| 9 | 0.0006 m dia fiber | 10.0 | 0.3 | 0.0006 | 271 | 271 | 0.9 |
| 10 | 0.0006 m dia fiber | 10.0 | 0.3 | 0.0001 | 415 | 415 | 0.9 |
| 11 | Terminal Absorber | 10.0 | N/A | N/A | 578 | 144 | 0.9 |

Receiver Height = 10 m
Receiver Radius = 11 m
Air Flow Rate = 42.8 Kg/s
Product Design Temperature = 1367K

Aperture Height = 6.0 m
Blocking Factor = 0.05
Shroud Fill = No

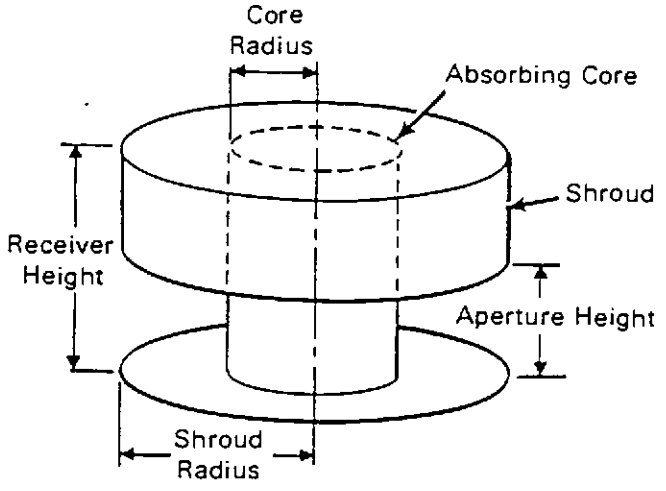


Schematic of Shroud

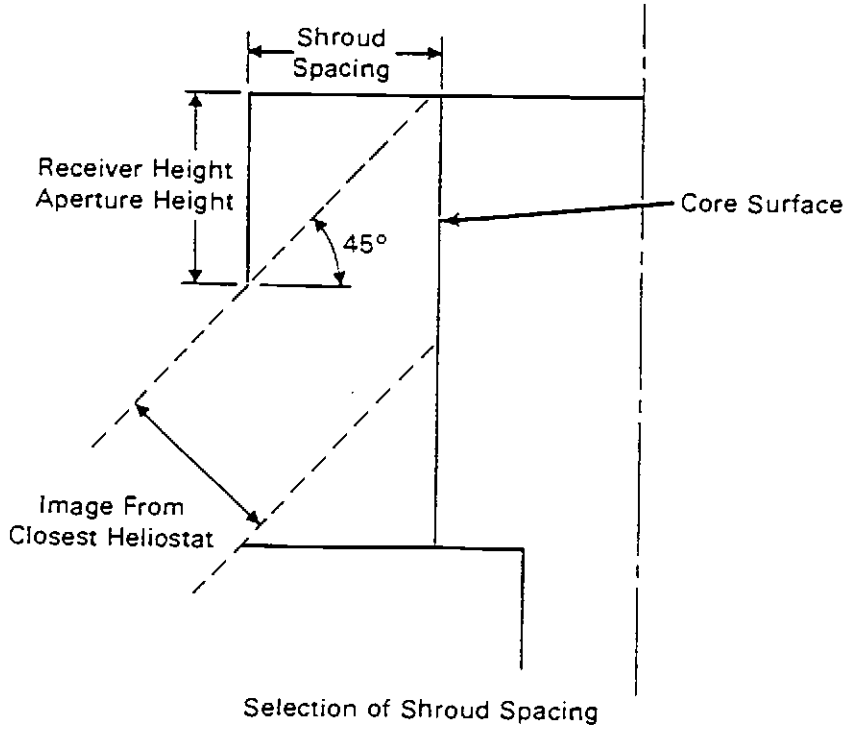


Selection of Shroud Spacing

Figure 7.6. Shroud Design

spacing between the core and the shroud must equal the receiver height minus the aperture height. The shroud spacing was kept constant for various aperture heights. The impact of varying the spacing was investigated in the sensitivity study. In all cases the requirement that the image from the nearest heliostat be able to strike the top of the fiber core was maintained.

### 7.7.2 Base Case Results

The results for the base case design are presented in Table 7.19. The base case shrouded-fiber design has a total receiver efficiency of 79.8% and a minimum flux ratio of 3.4. If we assume that convective losses are small, as they should be for a design which draws air into the receiver, then the total efficiency of the base case shrouded fiber design is approximately equal to the equivalent efficiency for the ceramic matrix receiver with a secondary concentration (Delaquil et al., 1983). The ceramic matrix receiver was the most efficient design considered in the Delaquil report. The flux ratio is a acceptable at 3.4 which implies that the peak flux can be 3.4 times as large as the average flux. The zone convective heat transfer coefficient is also of interest. The shroud convective heat transfer coefficient is 9.2 $W/m^2.K$ and is based on natural convection from the shroud walls. The convective heat transfer coefficient for the fiber zones vary from 310 $W/m^2.K$ to 630 $W/m^2.K$ demonstrating the very high heat transfer from small fibers. The convective heat transfer coefficient for the terminal absorber was

Table 7.19.

Shrouded Fiber Design Performance

| Zone | Zone Convective Heat Transfer Coefficient ($w/m^2 \cdot K$) | Zone Material Temperature (K) | Zone Air Exit Temperature (K) | Zone Flux Ratio | Zone Insolation (%) |
|---|---|---|---|---|---|
| 1 | 9.2 | 818 | 384 | 2.9 | 3.5 |
| 2 | 309.5 | 663 | 444 | 4.1 | 3.0 |
| 3 | 332.9 | 733 | 525 | 3.8 | 4.5 |
| 4 | 367.4 | 812 | 625 | 3.6 | 5.8 |
| 5 | 408.1 | 906 | 764 | 3.5 | 8.4 |
| 6 | 452.1 | 1000 | 906 | 3.7 | 10.1 |
| 7 | 500.4 | 1115 | 1061 | 3.6 | 13.9 |
| 8 | 549.3 | 1230 | 1213 | 3.5 | 18.9 |
| 9 | 592.7 | 1315 | 1311 | 3.9 | 17.6 |
| 10 | 629.6 | 1362 | 1362 | 5.2 | 11.6 |
| 11 | 5.0 | 1367 | 1362 | 46.5 | 0.7 |

Energy Balance

| | |
|---|---|
| Reflection Losses (w) | 1,238,923 |
| Convection Losses (w) | 0 |
| Reradiation Losses (w) | 11,542,768 |
| Useful Power (w) | 50,383,864 |
| Unaccounted Power (w) | 110,460 |
| Total | 63,276,014 |

Receiver Efficiency

| | |
|---|---|
| Receiver Absorptivity | 0.980 |
| Receiver Thermal Efficiency | 0.814 |
| Receiver Total Efficiency | 0.798 |

conservatively assumed to be 5.0 $W/m^2.K$. The material temperature and air temperature distribution and flux ratio is shown graphically in Figure 7.7.

### 7.7.3 Sensitivity Studies

The base case design was the subject of a variety of sensitivity studies. Each one examined the impact of a design variable on the performance of the receiver.

#### 7.7.3.1 Swirl Velocity

The first sensitivity study examined the impact of varying the tangential velocity of the air as it enters the receiver. Four cases were considered, the base cases with the maximum tangential air velocity equal to 30 m/s. Three other cases were included. These consisted of designs with a maximum tangential air velocity of 6 m/s, 18 m/s and 42 m/s. It was assumed that the normalized air velocity profile would be constant for all four cases. The results are presented in Table 7.20.

The results indicate that reducing the maximum air velocity from 30 m/s to 18 m/s has a negligible impact on the receiver efficiency but does result in a 9% reduction in minimum flux ratio. The 6 m/s case has a more significant drop in both efficiency and minimum flux ratio. The 42.0 m/s base results in an insignificant increase in efficiency and minimum flux ratio. The results of the sensitivity study suggest that the swirl velocity can be varied to reduce flow-

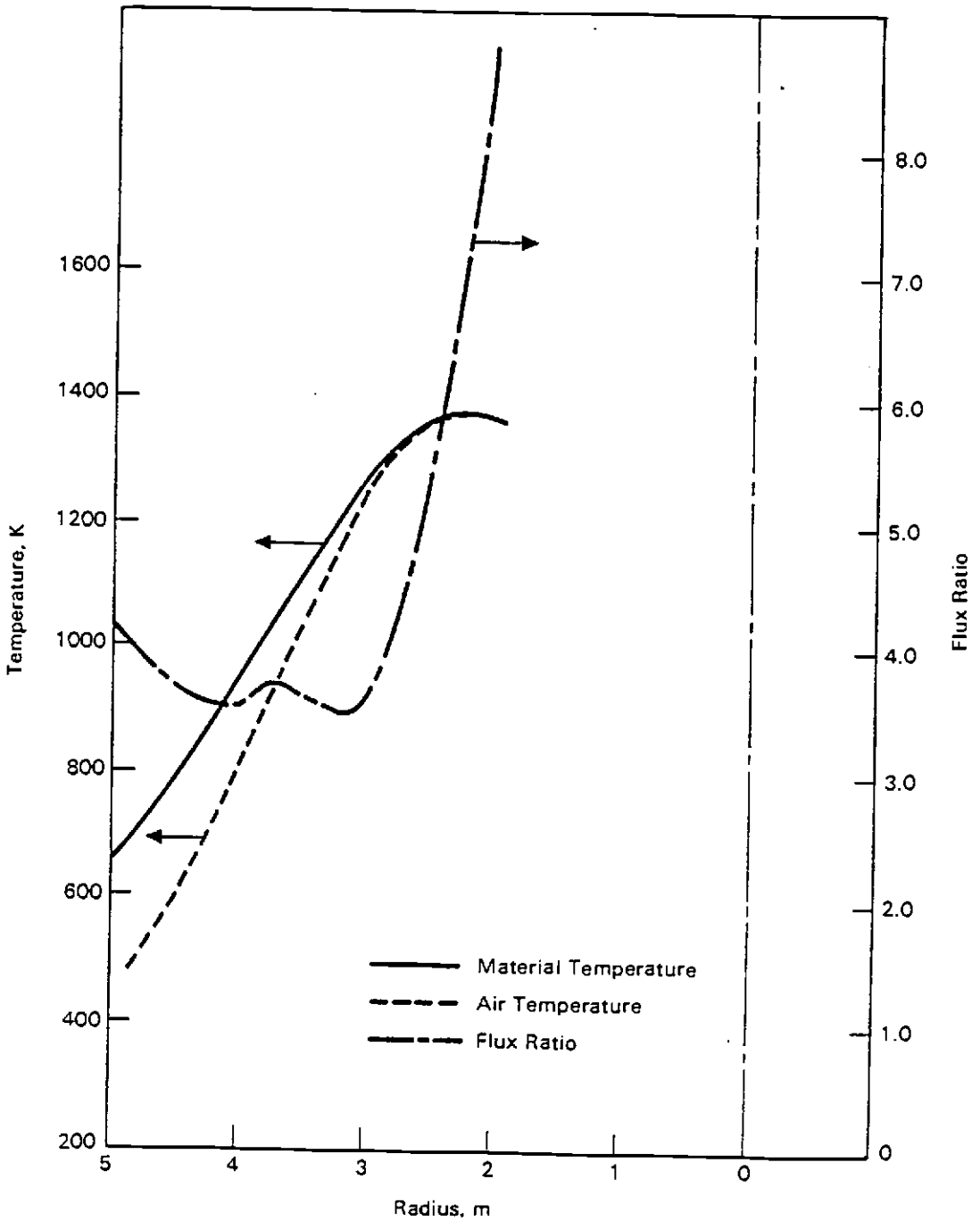


Figure 7.7. Temperature Distribution in Core for Shrouded Fiber design

induced fiber vibrations as long as the maximum velocity is above approximately 18 m/s.

Table 7.20.

Swirl Velocity Sensitivity Study

| | Maximum Velocity (m/s) | Receiver Efficiency | Minimum Flux Ratio |
|---|---|---|---|
| Base | 30.0 | 0.798 | 3.4 |
| Case 1 | 6.0 | 0.767 | 2.2 |
| Case 2 | 18.0 | 0.791 | 3.1 |
| Case 3 | 42.0 | 0.801 | 3.7 |

7.7.3.2 Fiber Diameter

The fiber diameter sensitivity study is related to the swirl velocity sensitivity study because both have a substantial impact on the convective heat transfer coefficient. Four cases were considered, the base case, and designs with absorbing fiber diameters of 0.0003 m, 0.0012 m, 0.0020 m. The results are presented in Table 7.21.

The impact of varying fiber diameter is primarily on minimum flux ratio where a doubling of the fiber diameter results in a 25% reduction in the minimum flux ratio. There is a reduction in receiver efficiency but it is not as severe as the reduction in minimum

Table 7.21.

Fiber Diameter Sensitivity Study

| | Fiber Diameter (m) | Receiver Efficiency | Minimum Flux Ratio |
|---|---|---|---|
| Base | 0.0006 | 0.798 | 3.4 |
| Case 1 | 0.0003 | 0.807 | 4.1 |
| Case 2 | 0.0012 | 0.781 | 2.6 |
| Case 3 | 0.0020 | 0.761 | 2.1 |

flux ratio. This suggests that there is not much opportunity for increasing the fiber diameter in order to improve the structural characteristics of the fiber. It should be noted that the increase in fiber diameter from 0.006 m to 0.0012 m increases the breaking strength from approximately 44.5 N (10 $lb_f$) to 186.8 N (42 $Lb_f$).

7.7.3.3 Rotation vs. Preswirl

Two methods for augmenting convection from the absorbing fibers have been considered; rotating a fraction of the absorbing fibers and inducing a free vortex by supplying angular momentum with a series of air jets at the shroud aperture. The two methods produce different velocity profiles. The rotation concept results in the highest tangential relative velocity occurring at the external row with the

relative velocity decreasing for interior zones until the innermost zones are reached. The interior zones are not rotated but the relative velocity increases because conservation of angular momentum leads to increasing air velocity. The preswirl method produces the lowest relative tangential velocity at the exterior zone with the relative tangential velocity increasing monotonically as the air moves deeper into the receiver. As Figure 7.8 demonstrates, the velocity distribution produced by the preswirl concept more closely approximates the distribution of insolation in the base case receiver. The performance analysis sensitivity study confirmed that the preswirl and rotation concepts have similar performance. The preswirl concept results in a receiver efficiency of 79.7% with a minimum flux ratio of 3.4 as compared to a receiver efficiency of 80.0% and a minimum flux ratio of 3.4 for the rotating design. In both cases the maximum fiber velocity was limited to 30 m/s.

#### 7.7.3.4. Shroud Packing

Energy convected away from the shroud is not lost as in other cavity designs because the heated air is being drawn into the receiver. In the base case, convection from the shroud was calculated based on the interior surface area of the shroud sides, roof, and floor. Convection was assumed to be limited to natural convection. In order to investigate the impact of adding a fiber packing to the shroud two additional cases were considered. In the first case enough fiber packing was added in order to provide 4000 $m^2$ of heat

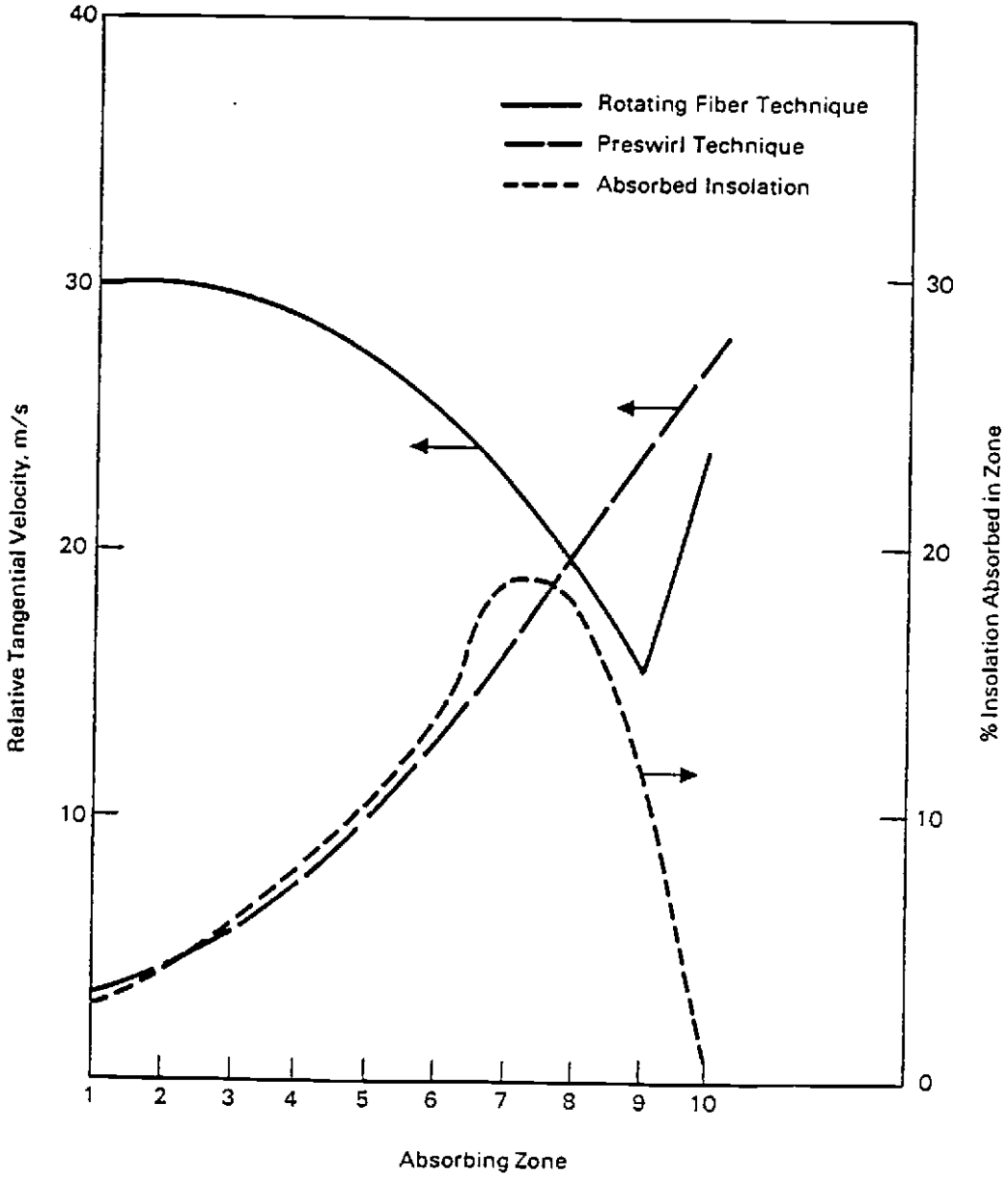


Figure 7.8. Velocity and insolation distribution for rotation and preswirl

transfer area with convective heat transfer coefficient based on natural convection from a fiber. The second case was similar except that 8000 $m^2$ of heat transfer area was added. Figure 7.9 shows be assumed the location of the fiber packing. The results are summarized in Table 7.22.

The results indicate a substantial performance improvement when fiber packing with 4000 $m^2$ of surface area is added. There is a 21% reduction in losses and a 10% improvement in flux ratio. Adding 4000 $m^2$ of surface area would result in the fibers filling 0.55% of the volume of the shroud with a fiber spacing of 0.0677 m or 13.5 diameters. The wide spacing should reduce the interference of one fiber on the natural convection from other fibers. The total mass of the 0.005 m diameter fibers is estimated to be approximately 20,000 kg. The 8000 $m^2$ case shows that additional packing above 4000 $m^2$ results in insignificant improvement in either receiver efficiency or flux ratio but with a substantial increase in fiber mass. Methods for augmenting convection from the fibers by forced convection offers the possibility for reducing the required heat transfer area and fiber mass but an investigation of these options was beyond the scope of the sensitivity study.

#### 7.7.3.5 Aperture Blocking

One method for reducing receiver thermal loss is to block a fraction of the circumferential area of the shroud aperture. An example of aperture blocking is shown in Figure 7.10 where 1/3 of the

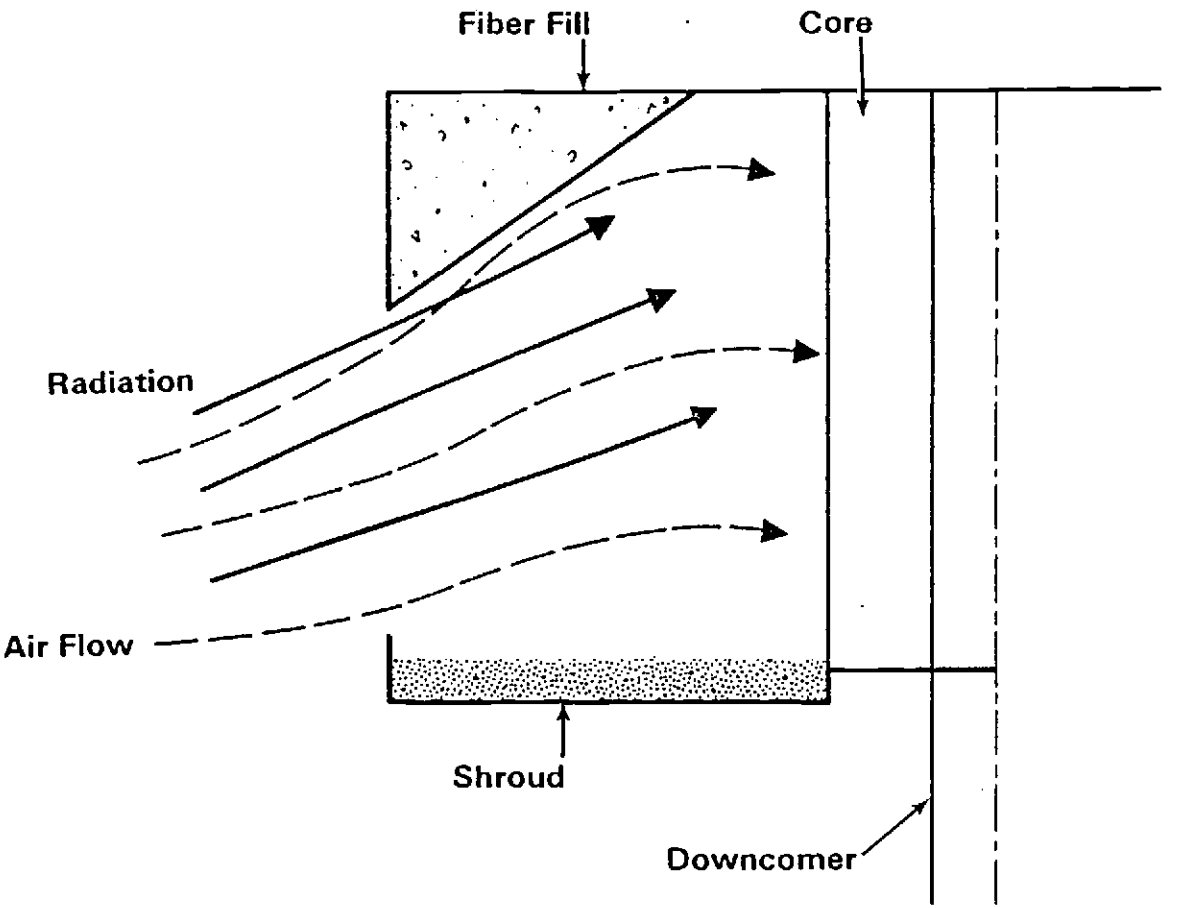


Figure 7.9. Shroud with packing

Table 7.22.

Shroud Packing Sensitivity Study

| Base | Heat Transfer Coefficient ($w/m^2 \cdot K$) | Receiver Efficiency (%) | Flux Ratio | Fiber Packing Volume Fraction | Fiber Spacing (m) | Fiber Mass kg |
|---|---|---|---|---|---|---|
| Base | 9.2 | 79.7 | 3.4 | -- | -- | -- |
| 4000 $m^2$ | 20.4 | 83.9 | 3.7 | 0.55% | 0.0677 | 20,000 |
| 8000 $m^2$ | 19.3 | 84.2 | 3.8 | 1.10% | 0.0479 | 40,000 |

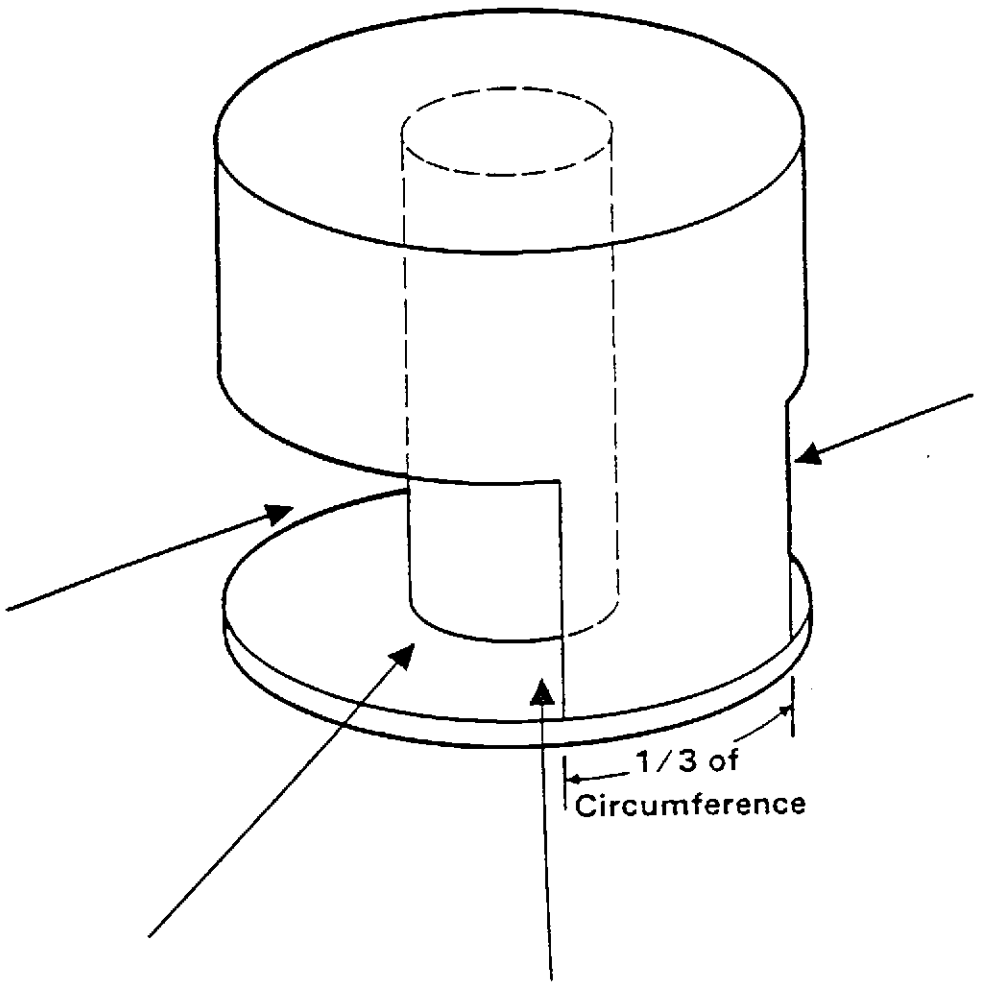


FIGURE 7.10. Shroud With Circumferential Blocking

aperture is blocked. The blocked area can either be combined in one area as shown in Figure 7.10 or be divided into two or more areas with apertures located between the blocked areas. The base case assumes that 5% of the aperture area is blocked. The blocked area is assumed to provide structural support for the roof. Two additional cases were considered, one involved aperture blocking of 25% of the aperture area while the second involved blocking 50% of the aperture area. The results are presented in Table 7.23.

Table 7.23.

Aperture Blocking Sensitivity Study

| | Aperture Blocking | Receiver Efficiency | Flux Ratio |
|---|---|---|---|
| Base | 0.05 | 0.797 | 3.4 |
| Case 1 | 0.25 | 0.819 | 2.7 |
| Case 2 | 0.50 | 0.857 | 1.8 |

The results indicate that aperture blocking can increase the receiver efficiency but at the cost of decreasing the flux ratio. This is caused by concentrating the flux which was spread over the whole aperture area into a smaller area, consequently the average flux is increased by a factor equal to 1/(1.0-aperture blocking).

7.7.3.6 Shroud Spacing

As indicated in Section 7.7.1 the distance between the absorber core and the shroud can be reduced so that it equals the receiver height minus the aperture height and still allows the image from the closest heliostat to strike the top of the absorbing area. The base case has a shroud spacing of 6.0 m, an aperture height of 6.0 m and a receiver height of 10.0 m so the minimum shroud spacing would be 4.0. Two alternative shroud spacings were considered. One design used a shroud spacing of 4.0 m while the second had a spacing of 5.0 m. The advantage of reducing the shroud spacing is that it results in a receiver with a smaller, overall radius. This would result in lower shroud cost, wind loading and tower cost. The results are presented in Table 7.24.

Table 7.24.

Shroud Spacing Sensitivity Study

| | Shroud Spacing | Receiver Efficiency | Minimum Flux Ratio |
|---|---|---|---|
| Base | 6 m | 0.79765 | 3.4 |
| Case 1 | 5 m | 0.79699 | 3.4 |
| Case 2 | 4 m | 0.79695 | 3.4 |

The results indicate that, over the range of shroud spacings considered, the shroud spacing has a negligible impact on either efficiency or flux ratio.

7.7.3.7 Product Temperature

The volumetric receiver may be used to produce hot air at temperatures other than 1367 K. In order to investigate the impact of product temperature on receiver efficiency, two additional cases were considered, one with a product temperature of 1089 K (1500 F) and 811 K (1000 F). The results are shown in Table 7.25. As expected, the lower product temperature results in a substantial improvement in efficiency and minimum flux ratio. The high minimum flux ratio implies that a substantial fraction of the aperture area can be blocked without exceeding a minimum flux ratio of 3.0. This would further improve the receiver efficiency. Case 2A is a design for producing 811 K product with a blocking factor of 0.5. At 811 K the predicted efficiency of .968 can be compared to the corresponding value of 0.876 for the Sanders receiver and 0.903 for a molten salt receiver (Delaquil et al., 1983).

7.7.3.8. Combined Shroud Packing and Aperture Blocking

The most attractive shrouded fiber design would include shroud packing and aperture blocking. Aperture blocking can improve receiver efficiency but at the cost of decreasing flux ratio. Two situations were considered-one where the minimum flux ratio was limited to

Table 7.25.

Product Temperature Sensitivity Study

| Case | Product Temperature (K) | Air Mass Flow Rate (kg/s) | Receiver Efficiency (%) | Minimum Flux Ratio |
|---|---|---|---|---|
| Base | 1367 | 42.8 | 0.797 | 3.4 |
| Case 1 | 1089 | 57.0 | 0.906 | 5.4 |
| Case 2 | 811 | 92.0 | 0.948 | 6.2 |
| Case 2a | 811 | 92.0 | 0.968 | 3.2 |

3.0, and one with a minimum flux ratio limited to 2.0. The base case design was included in the comparison. The results are presented in Table 7.26.

The results indicate that if a minimum flux ratio of 3.0 is acceptable then a receiver efficiency of 86.9% can be expected. If a minimum flux ratio of 2.0 is acceptable then an efficiency of 88% to 89% can be expected. The four cases with a flux ratio of 2.2 show that a variety of different designs can yield equivalent performance and minimum flux ratio. The selection among these four cases would be based on economics.

Table 7.26

Receiver Performance with Shroud Packing and Aperture Blocking

| Case | Radius (m) | Receiver Height (m) | Aperture Height (m) | Aperture Blocking | Receiver Efficiency (% | Minimum Flux Ratio |
|---|---|---|---|---|---|---|
| Base | 5 m | 10 m | 6 m | 0.25 | 0.864 | 3.0 |
| Base | 5 m | 10 m | 6 m | 0.45 | 0.890 | 2.2 |
| Case 1 | 5 m | 7.5 m | 6 m | 0.35 | 0.883 | 2.2 |
| Case 2 | 3.75 m | 10.0 m | 6 m | 0.30 | 0.887 | 2.2 |
| Case 3 | 2.5 m | 15.0 m | 6 m | 0.25 | 0.891 | 2.2 |

# CHAPTER 8.0

# CONCLUSIONS

This investigation of the Volumetric Air Heating Receiver emphasized two areas; analytical model development and conceptual design studies. In a similar manner the conclusions will be divided into two areas. Section 8.1 will present conclusions regarding the analytical model. Section 8.2 will describe the conclusion based on the design study reported in Chapter 7. In addition, section 8.3 will identify areas of possible future research. Section 8.4 presents a summary of conclusions.

## 8.1 CONCLUSIONS REGARDING THE ANALYTICAL MODEL

The analytical models used in this study were the result of a detailed literature review followed by extensive model development and experimental verification. In some cases the resulting analytical models were unique, therefore it is appropriate to review the models and draw conclusions on their suitability.

### 8.1.1 Radiation Heat Transfer Model

The Monte Carlo radiation heat transfer model proved to be an efficient and flexible design tool with accuracy appropriate to the level of detail in the design study. Other specific observations include:

- The Monte Carlo model allowed the inclusion of details, such as non-diffuse, non-gray surfaces, which could not have been simulated by any other method. This is particularly true when the large number of surfaces are considered.
- The cell to cell method of tracing a photon's path proved to be relatively simple to program and efficient to run. When the large number of surfaces is considered the alternative Monte Carlo method of calculating the distance between each surface, and the emitting point followed by identifying the shortest path would have proved to be very time consuming. As an example, if 100 surfaces were arrange in 10 zones, the cell to cell approach involves 20 major calculations per photon (10 calculations of photon impact locations, plus 10 zone to zone calculations) assuming that there is 10 photons/surface interactions. The alternative method would include 1000 major calculations per photon (100 impact location calculations for each of 10 interactions).
- The accuracy of the Monte Carlo model, based on a comparison with analytical and experimental results, was adequate for the level of detail used in the design study. The comparison with analytical results was excellent. The comparison with experimental results was

adequate particularly when the uncertainties in the experimental analysis were considered.

### 8.1.2 Convective Heat Transfer Model

The convective heat transfer model for convection between fins and the air includes substantial uncertainties, particularly in determining the proper way to model the forced convection. The natural convection and mixed convection models are based on correlations developed from experimental investigations but the physical arrangement in the volumetric receiver is quite different from that used in the experimental investigations. Fortunately, the uncertainties did not have a substantial effect on the overall results because the fin designs proved to be unattractive.

The convective heat transfer from fibers is better understood. A substantial body of experimental data exists and it has been used to develop correlations which are often used with hot wire anemometry. Natural and mixed mode convection are not significant factors because of the high forced convection associated with flow past very small diameter fibers.

### 8.1.3 Air Flow Modeling

The primary area of uncertainty associated with air flow modeling is the suitability of inducing a preswirl. Almost no work has been done in this area and it is difficult to draw any conclusions concerning preswirl. It appears that air can be successfully

distributed using manifold orifice designs but convective loss calculations are still uncertain.

### 8.1.4 Performance Model

The performance model proved to be efficient to operate and give reasonable results but the uncertainty in surface properties, heat transfer coefficients, air flow distribution, and statistically calculated exchange factors, all create uncertainties in the results. Given these limitations the performance model successfully fulfills its role as a tool for screening various designs. One clear conclusion is that the transient approach was superior to the steady state approach because of stability problems with the steady state approach.

## 8.2 CONCLUSIONS BASED ON PERFORMANCE RESULTS

The analytical models were used to investigate two fin designs, one fiber design with a fixed absorbing array and two fiber designs with augmented convection. In addition, detailed parametric investigations were conducted on the reflecting row fiber designs and the shrouded fiber designs. This section summarizes the conclusions drawn from the results presented in Chapter 7.0.

### 8.2.1 Radial Fin Design

The major problem with the radial fin design is the low convective heat transfer coefficient between the fins and the air. This results in both high material temperatures and thermal losses. Even

if convective heat transfer was increased by a factor of five, the receiver efficiency is still low and the design is not competitive with other concepts. Based on these results it was concluded that the radial fin design was not attractive and should not be investigated further.

### 8.2.2 Staggered Fin Design

As with the radial fin design, the staggered fin design has a major problem with the low convective heat transfer between the fins and the air. This results in high material temperatures and thermal losses. Even if convective heat transfer was increased by a factor of five, the receiver efficiency is still low and the design is not competitive with other concepts. Based on these results, it was concluded that the staggered fin design was not attractive and should not be investigated further.

### 8.2.3 Non Augmented Fiber Design

The non-augmented fiber design demonstrates better convective heat transfer than either fin design. This is due to the high convective heat transfer from very small ceramic fibers. Unfortunately the superior heat transfer is still not sufficient to make the non-augmented fiber design competitive with other concepts.

### 8.2.4 Reflecting Row Fiber Design

This concept includes a reflecting row for geometric loss reduction and augmented convection caused by inducing a preswirl. The results presented in section 7.6 indicate that convective heat

transfer resulting from the preswirl is sufficient to maintain the fiber at suitable temperature but the reflecting row concept did not prove to be successful. Based on the results of an extensive parametric study of the reflecting rows, one reflecting row design was selected. The performance of this design showed that the reflecting row temperature was approaching the upper temperature limit for the reflecting zone material. This was true even using optimistic assumptions for material optical properties. When more realistic optical properties were assumed, the reflecting row temperatures exceeded their maximum material temperature. While the reflecting row design does demonstrate high thermal efficiency, the high temperatures in the reflecting rows represent a critical weakness which prevents this concept from being a viable design.

### 8.2.5 Shrouded Fiber Design

This concept consists of a fiber absorbing array with preswirl and is enclosed in a shroud. The shroud replaces the reflecting row as the geometric loss reducer. A parametric study of shroud designs resulted in a base case design with

- 5.0 meters radius fiber filled core
- 10.0 meter receiver height
- 11.0 m shroud radius
- 6.0 m aperture height

This design has a predicted receiver efficiency of 80% and maximum flux ratio of 3.6. The predicted efficiency is approximately equal

to the next best high temperature air heating receiver reported by Delaquil et al. (1983).

A variety of sensitivity studies were conducted in order to investigate possible design improvements.

- o Swirl Velocity - Decreasing swirl velocity caused a small decrease in efficiency but substantially decreased minimum flux ratio.
- o Fiber Diameter - Increasing fiber diameter caused a small decrease in receiver efficiency but substantially decreased minimum flux ratio.
- o Rotation vs. Preswirl - Convective heat transfer augmentation by either rotation or preswirl demonstrates essentially similar performance. Therefore the selection of augmentation technique should be based on other factors such as cost.
- o Shroud Packing - Shroud packing results in a substantial increase in receiver efficiency and flux ratio.
- o Aperture Blocking - Aperture blocking results in a substantial increasing in receiver efficiency but has an accompanying decrease in flux ratio.
- o Shroud Spacing - The spacing between the core and the shroud has no significant impact on receiver efficiency or flux ratio.
- o Product Temperature - Decreasing product temperature increases efficiency and minimum flux ratios. In the

case of 811K product, the shrouded fiber design shows a distinct improvement in efficiency when compared to either a molten salt receiver or other air heating receiver (DeLaquil et al., 1983).

- Modified Base Case - The base case design was modified to include both shroud packing and aperture blocking. This resulted in a receiver efficiency of 86.9% for a minimum allowable flux ratio of 3.0 and 88.0 to 89.0% for a minimum allowable flux ratio of 2.0.

In summary, the shrouded fiber design with preswirl does show a significant improvement in performance when compared to other high temperature designs. In the case of 1367K product, the reduction in thermal losses is around 35%. If the product is air at 811K, the reduction in thermal losses is around 65%.

### 8.2.6 Summary of Performance Conclusions

The fiber design with preswirl for convective augmentation and a shroud for geometric loss reduction was selected as the most attractive design. Parametric studies indicated that the fiber design should include shroud packing and 25% aperture blocking. The resulting design demonstrates a significant efficiency increase when compared to other high temperature designs. The attainment of these performance improvements depend on the successful application of the "Preswirl" technique and the structural suitability of the ceramic fibers for this application.

## 8.3 SUGGESTED FUTURE RESEARCH

Based on the results of this study several areas for future research have been identified. These include, preswirl augmented convective heat transfer, ceramic fiber structural properties and economic optimization of the volumetric receiver.

### 8.3.1 Preswirl

The combination of preswirl and small heated fibers produced very high convective heat transfer with small parasitic energy consumption. This technique, if successful, could have application outside of solar thermal technology. The main area of uncertainty is in inducing the initial angular velocity. The use of multiple slot jets was selected for this study but a literature review indicated that there is almost no experience in this area. Future research could investigate the interaction between the heated fibers and the heat transfer fluid as it spirals into the inlet manifold.

### 8.3.2 Ceramic Fiber Structural Properties

The Nextel 312 ceramic fibers have many unique properties which may be of use to high temperature solar thermal applications. The combination of flexibility, good tensile strength, suitability for high temperatures and high absorptivity could be useful in future solar thermal designs. The primary uncertainty with the ceramic fibers was their structure suitability in an environment that includes high radiation flux, large temperature gradients, high air flow velocities and flow induced vibrations. An investigation of

fiber suitability including schemes for weaving the fibers into "fish net" absorbing surfaces would help in establishing ceramic fibers as a viable absorbing surface. As associated study could investigate cost effective methods of attaching the fibers to the receiver's surfaces. This was also an area of concern given the high ($1300^{o}K$) material temperatures.

### 8.3.3 Economic Optimization

The volumetric receiver has not been the subject of a careful design optimization. The actual value of efficiency enhancing devices such as shroud packing would depend on the cost of the enhancement and the value of the improved efficiency. In addition, the high cost components can be identified and lower cost design modification developed.

### 8.3.4 Optical Evaluation

The selection of the aperture height should be based on a trade-off study between the intercept losses and the thermal losses. The analysis of the heliostat field optics was beyond the scope of this study but future investigations should consider the impact of heliostat field performance on the receiver aperture design.

## 8.4 SUMMARY

The results of this study indicate that the volumetric receiver is the most efficient receiver concept for producing high temperature air for process heat applications. While economic factors were

beyond the scope of this study, PNL did develop a preliminary cost estimate (Drost et al., 1985) which indicated the cost of the volumetric receiver was higher than competing concepts. The net effect of efficiency improvements and higher cost resulted in the cost of energy produced by the volumetric receiver being essentially equal to competing designs. Based on this result PNL decided not to pursue the volumetric receiver because the potential efficiency improvements were not sufficient to justify the large scale, expensive research required to remove uncertainties in the preswirl concept and fiber viability. As a member of the PNL project the author concurs with this recommendation.

While it may not be appropriate to continue large scale and expensive research on the volumetric receiver, the concept is still the most efficient receiver for producing high temperature process heat and the design has not been the subject of a cost reducing optimization study. In addition, even if the complete concept does not ultimately appear attractive, various aspects of the concept, such as preswirl and ceramic fiber absorbing arrays, may be useful in other applications. Therefore, it appears that small scale research on various theoretical aspects of the volumetric receiver is justified, as is innovative design investigations into alternative concept configurations.

# REFERENCES

Apley, et al., 1980, Assessment of Generic Solar Thermal Systems for Large Power Applications, Vol. I, PNL-3533 Vol. I, Pacific Northwest Laboratory, Washington.

Bejan, A., and D. Poulikokos, V. 1980. "Fin Geometry for Minimum Entropy Generation in Forced Convection." Journal of Heat Transfer. 104:616-623.

Bird, S. P. et al. 1981. Assessment of Generic Solar Thermal Systems for Large Power Applications Vol. I, PNL-3533, Vol. I, Pacific Northwest Laboratory, Richland, Washington.

Bird, S. P. et al. 1982. Evauation of Solar Air Heating Central Receiver Concepts. PNL-4003, Pacific Northwest Laboratory, Richland, Washington.

Carnahan et al. 1969. Applied Numerical Methods, John Wiley & Sons, New York, New York.

Clausing, A. M. 1981. "An Analysis of Convective Losses from Cavity Solar Central Receivers." Journal of Solar Energy. Vol. 27, No. 4, pp. 295-300.

Corlett, R. C. 1966. "Direct Monte Carlo Calculations of Radiative Heat Transfer in Vacuum." Journal of Heat Transfer. 88(4):376-382.

DeLaquil, P., III, C. L. Young and J. E. Noring. 1983. Solar Central Receiver High Temperature Process Air Systems. SAND82-8254, Sandia National Laboratories, Livermore, California.

Drost, M. K. et al. 1985. Analysis and Design of the Volumetric Air Heating Receiver, Sandia Natural Laboratories, Livermore, California.

Drost, M. K., and L. L. Eyler. 1981. Preliminary Evluation of the Volumetric Air Heating Receiver. Paper No. 81-WA/Sol-26, American Society of Mechanical Engineers Winter Annual Meeting, Washington D.C., November 1981.

Duffie, A. J. and W. A. Beckman. 1974. Solar Energy Thermal Processes. John Wiley, New York.

Emery, A. F., C. J. Kippenhan, H. Mortazavi and R. Weiting. 1981. Computation of Radiation View Factors for Surfaces with Obstructed Views of Each Other. Paper No. 81-HT-57, In Proceedings from the 20th Joint ASME-AIChe National Heat Transfer Conference, Wisconsin, August 1981.

Halbleib, J. A. 1979. ACCEPT: A Three-Dimensional Electron/Photon Monte Carlo Transport Code Using Combinational Geometry. SAND79-0415, Sandia National Laboratories, Alburquerque, New Mexico.

Hammersley, J. M. and D. C. Handscomb. 1964. Monte Carlo Methods, John Wiley & Sons, Inc., New York.

Howell, J. R. 1968. "Monte Carlo Applications in Heat Transfer." In Advances in Heat Transfer. Vol. 5.

Howell, J. R., and R. R. Bannerot. 1974. The Evaluation of Surface Geometry Modification to Improve the Performance of Solar Energy Collectors. NSF/RANN/SE/GI-41003/TR/74/1. National Science Foundation.

Kays, W. M., and M. E. Crawford. 1980. Convective Heat and Mass Transfer, 2nd ed., McGraw-Hill, pp. 134-139.

Laity, W. W. et al., 1979, Assessment of Solar Options for Small Power Systems Applications, Vol. I: Executive Summary, PNL-4000 Vol. I, Pacific Northwest Laboratory, Richland, Washington.

Los Alamos Scientific Laboratories. 1978. MCNP: A General Monte Carlo Code for Neutron and Photon Transport. Los Alamos Scientific Laboratory, NW(USA), July 1978.

Mishkin, M. and Kowalski, G. J. 1983. Application of Monte Carlo Techniques to Steady-State Radiative and Conductive Heat Transfer Problems Through a Participitating Medium. ASME Paper No. 83-WA/HT-27. American Society of Mechanical Engineers.

Modest, M. F. 1978. "Three Dimensional Radiative Exchange Factor for Non-Gray, Non-Diffuse Surfaces." Numerical Heat Transfer. 1:403-416.

Morgan, V. T. 1973. "The Heat Transfer from Bare Stranded Conductors by Natural and Forced Convection in Air." International Journal of Heat and Mass Transfer. 16:2023-2034.

Morgan, V. T. 1975. "The Overall Convection Heat Transfer from Smooth Circular Cylinders." In Advances in Heat Transfer. 8:199-264.

Siebers, D. L., R. G. Schwind and R. J. Moffat. 1983. Experimental Mixed Convection Heat Transfer from a Large Vertical Surface and Horizontal Flow. HMT-36, Stanford University, California.

Siegel, R. and J. R. Howell. 1972. Thermal Radiation Heat Transfer. McGraw-Hill, New York, New York.

Toor, J. S. 1967. Radiant Heat Transfer Analysis Among Surfaces Having Direction Dependent Properties by the Monte Carlo Method. M. S. Thesis, Purdue University.

Toor, J. S., and R. Viskanta. 1968. "A Numerical Experiment of Radiation Heat Interchange by the Monte Carlo Method." Journal of Heat and Mass Transfer. 11:883-897.

Viskanta, R., et al. 1978. "Radiation Characteristics of Multiple-Plate Glass Systems." International Journal of Heat and Mass Transfer. 21:815-818.

Weiner, M. M., et al. 1965. Radiative Interchange Factors by Monte Carlo. ASME Paper No. 65-WA/HT-51. American Society of Mechanical Engineers.

Wieting, A. R. 1975. "Empirical Correlations for Heat Transfer and Flow Friction Characteristics of Rectangular Offset-Fin Plate-Fin Heat Exchangers." Journal of Heat Transfer, 97(3):488-490.

Welty, J. R., C. E. Wicks, and R. E. Wilson. 1976. Fundamentals of Momentum, Heat and Mass Transfer. John Wiley and Sons, Inc., New York.

Yang, R. S. 1981. Heat Transfer Throughout a Randomly Packed Bed of Spheres by the Monte Carlo Method. Ph.D. Thesis, University of Texas.

3M Company. Properties of 3M Nextel 312 Ceramic Fibers, 3M Company, St. Paul, Minnesota.

# APPENDICES

# APPENDIX A

## RATS USERS GUIDE

# APPENDIX A

## RATS USERS GUIDE

The RATS (Radiation And Thermal Simulation) computer code is designed to use a transient simulation to obtain an equilibrium temperature distribution and performance parameters for volumetric type solar central receiver. The users guide will describe the important features of the code with particular emphasis on the information required to run the code. The theoretical justification for the models used in RATS is included in the body of this report. Section A.1 will describe the general approach used in the code. Section A.2 will discuss the code structure and the contents of the subroutines. Section A.3 will present the code inputs while Section A.4 will present a description of the codes output.

### A.1.0 GENERAL APPROACH

Program RATS is written in FORTRAN 77 for a CDC 3300 computer. It is intended to be used as a design tool in the design and analysis of a variety of volumetric receiver designs. The required output consists of the air and material temperatures in a volumetric receiver in addition to reradiation losses and parasitic power consumption. The method used in RATS consists of using a transient simulation to obtain the equilibrium temperature distribution. The receiver is assumed to start at ambient temperature and solar energy is added to the various zones of the receiver causing the zone

temperature to increase until the loss of energy from the zone by radiation and convection equals the amount of energy being added to the zone by insolation. A fictitious thermal mass is assigned to each zone and can be adjusted to avoid large temperature variations between time steps. Large temperature swings can cause zone temperatures to become negative which is both physically impossible and causes the program execution to terminate with one of a variety of error messages.

At time step t = 0, the receiver is assumed to be at ambient temperature. During successive time steps, energy in the form of insolation is added to the receiver. At any time step t, all temperatures are known from the previous time step calculations and the computational procedure consists of the following steps:

1) With all temperatures known at time t, the program calculates the net radiation heat transfer, convection to the air and insolation.
2) The program conducts a heat balance on each zone to determine the energy added to the zone during time step t.
3) The program calculates the t + 1 zone temperature based on the energy added to the zone and the fictitious thermal mass.
4) The zone temperatures at time step t + 1 are compared with those at time step t. If the zone temperatures

have converged the receiver has reached its equilibrium temperature.

5) The product temperature is compared with the design product temperature. If the produced temperature has not converged to the design temperature the amount of energy added to the zones as insolation is modified and a new equilibrium temperature distribution is obtained. This procedure is repeated until the product temperature approximately equals the desired air temperature.

6) After both zone temperature and produce temperature has converged. The parasitic power requirements are calculated and the results printed.

The results of a large number of simulations demonstrate that for the cases considered, the computer code always converges if the assumed thermal mass is sufficiently large. The original version of the code calculated a steady state temperature distribution. This approach resulted in many problems with obtaining convergence and was ultimately dropped for that reason. Increasing thermal mass has two undesirable characteristics. First, the number of time steps required for zone temperature convergence are increased. This results in an increase in computer costs. Second, the change in zone temperatures between time steps is small. If the convergence criteria is too large, this can result in the apparent convergence of zone temperatures long before the receiver has reached the steady state temperature distribution.

The output from RATS includes reflection losses and convective losses to ambient. Neither of these values are calculated in the code. They are input by way of the isolation distribution for reflection losses or by variable CVLPCT for convection losses. These results are included for completeness.

## A.2.0 CODE STRUCTURE

The RATS computer code consists of eight subroutines and three functions. The code includes two major iterative loops, the interior loop obtains zone temperature convergence. The exterior loop obtains produce temperature convergence. The structure of the code is shown on the flow chart in Figure A1.

The program driver RATS calls subroutine RATIN which reads input data from the appropriate data file, RATST which calculates non-temperature dependent variables and sets initial conditions and EFACT which processes exchange factors to insure reciprocity. With the initial conditions set, RATS call subroutine RATQ, which calculates the net radiation heat transfer between individual receiver zones and between the zones and ambient. This is followed by a RATTP which calculates convective heat transfer. The coefficients are calculated by calling subroutine CONV which determines the convective heat transfer coefficients. RATTP then calculates the new zone temperatures. Zone temperature convergence is checked in RATS and a new time step is executed if zone temperatures have not converged. If zone temperature convergence has been obtained, product temperature

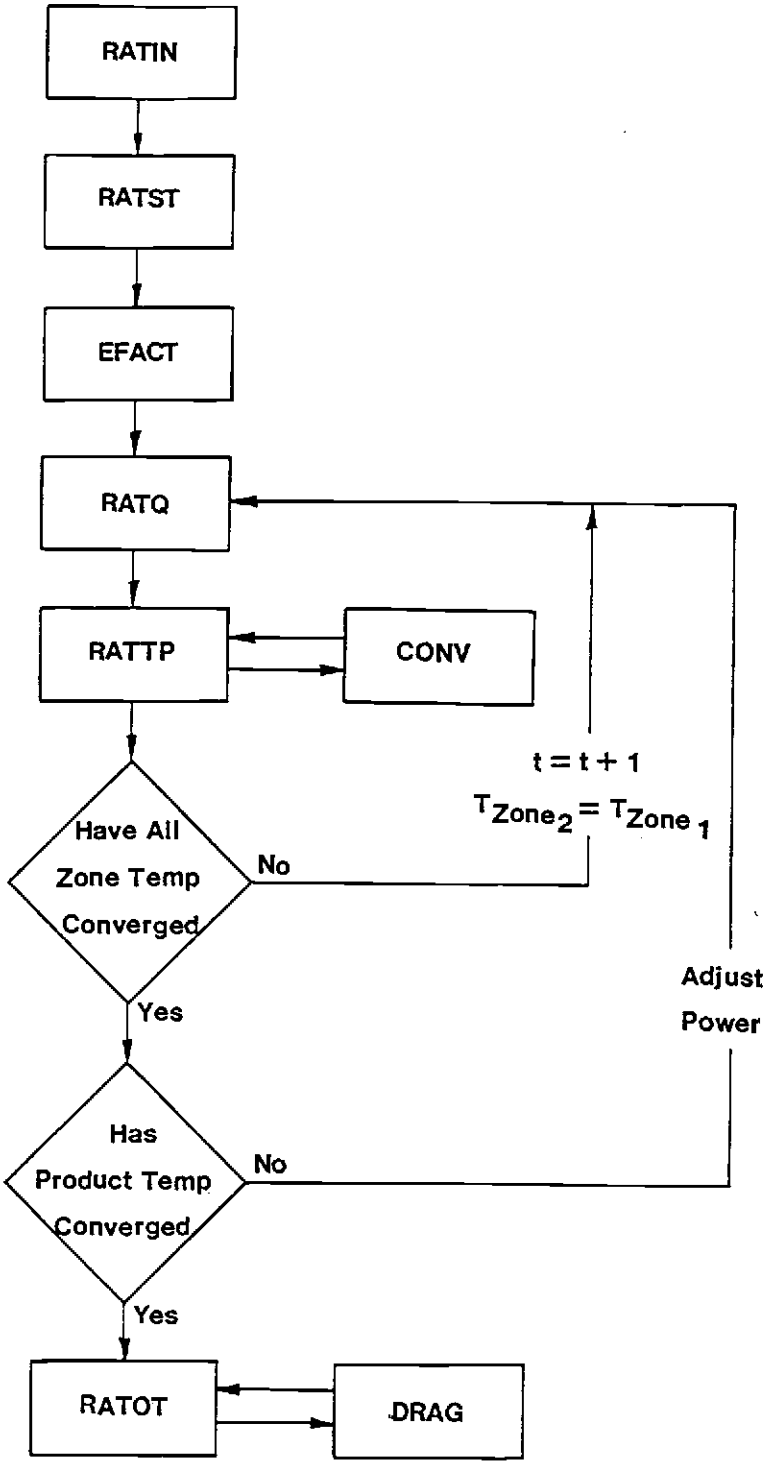


Figure A1. RATS Structure

convergence is checked and a new power level is assigned if product temperature convergence does not meet the convergence criteria. When both convergence criteria have been met RATS calls subroutine RATOT which prints out a summary of both inputs and results. RATOT calls subroutine DRAG to calculate parasitic power requirements for ceramic fiber volumetric receiver designs with rotating fiber zones.

Each subroutine will now be discussed, but a detailed presentation of the analytical model is not included. The development, description and verification of the analytical model is included in the body of the report.

RATIN - Subroutine RATIN reads input data from the appropriate data file. The data is arranged in three groups; control variables and general data, zone properties, and exchange factors. The various input parameters are described in A.3.0.

RATST - Subroutine RATST executes a variety of tasks which must be completed before the transient simulation starts. the zone radius, and flow areas are calculated. The equilibrium air, and zone temperatures are estimated so that the fictitious thermal mass can be calculated. Initial zone and air temperatures are set equal to ambient temperature and initial insolation rate is calculated based on the design power level. Zone material temperature limits are set based on zone material and both convection losses to the surroundings and reflective losses to the surrounding are calculated.

In the flow area calculations, the flow area is reduced to account for flow area being blocked by fins or pins. This is calculated based on the flow area ratio ZFARA except for ceramic fibers where the analytical model has aggregated many rows into one row. Using ZFARA in this case would produce an unjustifiably high air flow velocity, therefore, all fiber zones are assumed to have individual fibers separated by 20 diameters. Therefore, a constant value of .95 is used for ZFARA.

EFACT - Subroutine EFACT processes the input exchange factors to insure that reciprocity relations are maintained. Simulations using RATS have indicated exchange factor reciprocity between zones must be obtained or the code will not converge. If exchange factors are not processed to insure reciprocity the sum of the net radiation between all zones, including the surroundings as one zone, will not be zero. This results in an unjustified addition or deduction in the receiver energy balance during each time step which results in either an inaccurate answer or non convergence caused by a constantly increasing zone temperatures. It is expected that the exchange factors will be calculated by a Monte Carlo model similar to that in the VORVFM computer code. Due to the statistical nature of Monte Carlo modeling, it is unlikely that exchange factor reciprocity will be accurately maintained, therefore, EFACT calculated all of the exchange factors by assuming exchange factors from the internal

to external zones are correct and then using the receprocity relation to calculate the exchange factors from the external to internal zones. The appropriate reciprocity relation is

$$B_{ij}A_i\varepsilon_i = B_{ji}A_j\varepsilon_j$$

The exchange factor from a zone to itself is calculated by subtracting the sum of the exchange factors to other zones from 1.00.

RATQ - Subroutine RATQ calculates the net radiation heat transfer between zones using the exchange factors calculated in EFACT. The reradiation losses is the net radiation heat transfer to the surrounding (designated Zone (0)).

RATTP - Subroutine RATTP calculates the convective heat transfer for time step t + 1 based on the zone temperature and air temperature at time t. The convective heat transfer coefficients are calculated by subroutine CONV which is called in RATTP. They are used to calculate the t + 1 zone exiting air temperature which is then used to calculate the t + 1 bulk air temperature. An energy balance for the air in a zone gives the amount of energy convected away from the zone. An energy balance on the material in the zone determines how much energy is added to the zone material and this along with the fictitious thermal mass is used to determine the new zone temperature. The final calculation checks all zones for convergence. If any zone does not converge a flag JA is set equal to 0, otherwise it is

set equal to 1. The driver checks for JA = 1 in which case convergence has been obtained.

CONV - Subroutine CONV calculates the convective heat transfer coeffieients for either fins or fibers. Both forced and natural convective heat transfer coefficients are calculated and combined into one convective heat transfer coeffieient.

RATOT - Subroutine RATOT calculates several performance figures-of-merit and and then prints out results. The performance parameters calculated in RATOT includes reflection losses, receiver efficiencies, useful energy added to the air, zonal reradiation losses, the flux ratio and parasitic power requirements. RATOT calls subroutine DRAG in order to calculate parasitic power requirements. Subroutine RATOT also prints out a summary of the results.

DRAG - Subroutine DRAG determines which zones, if any, consist of rotating ceramic fibers, for these zones DRAG calculates the number of fibers and drag per fiber. The total drag on the rotating zones is then calculated along with the installed power required to overcome the drag.

FUNCTION CP - This function calculated the value of the constant pressure specific heat (J/KG-K) of air as a function of temperature using

$$CP = 1000* (A0 + A1*T + A2*T^2 + A3*T^3 + A4*T^4 + A5*T^5)$$

where A0 = 1.0928185

A1 = -7.30627956E-04

A2 = 1.93144568E-06

A3 = -1.80015117E-09

A4 = 7.72805428E-13

A5 = -1.25104697E-16

FUNCTION VISC - This function calculates the value of the temperature dependent viscosity (KG/M-S) of air using

$$VISC = A0 + AA*T + A2*T^2 + A3*T^3$$

where A0 = 3.98007586E-06

A1 = 5.49121523E08

A2 = -2.17252314E-11

A3 = 4.84816881E-15

FUNCTION COND - This function calculates the value of the thermal conductivity of air (KW/M-K) using

$$COND = A0 + A1*T = A2*T^2 + A3*T^3$$

where A0 = 3.8913544E-6

A1 = 8.10317932E-8

A2 = -2.35657904E-11

A3 = 6.4678539E-15

## A.3.0 INPUT PARAMETERS

The input data for RATS consists of three groups; control variables and general receiver characteristics, zone characteristics and

exchange factors. The data in the first two groups are determined from the receiver design. The data in the third group are normally taken from the output of VOREFM code while one variable (QINSF) is taken from the output of the VORRUM computer code. In the current version of the code, the data is entered from a separate data file. The input data file, including the appropriate format, is shown graphically in Figure A.2. A sample data file is shown in Figure A.3. In this section each input will be described separately.

INPUTS

EPS - This represents the convergence criteria for zone temperature. When the difference between the t + 1 and t time step zone temperature divided by the time step t zone temperature is less than EPS for all zones the receiver temperature distribution has converged.

EPS2 - This represents the convergence criteria for produce exit temperature. When the difference between the calculated produce temperature and the design product temperature (TAIRE) divided by the design produce temperature is less than EPS2 the calculated product temperature has converged to the design produce temperatures.

ITMAX - This is the maximum number of iterations to obtain zone temperature convergence. If two temperatures have not converged, a warning comment is printed and the results for the last iteration are output.

| EPS | EPS2 | ITMAX | ITMAX2 |
|---|---|---|---|
| F10.4 | F10.4 | I10 | I10 |

| N | POWERL |
|---|---|
| I10 | F12.2 |

| TAIR1 | RCVRR | RCVRH | AIRMAS | PINDI | RPM | ETS | TAIRE |
|---|---|---|---|---|---|---|---|
| F10.4 | F10.4 | F10.4 | F10.4 | F10.4 | F10.4 | F10.4 | F10.4 |

| EMEFF | CVLPCT |
|---|---|
| F10.4 | F10.4 |

| | |
|---|---|
| QINSF | 6F12.2 |
| ZTHCH | 8F10.4 |
| ZFARA | 8F10.4 |
| ZHIGH | 8F10.4 |
| ZEMIS | 8F10.4 |
| ZSARA | 8F10.4 |
| ZRADA | 8F10.4 |
| IZONE | 8I10 |
| IROT | 8I10 |
| DRAGF | 8F10.4 |

| F(0,0) | F(0,1) | F(0,2) | F(0,3) | F(0,4) | F(0,5) | F(0,6) | F(0,7) | F(0.8) | F(0.9) | 10F8.6 |
|---|---|---|---|---|---|---|---|---|---|---|

.
.
.

Figure A.2 Input Format

PROGRAM RATS

PROGRAM RATS DETERMINES THE ZONE TEMPERATURE
RERADIATION LOSSES AND PRODUCT TEMPERATURE
FOR THE VOLUMETRIC AIR HEATING RECEIVER

INPUT ZONE PROPERTIES

| ZONE NO. | ZONE DEPTH (M) | ZONE FLOW AREA RATIO | ZONE HEIGHT (M) | ZONE CONVECTIVE HEAT TRANSFER AREA (SQR-M) | ZONE RADIATION HE AT TRANSFER AREA (SQR-M) | ZONE MTRL | ZONE EMISSIVITY | ZONE RELATIVE VELOCITY RATIO | ZONE INSOLATION (WATTS) |
|---|---|---|---|---|---|---|---|---|---|
| 1 | 2.10 | .950 | 5.00 | 3142.00 | 3142.00 | 2 | .20 | 1.0000 | 4962338.70 |
| 2 | .60 | .964 | 5.00 | 28.88 | 28.88 | 1 | .90 | .3400 | 2231543.56 |
| 3 | .60 | .952 | 5.00 | 34.31 | 34.31 | 1 | .90 | .4500 | 2649316.71 |
| 4 | .60 | .938 | 5.00 | 38.90 | 38.90 | 1 | .90 | .6300 | 3222079.96 |
| 5 | .60 | .902 | 5.00 | 53.75 | 53.75 | 1 | .90 | .8600 | 4782542.95 |
| 6 | .60 | .867 | 5.00 | 64.62 | 64.62 | 1 | .90 | 1.2000 | 5606334.62 |
| 7 | .60 | .800 | 5.00 | 83.40 | 83.40 | 1 | .90 | 1.7200 | 7587694.72 |
| 8 | .60 | .647 | 5.00 | 132.60 | 132.60 | 1 | .90 | 2.4400 | 10992769.21 |
| 9 | .60 | .500 | 5.00 | 165.90 | 165.90 | 1 | .90 | 3.5400 | 9523199.95 |
| 10 | .60 | .142 | 5.00 | 254.90 | 254.90 | 1 | .90 | 5.0100 | 6464257.93 |
| 11 | .60 | .900 | 5.00 | 289.00 | 72.00 | 3 | .80 | 1.0000 | 318309.10 |

OTHER INPUT DATA

CONTROL VARIABLES
ZONE TEMP CONVERGENCE CRITERIA = .00001
PRODUCT TEMP CONVERGENCE CRITERIA = .005
ZONE TEMP ITERATION LIMIT = 800
PRODUCT TEMP ITERATION LIMIT = 11
FICTIOUS THERMAL MASS MULTIPLIER = 125.

RECEIVER DESIGN DATA
RECEIVER RADIUS (M) = 10.
RECEIVER HEIGHT (M) = 5.
FIBER DIAMETER (M) = .0006
ROTATION SPEED (RPM) = 25.
AIR MASS FLOW RATE (KG/SEC) = 42.8
PRODUCT DESIGN TEMPERATURE (K) = 1367.

SHROUD DESIGN DATA
APERATURE HEIGHT (M) = 4.99
APERATURE BLOCKING FACTOR = 0.
SHROUD FIBER FILL INDICATOR = 0
FIBER FILL FIBER DIAMETER (M) = .005

AMBIENT CONDITIONS
AMBIENT AIR TEMPERATURE (K) = 294.
AMBIENT TEMPERATURE FOR RADIATION
HEAT TRANSFER (K) = 294.

EXTERNALLY CALCULATED PERFORMACE PARAMETERS
REFLECTION LOSS (%) = 3.005599999999
CONVECTIVE LOSS (%) = 0.

Figure A3. Sample Data

ITMAX 2 - This is the maximum number of iterations to obtain product temperature convergence. If the calculated and design product temperatures have not converged, a warning comment is printed and the results for the last iteration are output.

N - This is the maximum number of zones in the receiver with ambient being zone 0 and the terminal absorber being zone N.

POWERL (watts) - This represents the design power level (power being transferred to the air).

TAIR1 ($^{O}$K) - ambient temperature.

RCVRR (meters) - outside radius of external receiver zone.

RCVRH (meters) - height of external receiver zone.

AIRMAS (Kg/sec) - air mass flow rate. Note that, POWERL, AIRMAS, and TAIRE are not independent, when two are specified (normally POWERL and TAIRE). The third must be calculated.

PINDI (meter) - The diameter of one ceramic fiber in a fiber design. If no fiber zones are included in the design this variable should be set to zero.

RPM (revolutions per minute) - The rotation speed for rotating components of the rotating fiber design. For non-rotating designs this should be set to zero.

ETS - This represents the thermal mass multiplier. The variable determines the amount of fictitious thermal mass added to the receiver for the transient calculations. A large ETS means that the zone temperature will increase slowly from time step to time step. If the program is not converging or terminates due to negative zone

temperatures ETS should be increased. An increase in ETS can require a decrease in EPS because temperature may converge even if the equilibrium temperature distribution has not been obtained. An increase in EPS is required if "unaccounted energy" in the output is a significant fraction of the energy added to the receiver.

TAIRE ($^{o}$R) - design product temperature

EMEFF - This represents the efficiency of motor and rotating mechanism. EMEFF is the installed power divided by power to overcome drag.

CVLPC(%) - This represents convective losses and is calculated external to the code. CVLPCT equals convective losses divided by design power level multiplied by 100.

QINSF(I) - This represents the decimal fraction of energy absorbed in Zone I. The summation of QINSF for all zones should equal 1.0 minus reflection losses in decimal fractions.

ZTHCH (I) (meters) - Depth of Zone (I).

ZFARA (I) - Ratio of flow surface area to total surface area in Zone I. The surface area of a cylinder with the zone average radius and height equals the flow area plus the area blocked by fins or fibers. ZFARA(1) represents the flow area divided by the total surface area for zone I.

ZHIGH (I) (meters) - The height of the zone, normally equal to RCVRH.

ZEMIS(I) - emissivity for Zone (I). Note that the zone emissivity is modeled as a constant and not as being temperature dependent.

ZSARA(I) (Sqr-meters) - Surface area in Zone (I) for convection. Normally this is the sum of all surface in the zone. For a fiber design this would be given as the surface area of one fiber times the total number of fibers in the zone.

ZRADA (I) (sqr-meters) - Surface area in Zone (I) for radiation heat transfer. Normally this equals ZSARA with the possible exception of the terminal absorber where convection occurs from the internal surface but radiation heat transfer from the internal surface is ignored because that surface of the terminal absorber primarily "sees" itself.

IZONE (I) - Zone material indicator ( 1 = Nextel 312 Fiber, 2 = Aluminum, 3 = silicone carbide, 4 = shroud).

IROT (I) - Zone rotation indicator (0 = zone does not rotate, 1 = zone does rotate).

DRAGF (I) - Zone relative velocity coefficient. This represents the actual zone relative velocity for a fiber moving through the air divided by the ideal relative velocity, where the ideal velocity assumes no circumferential acceleration of the air. By proper selection RPM and DRAGF any pin to air relative velocity profile can be obtained. This allows the simulation of designs using preswil where the relative pin to air velocity profile is calculated external to the code.

F (I,J) - Exchange factor from Zone I to Zone J. The first line (or lines if more than ten zones are involved) consists of F (0, J)

where J ranges from 0 to n. The last line (or lines) consists of F (n, J) where J ranges from 0 to n.

## A.4.0 DESCRIPTION OF OUTPUT

The output from RATS consists of two components, a summary of the input variables and the results. A sample of the output is included in Figure A.4. Except where the output is self explanatory, each output parameter will now be briefly described.

Zone Depth - see ZTHCK

Zone Flow Area ratio - see ZFARA

Zone height - see ZHIGH

Zone convective heat transfer areas - see ZRADA

Zone material indicator - see IZONE

Zone emissivity - see ZEMIS

Zone relative velocity ratio - see DRAGF

Zone insolation (watts) - This represents the amount of energy absorbed in a given zone. It is calculated from QINSF and the current POWERL adjusted to insure the proper air exit temperature.

Zone temperature convergence criteria - see EPS

Product temperature convergence criteria - see EPS2

Zone temperature iteration limit - see ITMAX

Product temperature Iteration limit - see ITMAX2

Receiver radius - RCVRR

Fiber diameter - see PINDI

RESULTS

| ZONE NO. | ZONE EXCHANGE FACTOR | ZONE CONVECTIVE HEAT TRANS COEFFICIENT (W/SQR-M-K) | ZONE MATERIAL TEMP (K) | ZONE BULK AIR TEMP (K) | ZONE EXIT AIR TEMP (K) | ZONE NET RADIATION HEAT TRANS (WATTS) | ZONE CONVECTION TO AIR (WATTS) | ZONE RADIATION LOSS TO AMBIENT (WATTS) | ZONE FLUX RATIO |
|---|---|---|---|---|---|---|---|---|---|
| 1 | .3160 | 7.48 | 612.48 | 360.83 | 427.66 | -815019.0 | 5768728.1 | 1499992.3 | 1.1 |
| 2 | .2528 | 354.11 | 718.23 | 457.95 | 488.24 | -422748.7 | 2649618.0 | 96350.0 | 3.9 |
| 3 | .2413 | 381.17 | 766.93 | 523.87 | 559.50 | -511607.3 | 3155638.1 | 142993.8 | 3.9 |
| 4 | .2337 | 420.29 | 832.45 | 601.07 | 642.64 | -525336.8 | 3741683.1 | 219298.4 | 3.8 |
| 5 | .2170 | 458.47 | 914.53 | 699.02 | 755.41 | -411628.4 | 5186987.3 | 411883.6 | 3.6 |
| 6 | .1924 | 502.59 | 1006.03 | 817.78 | 880.11 | -84620.4 | 5883528.6 | 645105.2 | 3.5 |
| 7 | .1556 | 555.79 | 1110.64 | 951.12 | 1022.13 | 703228.1 | 6876811.0 | 1002624.9 | 3.3 |
| 8 | .1202 | 609.75 | 1225.19 | 1103.71 | 1185.30 | 2877383.1 | 8106701.2 | 1628525.8 | 3.1 |
| 9 | .0567 | 667.87 | 1311.61 | 1241.34 | 1297.39 | 3831680.4 | 5685111.3 | 1416945.2 | 3.4 |
| 10 | .0193 | 717.14 | 1362.70 | 1329.12 | 1360.84 | 3201924.7 | 3258255.4 | 863761.0 | 4.5 |
| 11 | .0004 | 5.00 | 1382.01 | 1361.13 | 1381.42 | 287938.8 | 30183.0 | 4755.6 | 11.0 |

RECEIVER ENERGY BALANCE

| | | |
|---|---|---|
| POWER STRIKING RECEIVER (W) | 60299877.3 | |
| REFLECTION LOSSES (W) | | 1759489.9 |
| CONVECTION LOSSES (W) | | .0 |
| RERADIATION LOSSES (W) | | 8130005.1 |
| POWER ADDED TO THE AIR (W) | | 50343023.1 |
| UNACCOUNTED POWER | | 68167.9 |
| TOTAL | | 60298686.0 |

RECEIVER EFFICENCIES
RECEIVER ABSORPTIVITY = .970788372471
RECEIVER THERMAL EFFICENCY = .8609614486448
RECEIVER TOTAL EFFICENCY = .8356113636843

NUMBER OF ITERATIONS TO CONVERGE = 221

Figure A.4. Sample Output

Rotation speed - see RPM

Air mass flow rate - see AIRMAS

Product design temperature - see TAIRE

Ambient air temperatures - see TAIRI

Ambient temperature for radiation heat transfer (K). The model used in RATS assumes that ambient temperature for radiation heat transfer (Sky temperature) equals ambient air temperature.

Reflection losses - This represents the reflection losses (or 1.0 - receiver absorpitivity) in percent. It is calculated by subtracting the sum of QINSF for all zones from 1.0.

Convection loss - see CVLPCT

Zone exchange factor - Zone exchange factor represents the exchange factor between the zone and ambient. It is an indication of the geometric loss reduction due to receiver geometry.

Zone convective heat transfer coefficient (W/SQR -M-K) - This is the convective heat transfer coefficient between the zone surfaces and the air calculated in subroutine CONV.

Zone material temperature ($^{O}$K) - Zone material temperature is the temperature of the absorbing surface (either fin or fiber) in the specified zone.

Zone bulk air temperature ($^{O}$K) - Zone bulk air temperature is the average or bulk air temperature for the zone and is calculated by averaging the inlet and outline air temperatures. Air properties such as viscosity, conductivity and density are calculated based on bulk air temperature.

Zone exit air temperature ($^{o}K$) - This output is the temperatures of the air exiting the zone. The exit air temperature from zone n (the interior zone) is the calculated product temperature.

Zone net radiation heat transfer (watts) - Zone net radiation heat transfer is the net rate that energy is being added to the zone by radiation heat transfer, a negative value implies that energy is being added to the zone and a positive value implies that energy is leaving the zone.

Zone convection to air (watts) - Zone convection to the air represents the rate at which energy is being used to heat air in the zone.

Zone radiation loss to ambient - This is the net rate that energy is being radiated from the zone to ambient and it represents a loss.

Zone flux ratio - The zone flux ratio is the ratio of the maximum allowable flux on the zone (based on material temperature limits) to the calculated average flux. A value of 2 would imply that a flux multidistribution of up to 200% compared to the average flux could be tolerated without exceeding material temperature limitations.

Power striking receiver (watts) - This is the rate that thermal energy strikes the receiver. The energy can be lost by reflection, convection or reradiation or it can be transferred to the air in which case it becomes a useful product. This value

should equal the total of the various components of the energy balance included in the performance summary.

Reflection losses (watts) - Reflection loss is the rate at which thermal energy, which strikes the receiver, is lost due to reflection.

Convection losses (watts) - Convection loss is the rate at which thermal energy which is absorbed by the receiver is lost due to convection to the surrounding.

Reradiation losses (watts) - Reradiation loss is the rate at which thermal energy is absorbed by the receiver is lost due to reradiation to the surroundings.

Power added to the air (watts) - This is the rate that thermal energy is transferred to the product air and it represents the useful output of the receiver.

Unaccounted power (watts) - Unaccounted power is the energy added to the zone which contributes to raising the zone temperature. When equilibrium conditions have been attained, the unaccounted power should be small compared to the total power striking the receiver. If unaccounted power is not small relative to the power striking the receiver then EPS should be reduced.

Receiver absorbitivity - receiver absorbitivity is equal to 1.0 minus reflection losses and is reported as a decimal fraction.

Receiver thermal efficiency - receiver thermal efficiency equals the rate of energy being transferred to the air divided by the rate of energy being absorbed on the receiver.

Receiver total efficiency - this is the product of receiver absorbi-
tivity and thermal efficiency.

# APPENDIX B

## VORRUM USERS GUIDE

# APPENDIX B

## VORRUM USERS GUIDE

The VORRUM (Volumetric Receiver Radiation Utilization Model) computer code determined the distribution of absorbed incident radiation (radiation from the heliostat field) for a volumetric solar central receiver using a Monte Carlo type simulation. The users guide will describe the important features of the code. The theoretical justification for the models used in VORRUM is included in the body of the report. Section B1 will describe the general approach used in the code. Section B2 will discuss the code structure and the contents of the subroutines. Section B3 will present the code inputs while Section B4 will present a description of the codes output.

### B.1.0 GENERAL APPROACH

The VORRUM computer code is written in FORTRAN 77 for a CDC 3300 computer and requires access to the IMSL math pack. It is intended to be used as a design tool in the design and analysis of a variety of volumetric receive designs. The output consists of the distribution of absorbed radiation from the heliostat field and losses due to the reflection of insolation from the receiver.

The VORRUM computer code uses a Monte Carlo method to determine the distribution of absorbed insolation. The Monte Carlo approach is a statistical method of solving a physical problem which can be modeled as a series of probabilistic and deterministic events.

Energy entering the volumetric receiver is simulated by a large number of energy or photon bundles. The incoming photon bundles are followed as they proceed from one event to another with the results of each interaction being recorded. This process continues until a photon bundle either leaves the receiver or its energy drops below a minimum level. A large number of photon bundles are simulated with the results of all surface/bundle interaction being totaled. A sufficiently large number of bundles must be simulated to insure that variations in the results due to the random nature of the probabilistic events are small. The results can then be used to determine the fraction of the emitted energy which has been absorbed on each surface or zone.

The volumetric receiver includes fin shaped pins or small fiber arranged in rows. The regular spacing of the pins or fibers and the row arrangement is used to improve the efficiency of the computational method. The approach consists of dividing the receiver into computational cells where the cells are arranged so that solid surfaces are located on cell boundaries. With this arrangement, an energy bundle leaving one surface must strike one of the other three surfaces. The determination of the impacted surfaces and the location of impact is straight forward. An example of a computational cell along with the cell surface number convention is shown in Figure B.1. The arrangement of computational cells forming a receiver array is shown in Figure B.2. For fin shaped pins, the computational cell includes one fin which is located on the bottom (surface 2) of

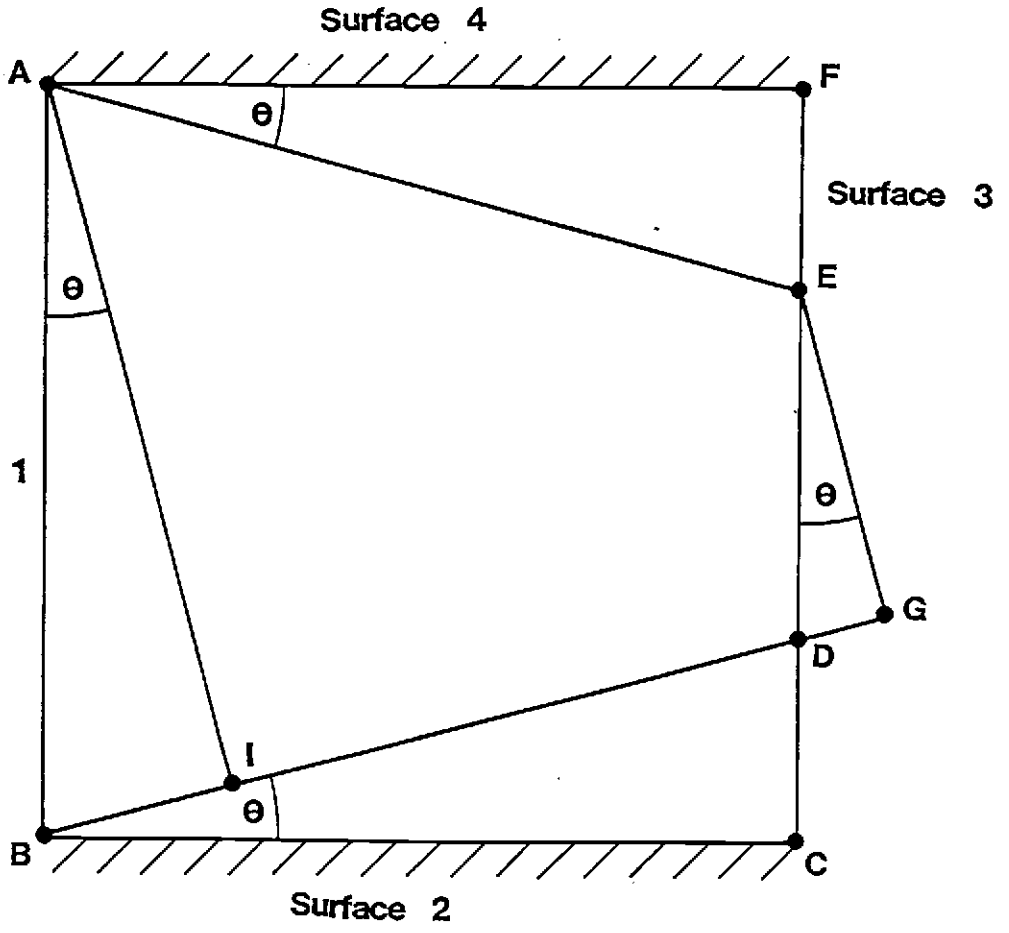


Figure B.1. Sample Computation Cell

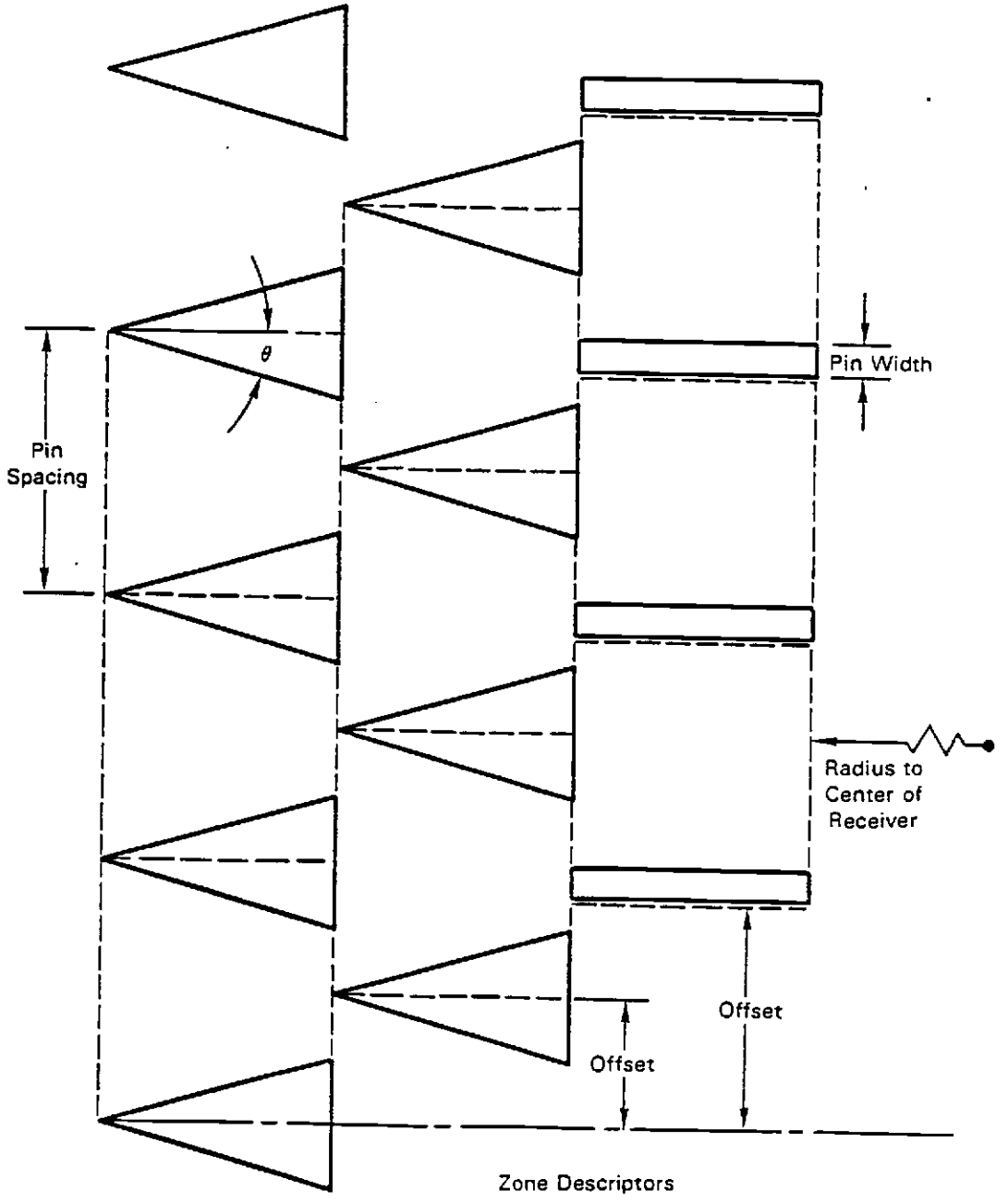


Figure B.2. Definition of Cell Parameters

the cell. For wedge shaped pins the computational cell boundary runs along the centerline of the wedge.

The results from VORRUM can be used to select an absorbing array design which gives a desired energy distribution or they can be used with the RATS computer code to determine the temperature distribution and performance of a volumetric receiver design. When used with RATS, the output from VORRUM does not require any processing before being used as an input to RATS.

As with all Monte Carlo codes, the demand for computer time can be substantial. The actual requirements for computing resources depends on the required accuracy. The user must consider this trade-off carefully and weigh the benefit of improved accuracy versus the cost of computer time. As a rule of thumb, a decrease in the standard deviation by one half will require the simulation of four times as many photons. The batch sizes used in this study ranged from 100 photons for screening studies to 1000 photons for preliminary design simulations. An actual design might require batch sizes of 10,000 to 100,000 depending on the required accuracy.

## B.2.0. CODE STRUCTURE

The VORRUM computer code consists of ten subroutines and one function. The code includes two major iteration loops. The first simulated NBATC number of batches. The interior iteration then simulates NPHOT photons for each batch.

The driver, VORRUM, calls subroutine INPUT which reads the input data from a data file. VORRUM then calls subroutine BATCH which simulates one batch of photons. BATCH is called NBATC times and the sum of energy absorbed in each zone is stored as ZTOTL. ZTOTL is a matrix with NBATC columns and NZOMX rows where NZOMX is the maximum number of rows. The ZTOTL matrix is supplied to subroutine STAT where the mean values and the standard deviations are calculated. VORRUM then calls subroutine OUTPUT which prints out a summary of the input variables and the results. The driver, VORRUM is shown in Figure B.3.

Each of the subroutines will now be discussed, but a detailed presentation of the analytical model is not included. The development, description and verification of the analytical model is included in the body of the report.

INPUT - Subroutine INPUT reads input data from the appropriate data file. The data is arranged in two groups; control variables and zone characteristics. The various input parameters are described in B.3.0 In addition INPUT calculates a large number of constant zone dimensions used later in the program. The definition of these zone dimensions are shown in Figure B.2. The definition of other variables are included in the comment statements in the code.

BATCH - Subroutine BATCH simulation the emission of NPHOT photons. The structure of BATCH is shown in Figure B.4. The initial emission point is selected and NPHOT/NICRM photon bundles are emitted from this location. NICRM is the number of emission points on the

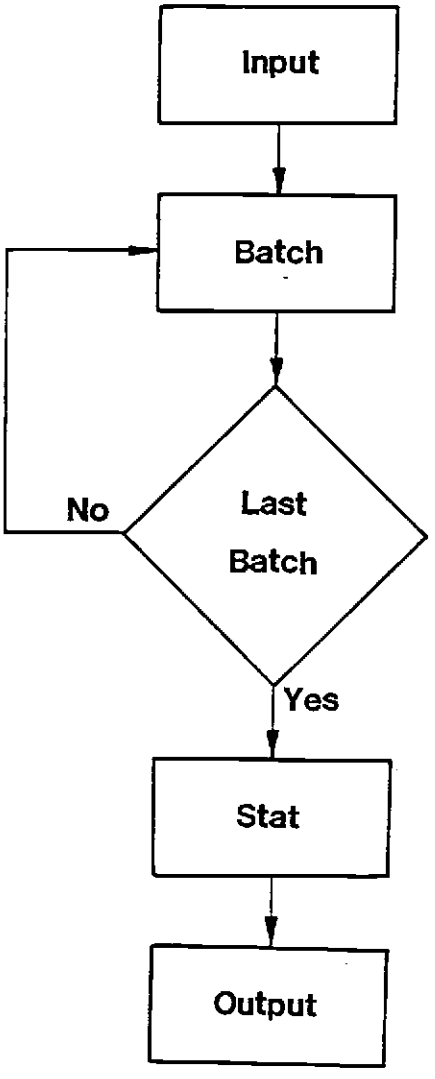


Figure B.3. VORRUM Flow Chart

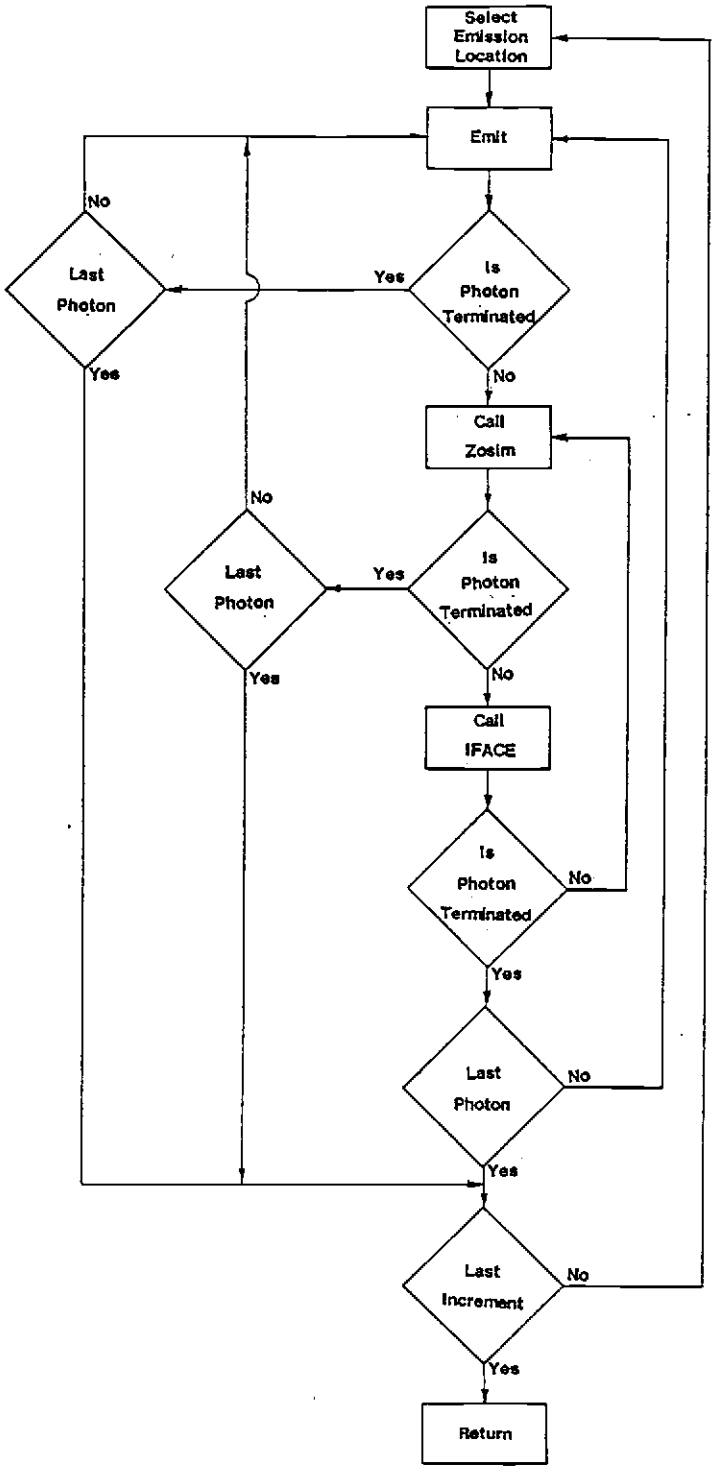


Figure B.4. Batch Flow Chart

emitting surface. An individual photon bundle history is initiated by calling subroutine EMIT which selects the original emission angle for a photon bundle entering the external zone. The photon bundle energy level is then checked to see if it has dropped below the minimum energy level. If the photon bundle energy has dropped below PHOEGM the photon bundle history is terminated and the number of photon bundles emitted from the first increment are checked to see if this bundle was the last emitted bundle for the first increment.

If the photon bundle was not terminated following EMIT then BATCH calls ZOSIM which determines the location and angle at which the photon bundle exits the currently occupied cell. Following ZOSIM, the photon bundle energy level is checked and if it's history is not terminated BATCH calls subroutine IFACE which takes the exiting location and angle from ZOSIM and calculates an inlet location and angle for the next cell. The photon bundle energy is again checked. If the photon bundle history is not terminated ZOSIM is called again. This process is continued until the photon bundle history is terminated due to the photon bundle energy falling below the minimum level or by the photon exiting the receiver.

When the last photon bundle emitted from the first emission location is simulated a new emission point is located and the process is repeated. This continues until all NPHOT photon bundles have been simulated and the results for one batch have been obtained.

EMIT - Subroutine EMIT calculates the emission point on the external surface of the external row of cells. The emission angle is selected

using an inverse error function supplied by the IMSL math pack. This approach insures that the distribution of inlet angles conforms to a Gaussian distribution with a standard deviation of AGDSD. EMIT also checks for a photon bundle striking a pin tip in the external row pins. If a pin tip is struck the energy level of the photon bundle is reduced by the product of the zone emissivity and the current photon bundle energy. The zone's absorbed energy total is increased by the same amount. The photon bundle is then assumed to exit the receiver and is considered a loss. EMIT also assigns the cell number (equal to NCELL1) and zone number (equal to 1).

ZOSIM - Subroutine ZOSIM takes the location and angle of the photon bundle entering a given cell and calculates the photon bundle exit location and angle. ZOSIM determines the emitting surface by checking the surface indicator NAME1. If NAME1 equals 1 subroutine SURF1 is called, otherwise SURF3 is called. These subroutines determine which surface in the cell has been struck by the photon bundle. ZOSIM then checks to see if the photon bundle has exited the cell (struck either surface 1 or 3) or if the photon bundle energy has dropped below the minimum level. In either case, control is returned to BATCH, otherwise ZOSIM determines which cell surface has been struck by the photon bundle by checking surface indicator NAME2. This is followed by an exit check and a photon bundle energy check. The procedure is continued until the photon bundle either exists the

cell or its energy drops below the minimum level. The structure of ZOSIM is shown in Figure B.5.

SURF1 - Subroutine SURF1 executes the emission of one photon bundle from surface 1, determines the surface struck by the photon bundle and the results of the event. SURF1 receives the emission location and incident angle from ZOSIM. SURF1 then determines which surface is struck by the photon bundle. If the surface is surface 3, the logical variable EXIT is assigned a true value and the exit location and angle are calculated. If surface 2 or 4 are struck SURF1 determines the photon bundle energy reduction (the produce of current photon bundle energy and surface emissivity), the location of the interaction and the incident angle. The surface emissivity can be a function of on the incident angle. After the surface has been determined and the location, angle and energy reductions calculated, control is returned to ZOSIM.

SURF2 - Subroutine SURF2 executes the emission of one photon bundle from surface 2. The location of the emission and the incident angle are supplied from ZOSIM. SURF2 checks for specular reflection. A random number is selected and if it is less than SPEC the reflections are specular and the emission angle is set equal to the incident angle, otherwise the emission is assumed to be diffuse and the angle is randomly selected. After the angle is selected, the surface being struck is determined. At this point SURF2 follows the logic des-

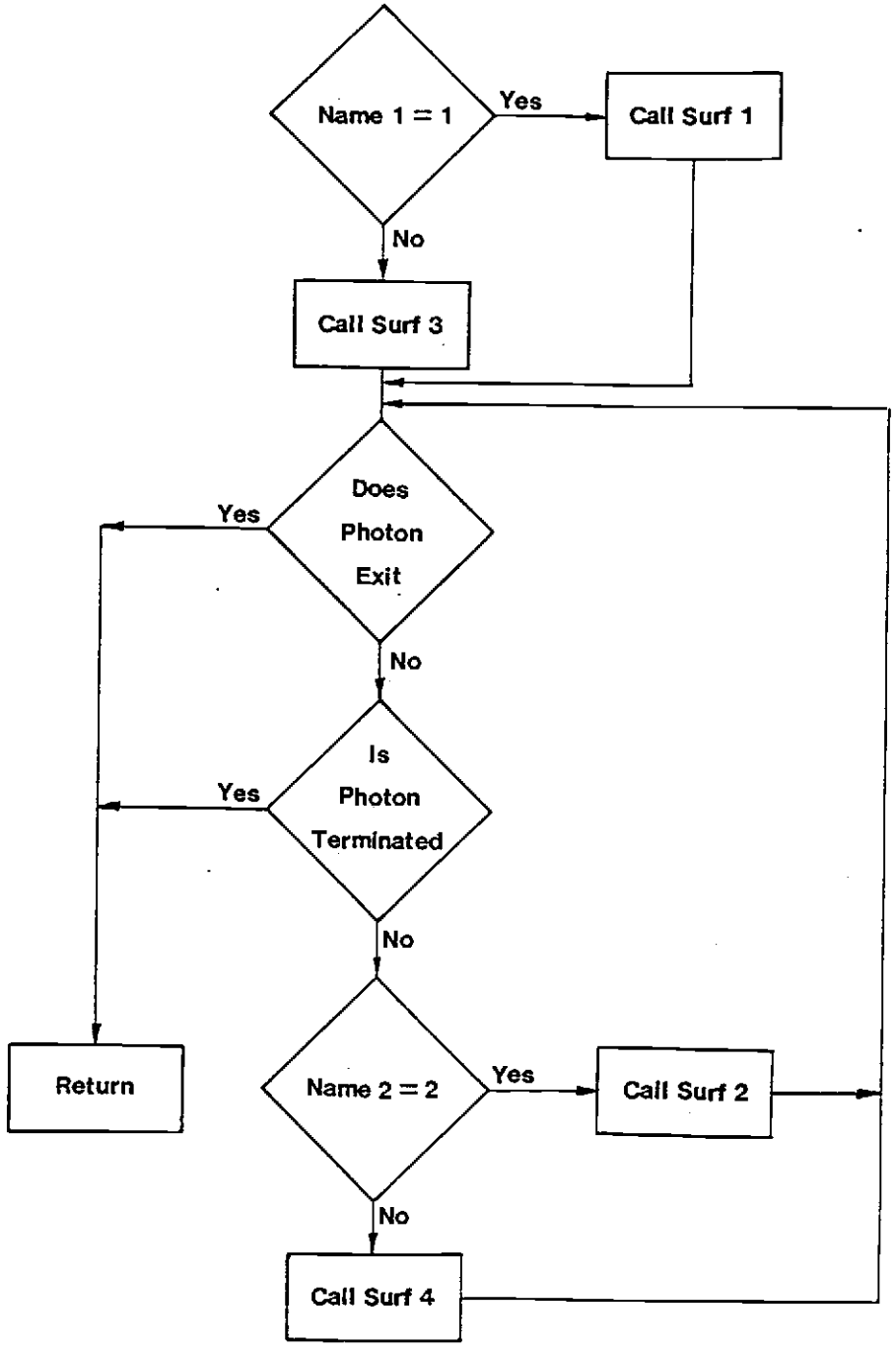


Figure B.5. ZOSIM Flow Chart.

cribed in SURF1 to determine the location incident angle and results of the photon bundle/surface interaction.

SURF3 - Subroutine SURF3 executes the emission of one photon bundle from surface 3, determines the surface struck by the photon bundle and the result of the event. The logic in SURF3 is similar to SURF1.

SURF4 - Subroutine SURF4 executes the emission of one photon bundle from surface4, determines the surface struck by the photon bundle and the results of the event. The logic in SURF4 is similar to SURF2.

IFACE - Subroutine IFACE takes the photon bundle exit location and angle from the currently occupied computational cell, calculated by ZOSIM and determines the inlet location and angle for the cell being entered by the photon bundle. IFACE first determines if the photon bundle is moving from an interior zone to and exterior zone or in the other direction. If the photon bundle is moving in the outward direction, IFACE checks to see if the photon bundle exits the receiver (enters zone 0). IFACE then calculates the arc length from the datum to the exiting location. The arc length is then used to determine the receiving cell number and the location of the incoming photon bundle relative to the receiving cell boundary. IFACE then checks to see if the photon bundle strikes a pin tip. If so, IFACE determines the energy reduction and reflection angle from the pin tip. The photon bundle is then assumed to enter the original doner cell at the old exit location with an inlet angle equal to the

reflection angle from the pin tip. Regardless of where or not a photon bundle strikes a pin tip the new inlet location angle, cell number and zone number are returned to BATCH.

In a similar manner, inward bound photon bundles are analyzed and the new inlet locations, angle, cell number and zone number are returned to BATCH. The one difference is that the photon bundle is checked to see if it is exiting the most interior zone in the inward direction, in which case the photon bundle is assumed to be absorbed in the interior zone.

STAT - Subroutine STAT calculates the mean and standard deviation of the NBATC results for each zone. In addition STAT calculates the total energy absorbed in the receiver and calculates the mean value and standard deviation in decimal fractions.

OUTPT - Subroutine OUTPT prints out a summary of the input data and the results. A description of the output variables is included in Section B.4.0.

EMIS - EMIS is a function which calculates the surface absorptivity (or emissivity) given the absorptivity (or emissivity) for a photon bundle striking the surface in the normal direction. If the emission model indicator IEMIS equals 0 the surface emissivity is assumed to be independent of emission angle and equal to the emissivity for a photon bundle striking the surface in the normal direction. For IEMIS equal to 1 the emissivity is calculated using a function of

incident angle. The emissivity model is described in the body of the report.

## B.3.0 INPUT PARAMETERS

The input data for VORRUM consists of two groups of data; control variables and zone characteristics. In the current version of the code, the data is entered from a separate data file. The input data file including the appropriate format is shown graphically in Figure B.6. A sample data file is shown in Figure B.7. In this section, each input will be described separately.

NBATC - This is the number of photon batches executed in the simulation.

NPHOT - NPHOT is the number of photon bundles included in each batch.

NICRM - This is the number of emission points on the external surface of the cell from which the photon bundles are initially emitted.

NZOMX - NZOMX is the total number of zones in the receiver with the external zone being zone 1 and the internal zone being NZOMX.

PHOEGM - PHOEGM is the minimum photon energy below which the photon history is terminated.

IEMIS - This is the emissivity model indicator. A value of 0 indicates a constant emissivity equal to EMISN which is given below. A value of 1 indicates an emissivity which is dependent on incident angle, in which case emissivity is calculated using function EMIS.

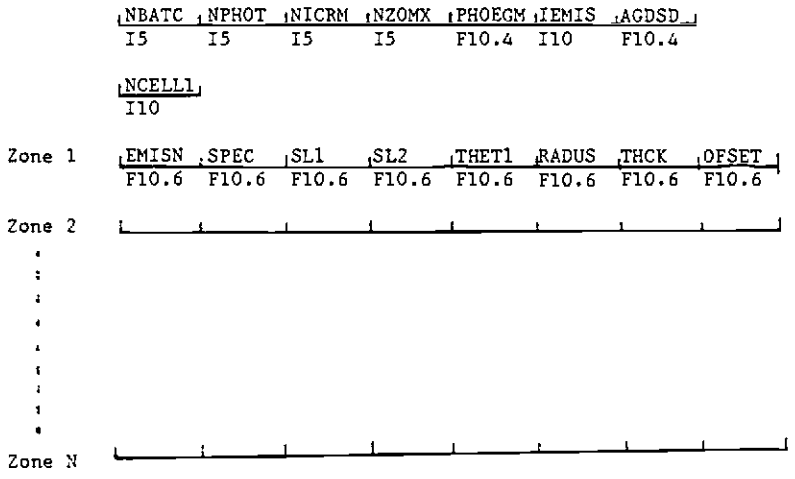


Figure B.6. Input Format

```
                    PROGRAM VORPUM


 PROGRAM VORPUM DETERMINES THE DISTRIBUTION OF
 INCIDENT ENERGY ON THE ZONES OF A VOLUMETRIC
 AIR HEATING RECEIVER.THIS PROGRAM SIMULATES
THE RADIATION HEAT TRANSFER IN THE VOLUMETRIC
RECEIVER USING A MONTE CARLO METHOD GIVEN
INSOLATION AND RECEIVER DESIGN CHARACTERISTICS


                    INPUT DATA

ZONE  EMISSIVITY SPECULARITY  PIN      ZONE     THETA     RADIUS    PIN      OFSET
                              SPACING  DEPTH                        WIDTH
  1     .2000      .9900      .1250    .6250    .0250     10.00     .0313    .000
  2     .0009     1.0000     1.2890   1.4750    .0000      9.39     .0000    .000
  3     .9000      .0000      .0130    .0005    .0000      7.90     .0005    .003
  4     .0000     1.0000     1.0860    .6000    .0000      7.90     .0000    .000
  5     .9000      .0000      .0100    .0005    .0000      7.30     .0005    .010
  6     .0000     1.0000     1.0040    .6000    .0000      7.30     .0000    .000
  7     .9000      .0000      .0080    .0005    .0000      6.70     .0005    .007
  8     .0500     1.0000      .9213    .6000    .0000      6.70     .0000    .000
  9     .9000      .0000      .0051    .0005    .0000      6.10     .0005    .003
 10     .0000     1.0000      .8388    .6000    .0000      6.10     .0000    .000
 11     .9000      .0000      .0037    .0005    .0000      5.50     .0005    .010
 12     .0000     1.0000      .7563    .6000    .0000      5.50     .0000    .000
 13     .9000      .0000      .0024    .0005    .0000      4.90     .0005    .007
 14     .0000     1.0000      .6738    .6000    .0000      4.90     .0000    .000
 15     .9000      .0000      .0011    .0005    .0000      4.30     .0005    .003
 16     .0000     1.0000      .5913    .6000    .0000      4.30     .0000    .000
 17     .9000      .0000      .0006    .0005    .0000      3.70     .0005    .010
 18     .0000     1.0000      .5088    .6000    .0000      3.70     .0000    .000
 19     .9000      .0000      .0001    .0005    .0000      3.10     .0005    .007
 20     .0000     1.0000      .4263    .6000    .0000      3.10     .0000    .000
 21     .8000      .0000      .4000    .2000    .0000      2.50     .0250    .000
 22    1.0000      .0000      .3163   2.3000    .0000      2.30     .0000    .000


CONTROL VARIABLES
     NUMBER OF BATCHES=20
     NUMBER OF PHOTON BUNDLES PER BATCH=100
     NUMBER OF ZONES=22
     NUMBER OF INCREMENTS IN INLET CELL=10
     MINIMUM PHOTON ENERGY FOR TERMINATION OF
       PHOTON HISTORY=.001
     STANDARD DEVIATION OF INLET ANGLE
       DISTRIBUTION =.1
     CELL NUMBER FOR INITIAL
       EMISSION=17
```

Figure B.7. Sample input

AGDSD - AGDSD is the standard deviation of Inlet angle distribution for the initial emission into NCELL1.

NCELL1 - This is the number of the cell into which the photons are emitted for the initial emission.

EMISN(I) - EMISN(I) is the normal emissivity for any surface in zone I (emissivity for radiation with a direction normal to the surface).

SPEC(I) - SPEC is the specularity of zone I (probability in decimal fractions that a reflection from any surface in the zone will be specular).

SL1(I)(meters) - This is the width of a computational cell in zone (I). SL1 is shown graphically in Figure B2.

SL2(I)(meters) - This is the depth of a computational cell in zone (I). SL2 is shown graphically in Figure B.2.

THET1(I) (radians) - THET1 is the wedge half angle for wedge shaped pins in zone (I). THET1 is shown in Figure B.2.

RADUS(I) (meter) - RADUS(I) is the radius of the cylinder forming the external surface of zone (I). RADUS is measured from the centerline of the receiver.

THCK(I)(meter)- THCK(I) is the pin thickness for non-wedge shaped pins in zone (I). THCK is shown in Figure B.2.

OFSET(I)(meter)- OFSET is the arc length from the datum to the boundary of the first cell in the zone. OFSET is shown in Figure B.2.

## B.4.0 OUTPUT PARAMETERS

The output from VORRUM consists of two components, a summary of the input variables and the results. A sample of the output's shown in Figure B.8. Except where the output variable is explained in Section B.3, each output variables will now be explained.

emissivity - see EMISN

specularity - see SPEC

pin spacing - see SL1

Zone Depth - see SL2

THETA - see THET1

Radius - see RADUS

Pin Width - see THCK

Offset - see OFSET

Number of batches - see NBATC

Number of photon bundles per batch - see NPHOT

Number of Zones - see NZOMX

Number of Increments in inlet cell - see NICRM

Minimum Photon Energy for Termination of photar history - see PHOEGM.

Standard Deviation of inlet angle Distribution - see AGDSD

Cell number for initial emission - See NCELL1

Percent Incident Radiation Absorbed in Zone - this is the percentage of the incident solar radiation from the heliostat field which is absorbed in the zone. The summation of this value for all

RESULTS

DISTRIBUTION OF INCIDENT RADIATION AMONG RECEIVER ZONES IN PERCENT

| ZONE | PERCENT INCIDENT RADIATION ABSORBED IN ZONE | STANDARD DEVIATION |
|---|---|---|
| 1 | 8.4590 | .9721 |
| 2 | .0000 | .0000 |
| 3 | 3.5971 | 1.3135 |
| 4 | .0000 | .0000 |
| 5 | 4.3305 | 1.7211 |
| 6 | .0000 | .0000 |
| 7 | 6.1422 | 2.4538 |
| 8 | .0000 | .0000 |
| 9 | 6.8932 | 1.3443 |
| 10 | .0000 | .0000 |
| 11 | 9.0088 | 2.7723 |
| 12 | .0000 | .0000 |
| 13 | 12.0037 | 2.3397 |
| 14 | .0000 | .0000 |
| 15 | 18.3085 | 2.9356 |
| 16 | .0000 | .0000 |
| 17 | 15.1083 | 3.6922 |
| 18 | .0000 | .0000 |
| 19 | 12.6276 | 3.2904 |
| 20 | .0000 | .0000 |
| 21 | .1073 | .1691 |
| 22 | .3764 | .5060 |
| REFLCT | 3.0372 | .6282 |

Figure B.8. Sample Output.

zones plus REFLCT should equal 1.0. This value in decimal factions is used for QINSF(I) in the RATS computer code.

Standard Deviation - This is the standard deviation of the value for "Percent Incident Radiation Absorbed in Zone" or REFLCT.

REFLCT - REFLCT is the percent of the incident solar radiation from the heliostat field which is reflected out of the receiver and lost to ambient. The receiver absorptivity equals 1.0 minus REFLCT.

# APPENDIX C

## VOREFM USERS GUIDE

# APPENDIX C

## VOREFM USERS GUIDE

The VOREFM (VOmetric Receives Exchange Factor Model) computer code determines the exchange factors between the various zones of a volumetric solar central receives using a Monte Carlo simulation. The users guide will describe the important features of the code. The VOREFM code is essentially a modified version of the VORRUM code, therefore this appendix will only discuss the areas where VOREFM differs from VORRUM. Section C.1 will describe the general approach used in the code. Section C.2 will discuss the code structure and contents of the subroutines. Section C.3 will present the code input and Section C.4 will present a discussion of the code outputs.

### C.1.0 GENERAL APPROACH

The VOREFM computer code is written in FORTRAN77 for a CDC 3300 computer and requires access to the IMSL math pack. It is intended to be used as a design tool in the design and analysis of a variety of volumetric receivers concepts. The required output is the exchange factor from the zone of interest to all other zones in the receiver including the surroundings. In order to supply all the required information for RATS, VOREFM must be run for each zone so that a complete matrix of exchange factors has been determined. VOREFM uses the same general Monte Carlo approach discussed in Section B.1 of Appendix B.

## C.2.0 CODE STRUCTURE

The VOREFM computer code consists of thirteen subroutines and one function. The code consists of two major iteration loops. The first simulate NBATC number of batchs. The interior iteration then simulate NPHOT photon bundles for each batch. Unlike VORRUM, the photon bundles are initially emitted from a representative surface in the zone currently being analyzed.

The driver VOREFM is identical to VORRUM. The main variations are in the subroutine BATCH, in addition to minor variations in INPUT. The subroutine EMIT in VORRUM has been replaced by four new subroutines EMIT1, EMIT2, EMIT3, and EMIT4. These subroutines will now be discussed. When there is no difference between VOREFM and VORRUM, this will be indicated and the reader will be referred to the VORRUM users manual.

INPUT - Subroutine INPUT is the same as in VORRUM except that several additional constants are calculated. These include the number of emission points on each surface of one pin or fiber in the row of interest. The emission points are chosen so that the number of emission points is proportional to the relative area of the surface compared to the overall area of the pin. All pin tips (excepting the wedge tip of a wedge shaped pin) are assigned at least one emission point. The number of photon bundles emitted from each emission point is then calculated. The number of photon bundles emitted from each point is calculated to insure that the energy emitted from a surface

is proportional to the area of that surface relative to the total surface area of the pin or fiber. The total number of photon bundles is then calculated by summing the product of emission points and photon bundles emitted per point. The NPHOT value input into the code is a target batch size, due to roundoff and allocation of photon bundles among surfaces of varying size, the actual NPHOT used in the code is calculated in INPUT.

BATCH - Subroutine BATCH is similar to that used in VORRUM except that BATCH now simulates the emission of photon bundles from four surfaces rather the one surface. First, batch simulates the emission of photon bundles from the sides of a pin. BATCH call subroutine EMIT2 or EMIT4 which provides the emission point and angle for the photon bundle. BATCH then calls ZOSIM and proceeds as in VORRUM. This is continued until all the photon bundles emitted from a pin's side have been simulated. BATCH then simulates photon bundle emission from the pin's tips by calling EMIT1 as EMIT3 which again provides the emission point and angle. BATCH then calls IFACE and continues as in VORRUM until all photon bundles in the batch have been simulated.

EMIT2 - Subroutine EMIT2 calculates the emission point and angle for photon bundles being emitted by surface2 in a computational cell. The surface is assumed to be a diffuse emitter and the emission angle is randomly selected.

EMIT4 - Subroutine EMIT4 is similar to EMIT2 except that photon bundles are emitted by surface4.

EMIT1 - Subroutine EMIT1 is similar to EMIT2 except that photon bundles are emitted by an internal pin tip so that the emission into the first computational cell is from surface1.

EMIT3 - Subroutine EMIT3 is similar to EMIT except that photon bundles are emitted by the exterior pin tip.

ZOSIM - See VORRUM users manual

SURF1 - See VORRUM users manual

SURF2 - See VORRUM users manual

SURF3 - See VORRUM users manual

SURF4 - See VORRUM users manual

IFACE - See VORRUM users manual

STAT - See VORRUM users manual

OUTPT - Subroutine output is similar to VORRUM except that the results are the exchange factors from the zone of interest (designated by NZOET) to all other zones including ambient.

EMIS - See VORRUM users manual

C.3.0 INPUT PARAMETERS

The input parameters for VOREFM are identical to VORRUM except that input variable AGDSD (Format=F10.4) is replaced by NZOET (Format=I10). NZOET is the zone number of the emitting zone.

C.4.0 OUTPUT PARAMETERS

The output parameters for VOREFM are identical to VORRUM except that the results are the exchange factors between the zone of interest and all other zones. RERADIATION is the exchange factor from the zone of interest to ambient.

# APPENDIX D

## SHROUD EXCHANGE FACTOR CALCULATIONS

# APPENDIX D

## SHROUD EXCHANGE FACTOR CALCULATIONS

The performance code RATS includes subroutine SHDEF which calculates the exchange factors between the shroud and ambient and all other surfaces. This is accomplished by determining the view factors between the core, shroud and the surroundings. The exchange factors will equal the view factors if all surfaces are assumed to be black.

The view factor calculation is based on modeling the core as a cylinder of finite length nested in a finite length cylinder with the radius of the shroud. The assumed shroud shape and surface numbering scheme is shown in Figure D1. First the view factors between nested cylinder with a length equal to the receiver height are determined. This gives the following view factors.

VF(1,3)

VF(1,4)

VF(3,1)

VF(3,4)

VF(4,3)

VF(4,1)

VF(1,1), VF(3,3) and VF(4,4) are assumed to equal 0.0.

Then the view factors between nested cylinders with a length equal to the aperture height are determined. This yields

VF(0,4)

VF(0,0)

VF(4,0)

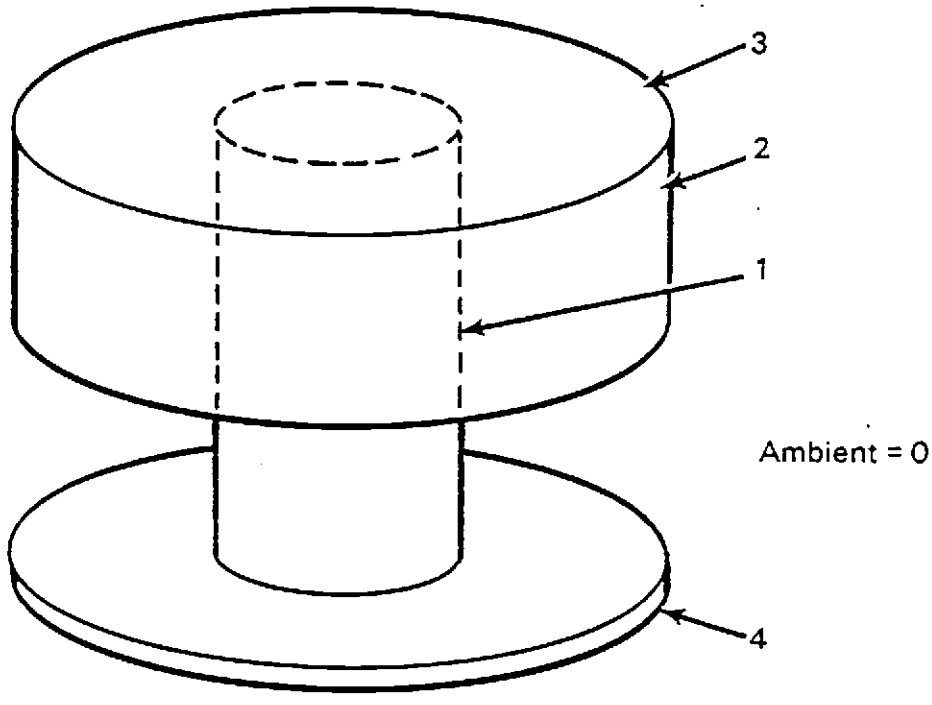


Figure D.1. Shroud Design

In a similar manner the view factors for nested cylinders with a length equal to the shroud height are determined, giving

VF(2,2)

VF(2,3)

VF(3,2)

The view factors involving the aperture, shroud and the ends can now be determined using equations D1, D2, D3 and D4.

D1 $VF(3,0) = 1.0 - VF(3,1) - VF(3,2) - VF(3,3) - VF(3,4)$

D2 $VF(4,2) = 1.0 - VF(4,0) - VF(4,1) - VF(4,3) - VF(4,4)$

D3 $VF(0,3) = VF(3,0)\ (A_3/A_0)$

D4 $VF(2,4) = VF(4,2)\ (A_4/A_2)$

At this point we know that the sum of the view factors from surface 0,1 and 2 must each equal 1.0 and that there are three reciprosity relations between surfaces 1 and 2, 1 and 0 and 2 and 0. These six equations allow for a solution in terms of the six remaining unknown view factors. The results are shown in equations D5 through D10.

D5 $VF(2,0) = ((A_0/A_1)\ C_0 + \frac{A_2}{A_1}\ C_2 - C_1)/\frac{A_2}{A_1}$

D6 $VF(0,1) = C_0 - A_2\ VF(2,0)/A_0$

D7 $VF(2,1) = C_2 - VF(2,0)$

D8 $VF(1,2) = A_2\ VF(2,1)/A,$

D9 $VF(1,0) = A_0\ VF(0,1)/A_1$

D10 $VF(0,2) = A_2\ VF(2,0)/A_0$

where

$C_0 = 1,0 - VF(0,3) - VF(0,4) - VF(0,0)$

$C_1$ = 1.0 - VF(1,3) - VF(1,4) - VF(1,1)

$C_2$ = 1.0 - VF(2,2) - VF(2,3) - VF(2,4)

The view factors may be effected by having some fraction of the circumference of the aperture blocked. The variable ABLK indicates the decimal fraction of the circumference which is blocked. The area of surface 2 is increased by an amount equal to the product of ABLK and the original aperture area. The area of the aperture is decreased by a similar amount. Equations D11 through D20 are used to calculate the following view factors modified for aperture blockage.

D11 VF(1,2) = VF(1,2) + ABLK (VF(1,0))

D12 VF(1,0) = VF(1,0)(1 - ABLK)

D13 VF(3,2) = VF(3,2) + ABLK (VF(3,0))

D14 VF(3,0) = VF(3,0)(1-ABLK)

D15 VF(4,2) = VF(4,2) + ABLK (VF(4,0))

D16 VF(4,0) = VF(4,0) (1,0-ABLK))

D17 VF(0,2) = VF(0,2) + ABLK (VF(0,0))

D18 VF(2,2) = VF(2,2) + VF(2,0) (ABLK)

D19 VF(0,0) = VF(0,0) (1,0-ABLK)

Reciprosity is used with equations D11 through D17 to find VF(2,1) VF(0,1), VF(2,3), VF(0,3), VF(2,4), VF(0,4), VF(2,0). At this point all significant view factors are known and the next step is to calculate exchange factors.

The exchange factor from zone j to ambient and the shroud is given by equations D20 and D21.

D20 $F(j,0) = \tilde{F}(j,0)$ (VF(1,0))

D21 $\tilde{F}(j,1) = F(j,0)\ (1.0 - VF(1,0))$

where $\tilde{F}\ (j,0)$ is the exchange factor from zone j to ambient taken from the Monte Carlo model results. The exchange factor indexing scheme corresponds to the convention used in the performance model with ambient being zone 0, the shroud being zone 1. The absorbing zones are 2 to N-1. The terminal absorber is zone N. The exchange factors from ambient and the shroud to the interior zone j is given by equation D22 and D23.

D22 $F(0,j) = \tilde{F}(1,j)\ (VF(0,1)/(1.0 - F(0,0)))$

D23 $F(1,j) = \tilde{F}(1,j)\ (1.0 - F(1,0) - F(1.1)))$

Exchanger factors between the shroud and ambient are given by equations D24 through D27.

D24 $F(0,0) = VF(0,0)$

D25 $F(0,1) = VF(0,2) + VF(0,3) + VF(0,4)$

D26 $F(1,0) = F(0,1)(A_0/(A_2 + A_3 + A_4))$

D27 $$F(1,1) = 1.0 - F(1,0) - \frac{(VF(1,2) + VF(1,3) + VF(1,4))A_1}{A_2 + A_3 + A_4}$$

This completes the calculation of all exchange factors which are influenced by the inclusion of a shroud in a volumetric receiver design.